

Dissertations and Theses

7-2018

Sensitivity Analyses of Optimized Attitude Estimators Using Sensor Fusion Solutions for Low- Cost MEMS Configurations

Ryan W. Hoffman

Follow this and additional works at: <https://commons.erau.edu/edt>



Part of the [Mechanical Engineering Commons](#)

Scholarly Commons Citation

Hoffman, Ryan W., "Sensitivity Analyses of Optimized Attitude Estimators Using Sensor Fusion Solutions for Low-Cost MEMS Configurations" (2018). *Dissertations and Theses*. 407.
<https://commons.erau.edu/edt/407>

SENSITIVITY ANALYSES OF OPTIMIZED ATTITUDE ESTIMATORS USING SENSOR FUSION SOLUTIONS FOR Low-COST MEMS CONFIGURATIONS

Ryan W. Hoffman

A thesis submitted in partial fulfillment of the requirements for the degree of
Master of Science in Mechanical Engineering

Embry-Riddle Aeronautical University

Daytona Beach, Florida

July 2018

Sensitivity Analyses of Optimized Attitude Estimators Using Sensor Fusion Solutions for Low-Cost MEMS Configurations

by

Ryan W. Hoffman

This thesis was prepared under the direction of and approved by the candidate's Thesis Committee Chair, Assistant Professor Dr. Hever Moncayo, and Thesis Committee Members: Associate Professor Dr. Marc Compere, and Assistant Professor Dr. Richard Prazenica. It was submitted to the Department of Mechanical Engineering in partial fulfillment of the requirements for the degree of Master of Science in Mechanical Engineering.

Thesis Review Committee:

Dr. Hever Moncayo
Committee Chair

7/20/2018

Date

Dr. Marc Compere
Committee Member

27 July 2018

Date

Dr. Richard Prazenica
Committee Member

7/25/2018

Date

E. Divo for Dr. Dhainaut

8/1/2018

Date

Dr. Eduardo Divo
Department Chair,
Mechanical Engineering

8/1/2018

Date

Dr. Maj Mirmirani
Dean, College of Engineering

Date

Dr. Christopher Grant
Vice Chancellor, Academic Support

8/6/18

Date

Abstract

Since the 1990's, there has been increased focus on creating navigation systems for small unmanned systems, particularly small unmanned aerial systems (SUAS). Due to size, weight, and cost restrictions, compared to larger more costly manned systems, navigation systems for SUAS have evolved to be quite different from the proven systems of the past. Today, there are many solutions for the problem of navigation for SUAS. The problem has now become choosing the most fitting navigation solution for a given application/mission. This is particularly true for evaluating solutions that are fundamentally different.

This research analyses the performance and sensitivity of four sensor fusion solutions for attitude estimation under multiple simulated flight conditions. There are three different hardware configurations between the four estimators. For this reason, each estimator is tuned to be experimentally optimal, as to provide a fair comparison between different estimators. With each estimator tuned to its highest performance, the estimators are compared based on their sensitivity to tuning error, sensor bias, and estimator initialization error. Finally the estimators' accuracy performances are directly compared.

This thesis also provides methods to tune different configuration estimators to their individual best performances. These methods show that choosing tuning parameters based on sensor noise covariance, as is typically done in research, does not produce optimal performance for all estimator formulations. After comparing multiple sensitivity and performance properties of the estimators, observations are provided regarding the efficacy of the analyses, including the applicability of the metrics used to determine performance. Some metrics were shown to be misleading for particular estimators or analyses. Ultimately, guidance is given for choosing performance metrics capable of comparing different solutions.

Table of Contents

Abstract.....	ii
Table of Contents.....	iii
List of Figures	v
List of Tables	vii
List of Acronyms.....	viii
List of Symbols	ix
1. Introduction - Attitude Estimation for Small Unmanned Applications.....	1
1.1. Problem Statement:.....	3
1.2. Objectives:	4
1.3. Literature Review	5
1.3.1. History of Navigation Systems	5
1.3.2. Current State of Attitude Solutions for SUAS	9
2. Theory	17
2.1. Coordinate Frames and Rotational Kinematics	17
2.1.1. Quaternion Rotations.....	24
2.2. Non-Linear Estimation Filters	27
2.2.1. Complementary Filter	27
2.2.2. Extended Kalman Filter	29
2.2.3. Unscented Kalman Filter.....	32
3. Attitude Estimation Formulations.....	34
3.1. Complementary Filter ("Method 1").....	34
3.2. Airspeed Aided Inertial Attitude Extended Kalman Filter ("Method 2")	37
3.3. GPS Aided Inertial Navigation Extended Kalman Filter ("Method 3")	44
3.3.1. Quaternion Formulation	48
3.4. GPS Aided Inertial Navigation Unscented Kalman Filter ("Method 4")	52
4. Experimental Setup.....	55
4.1. Simulation Environment	55
4.2. Flights	57
4.3. Noise Models	57

4.4. Monte Carlo Setup	58
5. Analyses, Results, and Observations.....	60
5.1. Optimal Tuning Parameters	61
5.1.1. Complementary Filter ("Method 1").....	61
5.1.2. Airspeed Aided Inertial Attitude Extended Kalman Filter ("Method 2")	73
5.1.3. GPS Aided Inertial Navigation Extended Kalman Filter ("Method 3")	80
5.1.4. GPS Aided Inertial Navigation Unscented Kalman Filter ("Method 4")	87
5.2. Sensitivity to Tuning Parameters	93
5.2.1. Complementary Filter ("Method 1").....	93
5.2.2. Airspeed Aided Inertial Attitude Extended Kalman Filter ("Method 2")	95
5.2.3. GPS Aided Inertial Navigation Extended Kalman Filter ("Method 3")	98
5.2.4. GPS Aided Inertial Navigation Unscented Kalman Filter ("Method 4")	102
5.2.5. Discussion.....	106
5.3. Bias Sensitivity.....	107
5.3.1. Complementary Filter ("Method 1").....	108
5.3.2. Airspeed Aided Inertial Attitude Extended Kalman Filter ("Method 2")	109
5.3.3. GPS Aided Inertial Navigation Extended Kalman Filter ("Method 3")	111
5.3.4. GPS Aided Inertial Navigation Unscented Kalman Filter ("Method 4")	112
5.4. Initialization Error	113
5.4.1. Complementary Filter ("Method 1").....	113
5.4.2. Airspeed Aided Inertial Attitude Extended Kalman Filter ("Method 2")	114
5.4.3. GPS Aided Inertial Navigation Extended Kalman Filter ("Method 3")	115
5.4.4. GPS Aided Inertial Navigation Unscented Kalman Filter ("Method 4")	117
5.4.5. Discussion.....	118
5.5. Baseline Comparison.....	119
6. Conclusions & Recommendations	123
6.1. Optimal Tuning.....	124
6.2. Metrics	125
6.3. Future Configurations	126
Bibliography	129

List of Figures

Figure 2-1: Inertial, Vehicle, and Body Frames; Source: (Modified from) (Beard & McLain, 2012)	19
Figure 2-2: Vehicle and Body Frames; Source: (jinsihou19, 2015)	20
Figure 2-3: Wind and Body Frames; Source: (Jirstrand & Gunnarsson, 2001)	20
Figure 2-4: Relation of Coordinate Frames.....	21
Figure 2-5: Gimbal Lock Example; Source: (Unknown, 2015)	25
Figure 2-6: 4 Axis Gimbal; Source: (DMahalko, 2018)	26
Figure 2-7: Standard Simple Complementary Filter	28
Figure 2-8: Complementary Filter Typical Application	29
Figure 2-9: EKF Equations	30
Figure 2-10: UKF Equations.....	32
Figure 3-1: Complementary Filter/Formulation for Attitude Estimation	36
Figure 3-2: Airspeed Aided Inertial Attitude EKF	41
Figure 3-3: GPS Aided Inertial Navigation EKF Pseudo Code Block Diagram	45
Figure 4-1: Simulation Environment Block Diagram.....	56
Figure 4-2: Monte Carlo Setup Pseudo Code Block Diagram.....	59
Figure 5-1: CF - Without Noise - Flight: Trim	62
Figure 5-2: CF - Without Noise - Flight: Elevator Pulse Input	63
Figure 5-3: CF - Without Noise - Flight: Short Steady Flight	64
Figure 5-4: CF - With Noise - Flight: Trim	66
Figure 5-5: CF - With Noise - Flight: Elevator Pulse Input.....	67
Figure 5-6: CF - With Noise - Flight: Short Steady Flight.....	68
Figure 5-7: CF - With Noise - Flight: Trim - Refined Tau.....	70
Figure 5-8: CF - With Noise - Flight: Elevator Pulse Input - Refined Tau.....	71
Figure 5-9: CF - With Noise - Flight: Short Steady Flight - Refined Tau.....	72
Figure 5-10: Airspeed Aided Attitude EKF - Theta Mean Error - Without Noise	74
Figure 5-11: Airspeed Aided Attitude EKF - Phi Mean Error - Without Noise.....	74
Figure 5-12: Airspeed Aided Attitude EKF - Theta Max Error - Without Noise.....	75
Figure 5-13: Airspeed Aided Attitude EKF - Phi Max Error - Without Noise	75
Figure 5-14: Airspeed Aided Attitude EKF - Theta Mean Error - With Noise	78
Figure 5-15: Airspeed Aided Attitude EKF - Phi Mean Error - With Noise	78
Figure 5-16: Airspeed Aided Attitude EKF - Theta Max Error - With Noise	79

Figure 5-17: Airspeed Aided Attitude EKF - Phi Max Error - With Noise	79
Figure 5-18: CF - Tuning Parameter Multiplier	94
Figure 5-19: Airspeed Aided Inertial Attitude EKF - Tuning Parameter Multiplier (Q and R)	96
Figure 5-20: Airspeed Aided Inertial Attitude EKF - Tuning Parameter Multiplier (Q Only).....	97
Figure 5-21: GPS Aided Inertial Navigation EKF - Tuning Parameter Multiplier (Q and R)	99
Figure 5-22: GPS Aided Inertial Navigation EKF - Tuning Parameter Multiplier (Q Only).....	100
Figure 5-23: GPS Aided Inertial Navigation EKF - Tuning Parameter Multiplier (Lower Portion of Q Only)	
.....	101
Figure 5-24: GPS Aided Inertial Navigation UKF - Tuning Parameter Multiplier (Q and R)	103
Figure 5-25: GPS Aided Inertial Navigation UKF - Tuning Parameter Multiplier (Q Only)	104
Figure 5-26: GPS Aided Inertial Navigation UKF - Tuning Parameter Multiplier (Lower Portion of Q Only)	
.....	105
Figure 5-27: CF - Gyro Bias Sweep (0-6deg/s).....	108
Figure 5-28: Airspeed Aided Inertial Attitude EKF - Gyro Bias Sweep (0-6deg/s).....	110
Figure 5-29: GPS Aided Inertial Navigation EKF -Gyro Bias Sweep (0-6deg/s)	111
Figure 5-30: GPS Aided Inertial Navigation UKF - Gyro Bias Sweep (0-6deg/s).....	112
Figure 5-31: Initialization Error - Complementary Filter.....	113
Figure 5-32: Initialization Error - Airspeed Aided Inertial Attitude EKF	114
Figure 5-33: Covariance - Initialization Error - Extended Kalman Filter (Method 2).....	115
Figure 5-34: Initialization Error - GPS Aided Inertial Navigation EKF	116
Figure 5-35: Covariance - Initialization Error - GPS Aided Inertial Navigation EKF	116
Figure 5-36: Initialization Error - GPS Aided Inertial Navigation UKF	117
Figure 5-37: Baseline Plot - Comparing All Estimators with Respect to Phi and Theta	121

List of Tables

Table 2-1: Relation of Coordinate Frames	21
Table 3-1: Airspeed Aided Inertial Attitude EKF Prediction Equations	42
Table 3-2: Airspeed Aided Inertial Attitude EKF Correction Equations	43
Table 3-3: GPS Aided Inertial Navigation EKF Prediction Equations.....	46
Table 3-4: GPS Aided Inertial Navigation EKF Corrections Equations.....	47
Table 3-5: GPS Aided Inertial Navigation EKF Prediction Equations - Quaternions.....	49
Table 3-6: GPS Aided Inertial Navigation EKF Correction Equations - Quaternions	50
Table 3-7: GPS Aided Inertial Navigation UKF Prediction Equations	53
Table 3-8: GPS Aided Inertial Navigation UKF Correction Equations.....	54
Table 4-1: Sensor Noise Properties.....	57
Table 5-1: Monte Carlo Results from EKF ("Method 3") - Without Noise - Theoretical Q/R.....	81
Table 5-2: Monte Carlo Results from EKF ("Method 3") - Without Noise - Theoretical Q/R – Divergent Q/R Combinations.....	82
Table 5-3: Monte Carlo Results from EKF ("Method 3") - With Noise.....	85
Table 5-4: Monte Carlo Results from EKF ("Method 3") - With Noise – Q/R Combinations with Traditional R Values.....	86
Table 5-5: Monte Carlo Results from UKF ("Method 4") - Without Noise - Theoretical Q/R	88
Table 5-6: Monte Carlo Results from UKF ("Method 4") - Without Noise - Theoretical Q/R – Divergent Q/R Combinations.....	89
Table 5-7: Monte Carlo Results from UKF ("Method 4") - With Noise	92
Table 5-8: Monte Carlo Results from UKF ("Method 4") - With Noise – Q/R Combinations with Traditional R Values	93
Table 5-9: Baseline Table - Comparing All Estimators with Respect to Phi and Theta	122
Table 6-1: Conclusions & Recommendations Summary	123

List of Acronyms

Symbol	Description
APL	Johns Hopkins Applied Physics Lab
CF	Complementary Filter
COTS	Commercial off-the-shelf
DCM	Direction Cosine Matrix
DoF	Degree of Freedom
DR	Dead Reckoning
EKF	Extended Kalman Filter
EOM	Equations of Motion
GN&C / GNC	Guidance, Navigation, and Control
GPS	Global Positioning System
IMU	Inertial Measurement Unit
INS	Inertial Navigation Systems
KF	Kalman Filter
MEMS	Micro Electro-Mechanical Sensors
NED	North, East, Down
PVA	Position, Velocity, Attitude
SUAS	Small Unmanned Aerial System(s)
UAS	Unmanned Aerial System(s)
UAV	Unmanned Aerial Vehicle(s)
UKF	Unscented Kalman Filter
w.r.t	With respect to
WWI/WWII	World War 1 and 2

List of Symbols

Symbol	Description
$a_{x y z}$	acceleration
A	State Transition Matrix (from Ax+Bu)
$A_{x y z}$	Acceleration from accelerometer
B	Control Transition Matrix (from Ax+Bu)
C	Observation Matrix
h	Observation
I	Identity matrix
K	Kalman gain
p	Body rotation about the body x axis
P	Error covariance matrix
q	Body rotation about the body y axis
$q_{\#}$	Quaternion component
\hat{q}	Quaternion vector
Q	Model/Input covariance matrix
r	Body rotation about the body z axis
R	Measurement covariance matrix
$R_{[toaxis]}^{[fromaxis]}$	Rotation matrix
u	Input (from Ax+Bu)
u	Airspeed vector component along body x axis
v	Airspeed vector component along body y axis
V_a	Airspeed
w	Airspeed vector component along body z axis
\hat{x}	State estimate
y	Mean of Observations (Ψ_k^i)
z	Measurement vector
α	Angle of Attack
α	Primary sigma point scaling factor
β	Angle of Sideslip
β	Secondary sigma point scaling factor
η	Weighting vector
θ	Pitch angle
κ	Tertiary sigma point scaling factor
λ	Compound sigma point parameter
σ	Standard deviation
τ	Time constant
ϕ	Roll angle
χ	Sigma points
ψ	Yaw angle
Ψ_k^i	Observation

1. Introduction - Attitude Estimation for Small Unmanned Applications

Navigation systems are a fundamental component of the growth in autonomous systems. Navigation systems provide a system with its position, velocity, and attitude (PVA) [1][2]. These systems continue to evolve as new problems or industry demands arise. Current industry demands include making smaller, less expensive, more accurate, and more reliable solutions for guidance, navigation, and control (GN&C) for many kinds and sizes of air/water/space craft. With these much lighter, smaller, and cheaper sensors, also came a new set of solutions to the navigation problem, particularly attitude determination. Solutions for determining attitude of spacecraft, commercial/military aircraft, missiles, submarines, and other large and/or higher cost applications have existed for decades. Capabilities and limitations of different solutions are well known throughout those industries. Size, weight, and/or cost preclude these solutions' use for small and/or inexpensive autonomous systems.

Sensors, a fundamental component of navigation systems, are inherently different between small lower-cost unmanned systems, and larger higher-cost systems. Due to this fundamental difference, some small unmanned systems attitude solutions have been developed independent of previous proven solutions. Previous proven attitude solutions for larger systems came from the Inertial Navigation Systems (INS) on board the vehicle, which contained only rate gyros and accelerometers for sensors. The concept of inertial navigation is to navigate without the need for any manmade references external to the vehicle itself. The INS sensors available to smaller low cost systems are much lower quality, therefore noisier. The smaller, low-cost solutions tend toward utilization of dissimilar additional sensors to address sensor quality/noise issues. Such dissimilar sensors include: magnetometers, infrared sensors, air data sensors, GPS, and cameras. These problems with the new, small, low cost systems require new sensor configurations and solutions. This is not to say that small unmanned systems were developed

completely independent of prior solutions; It is just to identify the fundamental differences between the problems.

Just as proven past solutions have not been adopted for these smaller low-cost systems, neither have their proven evaluation criteria. Without agreed upon performance and evaluation criteria, the best solutions to this new navigation for small unmanned systems problem cannot yet have been agreed upon. Like in the earlier days of previous navigation systems, multiple configurations have been, and are continuing to be developed. Also, like during the refinement of Inertial Navigation Systems, conflicting performance analyses and results emerged [3][4]. An interesting few lines from the "Foreward" in [4] illustrates history's repetition with the new generation of solutions to the latest navigation problem:

During this time [1971] different general configurations produced systems with very different types of performance, although with the same basic components. Accordingly, a common basis for meaningful comparison of the performance of these systems was lacking, and discussions by proponents and opponents of a given configuration generated more heat than light. This book... is the first definitive attempt that successfully provides a basis for a realistic comparison of performance of various inertial system configurations... The solution is not a simple, rule-of-thumb technique...

*-Walter Wrigley, Sc. D
Professor of Instrumentation and Astronautics
Educational Director, Charles Stark Draper Laboratory
Massachusetts Institute of Technology*

This analysis will evaluate only solutions that utilize only small low-cost sensors. It will also focus on methods of evaluation for these types of solutions, as to contribute toward a comprehensive common basis upon which to compare solutions.

1.1. Problem Statement:

The following is a list of Problem Statements addressed in this thesis.

1. Currently, there are many solutions to the problem of attitude estimation for small low-cost solutions. A good “fits all solution”, or single “industry standard” does not exist.

Evidence in [5] shows that a COTS solution does not perform as well as other algorithms-- including extremely simplified open source solutions. In order for an “industry standard” solution to exist, a robust, comprehensive, and common metric must be created in order to conclusively compare solutions.

2. There are apparently conflicting conclusions from different research groups [3].

It is hypothesized, by the author, that this is due to inconsistent testing methods, and even inconsistent solutions between the groups. Processes, algorithms, and test methods of these complex systems are not always detailed enough to enable replicable consistent baselines between researchers.

3. Researchers do not often provide insight to performance vs. complexity.

Additional complexity comes with potential unintended consequences and cost; therefore complexity should provide additional value in the form of performance. Additionally, it is valuable to know what performance "bare minimum" or simple solutions provide for the same reason it is valuable to know when you can use a tape measure vs. micrometer.

1.2. Objectives:

The following solutions toward each Problem Statement are the objectives of this thesis.

1. Solutions toward Problem Statement #1:

- a. Produce sensitivity analyses highlighting conditions that provide insight to behaviors and performance of different attitude estimation solutions.
- b. The intent is for these analyses to contribute toward a robust, comprehensive, and common metric for determining performance of attitude estimation. An agreed upon metric would enable conclusive comparisons of solutions, and identification of industry top performers.

2. Solutions toward Problem Statement #2:

- a. In order to contribute to replicability in future work, processes, algorithms, and test methods will be more detailed as to be replicable.
- b. It will be demonstrated that each solution is optimized, prior to evaluation against other solutions, in order to ensure that no sub-optimally tuned solution is compared to a more optimally tuned solution.

3. Solutions toward Problem Statement #3:

- a. Estimators with different levels of complexity will be compared to each other to provide insight to performance vs. complexity.

1.3. Literature Review

1.3.1. History of Navigation Systems

1.3.1.1. Early Navigation

Navigation, for quite some time, was defined as the determination of position and velocity with respect to some reference(s) [4]. Navigation has been, and continues to be a foundational component of many human advances. The oldest, and most basic, navigation problem humans encountered was how to get from their initial position to a desired destination within their line of sight. This problem quickly became more complex when destinations were no longer in line of sight. There are many large areas on Earth in which humans would have no line of sight references upon which to depend (i.e. deserts and oceans). Compasses were able to solve this problem up to a certain distance, depending on the skills of the human navigator. Navigation across Earth's most vast reference-less areas, though, required celestial navigation. Celestial navigation, or astronavigation, utilizes position of celestial bodies such as the sun and stars with respect to the observer to determine the observer's location on Earth.

Thus far, humanity's ability to navigate Earth was either limited (i.e. the compass/navigator), or depended on line of sight of Earth based or celestial references. Visibility, time of day/night, and time required for humans to make calculations limited navigation capability for many years. In the mid 1800s the gyro was first used as an inertial reference. Though, it was not until 1908 that the gyrocompass was invented—motivated by interference of magnetic compasses due to metal ships and the potential for submarine use in WWI. Multiple inventors came forward with the first gyrocompasses in 1908 [6], [7]. These gyrocompasses, though a fundamental step toward inertial navigation, did not provide position or velocity-- necessary components of a navigation system.

1.3.1.2. Inertial Navigation

The gyrocompass was the first inertial reference technology. In the 1910s, Sperry created the first gyroscopes that could indicate attitudes of bodies [6]. Other technologies were needed in order to navigate, though, as gyroscopes do not provide position or velocity. This was solved by radio navigation, which utilized radio signals from known locations on Earth to determine position and velocity. All of these technologies began to contribute to a system's ability to navigate autonomously, and quickly. Radio navigation, though, was limited due to radio range and had a significant disadvantage in WWII--being detectable by enemies.

Inertial navigation had significant motivation from the development of submarines and airplanes. Due to the dynamics of these vehicles, the term "navigation" began to incorporate not just position and velocity, but also attitude (PVA) [1][2]. Inertial navigation enables a vehicle to determine its PVA without use of any manmade references external to the vehicle itself—such that a vehicle can navigate without detection [8].

The first use of inertial navigation was the German V-2 missile in 1942 [7][8]. Early inertial navigation utilized gimbals and gyroscopes to directly determine attitude and accelerometers (integrated computationally) to determine velocity and position. Determining position and velocity in this manner is known as Dead Reckoning (DR). This type of configuration is known as gimbaled or stabilized. It should be noted that there are multiple classifications/configurations of gimbaled, or stabilized, INS with names both based on their physical configuration or the analytical means by which they determine PVA from their components [4][9][1]. For the purpose of this analysis, though, these will all be classified as one type of INS (gimbaled/stabilized) with the uniting characteristic that they measure attitude directly. This configuration matured to have high enough performance to be used in the Apollo's Inertial Navigation System (INS) [10] for man's first mission to the moon in 1969.

Though the gimbaled systems were well proven, the need for smaller, lighter, more reliable, and cheaper sensors drove the need for what is now known as Strapdown INS. Strapdown systems are mounted with respect to the vehicle's body. Strapdown systems do not measure attitude directly, nor do they measure acceleration with respect to the Earth (i.e. North and East) as the gimbaled systems did. Given that desired states are not directly measured, Strapdown INS required significantly more computations. Though computationally more complex, Strapdown INS were considered better overall due to their ability to decrease the size, weight, and cost while increasing reliability of INSs. Though a Strapdown INS was patented in 1956, due to the limitations of digital computers, they were not practical until the 1970s [4][1].

It is at this point in the chronology that the transition from gimbaled INS to Strapdown INS occurs and, for unrelated reasons, the INS problems of spacecraft diverge somewhat from that of aircraft. The sensors available to aircraft vs spacecraft, and the equations of motion are different enough that the INS configurations are not necessarily the same for the two applications, though they share similar components. For example, spacecraft have alternative methods to directly measure PVA such as star trackers and use of advantageous properties of their particular dynamics that are not relevant for aircraft. Because of these differences, the developments of INS for, or in relation to, spacecraft will not be reviewed any further.

Also around the time that Strapdown INS were gaining popularity in the 1970's [2], the Global Positioning System (GPS) was established. GPS was an amazing breakthrough in that it was a solution to the original navigation problem (position and velocity) without the use of more complicated to use and range limited radio navigation systems of the time. Like INS, the theory supporting GPS originated decades before, and implementation came when technology caught up. GPS has quite an interesting origin story. It was discovered somewhat accidentally in 1957 by a few employees at Johns Hopkins

Applied Physics Lab (APL). They wanted to see if they could pick up on signals Sputnik, the first manmade satellite, launched by Russia in 1957 was sending. Further intrigue allowed them to use the Doppler effect to estimate the position and velocity of the satellite. Inverting that process produces the fundamental concept of GPS [11].

Strapdown INS are typically comprised of rate gyros and accelerometers [9]. Given that Strapdown Systems measure gyro rate, each of their PVA outputs have an additional source of error—the integration of gyro drift. Gimbaled systems were susceptible to gyro drift, but their gyros measured attitude directly so the measurement errors were not increased by integrating input errors. Therefore, the success of strapdown systems is highly dependent on accurate body gyro measurements. There were multiple gyro technologies that were developed and used in different Strapdown INS configurations [9]. The Ring Laser Gyro (RLG), though, has been the most commonly used of these technologies since the 1990's [1]. Due to their standardization in INS, there is much documentation on RLG technologies [1][9]. For the purpose of this study, the most important characteristic of the RLG is its extreme accuracy for sensing gyro rates.

It's worth noting that, though INS have become extremely accurate, their DR solution for position and velocity and/or the accuracy of position or velocity of a target (i.e. runway or aircraft carrier) typically require the aid of additional sensors. This type of INS is known as aided-INS. Aided-INS utilize man made references external to the vehicle to aid navigation—typically position and velocity. Typical aiding sensors include radio, radar, and GPS.

1.3.1.3. Navigation for Small Unmanned Aerial Systems

In the 1990's the demand for unmanned systems, particularly small unmanned aerial systems (SUAS) began to emerge as supporting technologies came to maturity. The standard INS of the day, due to the

RLGs' size and cost, had limitations precluding use in SUAS applications. SUAS navigation research and development sought solutions to the size and cost problem in Micro Electro-Mechanical Sensors (MEMS). At the heart of a typical MEMS INS is an Inertial Measurement Unit (IMU) that, like its INS ancestors, consists of rate gyros and accelerometers. MEMS IMUs typically have 3 orthogonally aligned gyros and 3 orthogonal accelerometers. MEMS, though, have significantly more noise than sensors used in larger more expensive INS. Particularly, MEMS gyros have much more drift—on the order of degrees per second per second. Each output of PVA calculations is highly dependent on gyro rate, and highly affected by the integration of the drift error. Therefore MEMS based navigation has new or different problems compared to navigation systems of the past.

1.3.2. Current State of Attitude Solutions for SUAS

Solutions to the navigation problem for SUAS typically include additional sensors to supplement the noisy IMU. Typical sensors include one to three axis magnetometers, infrared sensors, air data sensors, GPS, and cameras. Unlike navigation solutions of the past, navigation for SUAS frequently utilizes non-inertial sensors to calculate, or aid in calculation of, attitude. Previously, the INS system generated attitude calculations and the INS was only aided in position and velocity calculations. This paradigm is not true for the SUAS navigation problem. This is not to say that an INS determination of attitude is not possible for small unmanned systems. IMU/magnetometer and IMU/airspeed sensor configurations have shown to provide attitude solutions complying with the definition of inertial navigation; though, these attitudes are not typically of sufficient accuracy for adequate DR of position and velocity.

Currently there are many partial and full navigation solutions for SUAS. There are four fundamental components to these new solutions, particularly for the new attitude solutions: the sensors, the mathematical formulations by which the sensors and vehicle dynamics relate, the filter, and the

computer/processor through and upon which the solution is implemented. Since these analyses are done in simulation, only the former three will be reviewed.

There are many terms used w.r.t. the small unmanned systems navigation problem and its solutions. For clarity, some of these terms will be related to the three fundamental components of interest of the new navigation solution described in the paragraph above. Specifically, "Sensor Fusion" and "State Estimation" (or "State Estimator") will be defined.

"Sensor Fusion" is a high level term that describes, generically, the combination of sensor data [12]. That is "Sensor Fusion" encompasses all of the terms described thus far as well as additional components and topics not covered in this thesis. A "State Estimator", or more generically "Estimator", combines the mathematical formulations and the filter(s) that operate on the sensors. Perhaps the simplest distinction between "estimator", "formulation", and "filter" is the example where states or solutions of interest are directly measurable by multiple sensors. In this case, "estimator" and "filter" are interchangeable, as there are no formulations by which to relate desired states to measurements. It is only in this form that filter theory can prove a filter to be an optimal estimator (see Section 2.2: Non-Linear Estimation)

1.3.2.1. Sensors

Sensors typical of SUAS attitude solutions are reviewed in this section. They are qualitatively ordered, based on the author's knowledge, from most to least successful or frequently implemented for attitude estimation. This qualitative ordering does not account for success or popularity in the estimation or measurement of position or velocity, as that is not the focus of this study. Only the following sensors are used in estimators in this analysis: IMU, GPS, and airspeed sensor.

1.3.2.1.1. Sensors Used for Estimators in this Analysis

The most common sensor used for attitude estimation, like previous INS, is the Inertial Measurement Unit (IMU). An IMU typically consists of 3 orthogonally aligned accelerometers and 3 orthogonal rate gyros. The IMU is used for most attitude estimation solutions as it provides direct measurement of body dynamics and, likely, because it is such a fundamental component of the previous proven INS attitude solutions. The IMU's main disadvantage is the gyro drift typical of the rate gyros used in the smaller IMUs.

The Global Positioning System (GPS) utilizes known position and velocity of satellites to triangulate the "unknown" position of GPS receivers on Earth. GPS's main advantage is that it directly solves the original navigation problem by directly providing position and velocity. Additionally GPS, alone, can be used to produce a rough low frequency attitude estimate that can help compensate the IMU's gyro drift [13]. GPS's main disadvantages are the availability and integrity of its calculation of position and velocity. GPS requires a strong signal to the satellite which is not always available indoors for low cost GPS, though this problem has had great improvement in recent years. The integrity problem, ironically, has only seen improvement by fusing IMU measurements with GPS measurements to provide better position and velocity estimates when the GPS signal is degraded. GPS calculation of position and velocity can be affected by buildings, trees, or the vehicle body interference between the satellite and the receiver. Additionally GPS signals are susceptible to jamming and spoofing, which has been a concern for military applications and is becoming more of a concern for civil applications.

There are multiple air data sensors typical of today's aircraft. Total and static pressure measurements are more typical for navigation solutions. Static pressure measurements provide a good low frequency measurement used for determining altitude. The combination of total and static pressure measurements provides an airspeed measurement. A Pitot-static tube and two pressure sensors, or a

single differential pressure sensor, provide the system with the airspeed measurement. The main advantages of this sensor are: provides indication of airspeed, which is a fundamental measurement for determining body forces for a fixed wing aircraft. Additionally, when in no wind this sensor provides measurement of total velocity, and can be coupled with instantaneous rotation rate of the gyros and accelerometer measurements to produce an attitude estimate via estimation of the gravity vector (see Section 3.2 Airspeed Aided Inertial Attitude Extended Kalman Filter) [14]. The main disadvantage of these sensors is that they are only valid at higher airspeeds. In the case of quad copters or vertical takeoff and landing (VTOL) SUAS, these sensors do not always provide valid measurements.

1.3.2.1.2. Other Sensors

Cameras capture images and video by recording light reflection from objects. Recent advances in artificial intelligence and machine vision have increased the versatility of the camera as a sensor. These new algorithms are enabling cameras to possibly be staged to replace multiple other sensors such as airspeed measurement devices, radio navigation arrays, and LIDAR. Applied solutions are emerging in this area at a significant rate; however, camera based solutions have one major disadvantage. That disadvantage is that since their "measurement" of anything is based on machine vision or image processing algorithms that do not have an easily quantifiable a priori error or error rate. Quite a few accidents have occurred recently in the autonomous automobile industry due to unforeseen failure modes of camera based algorithms in the autopilots.

Magnetometers have the ability to measure angles relative Earth's magnetic poles, directly. Multi-axis magnetometers have the ability to measure attitude, assuming a proper calibration of the sensors, and a general knowledge magnetic field in the vicinity of the vehicle. Given the lack of direct measurement of attitude of Strapdown systems, and the gyro drift problems of SUAS applications, a direct attitude measurement is quite appealing. The primary disadvantages to this sensor are the limited accuracy,

dependence on knowledge of the local magnetic field (a function of position and altitude), and interference due to metals and electricity in the vicinity of the vehicle. The latter of the disadvantages was what led to the pursuit of the gyrocompass many years before.

Infrared sensors utilize the reflection of heat and light off of the Earth's surface to provide a rough measurement of attitude. Their primary disadvantage is error due to inconsistent ground reflections. These inconsistencies come from different materials on Earth's surface (i.e. grass, concrete, or water). These different materials' reflection properties present a problem not many people have seen as worth pursuing. Horizon sensors were explored in the early days of SUAS for simple, rough, low-cost attitude stabilization [15].

1.3.2.2. Estimation

As stated previously, estimation requires combining the mathematical formulations and the filter(s) that operate on the sensors such that they produce estimate(s) of desired states. This requires both formulation and filtering. The following subsections will give a brief overview of formulations and filters for small unmanned systems.

1.3.2.2.1. Formulations

There are many formulations used to solve the navigation problem for small unmanned systems. Generally, researchers aim to solve for or estimate vehicle position, velocity, pitch/roll, yaw, gyro bias, or any and all combinations of these. There is a broad range of complexity and recursion between all the formulations. For example, some aim to solve for only pitch and roll using only the IMU; while others aim to solve for all states using a suite of sensors. Often, results highlight the comparison between filters, and do not discuss as much the impact of the filter inputs--the formulations. The focus on filters, without attention to filter inputs, is contributing to conflicting comparison results [3]. Regardless, the formulation is a significant part of the estimator or solution and should be carefully considered in

comparison just as much as, if not more than, the filters that provide the estimate or solution output. A good cross section of solutions utilizing IMU, GPS, and/or airspeed sensors exists within a few cited works that contain comparisons [2][5][14].

1.3.2.2.2. Filters

There are many filters for which to integrate into the estimation solution. For particular formulations, estimators can perform identically using multiple filters [16][3]. Filters typical of attitude estimation for small unmanned systems include: Complementary Filters (CF), Extended Kalman Filters (EKF), Unscented Kalman Filters (UKF), H-Infinity (H_∞), Particle Filters (PF), and Information Filters (IF). This analysis will only include solutions from the first three.

1.3.2.2.2.1. *Complementary Filter*

The complementary filter, as the name implies, involves combining two complementary inputs as to produce a filtered output. An explicit example is provided in the Complementary Filter Theory Section. Complementary filters are single input, single output (SISO), but can still be used to estimate multiple states individually [17]. Complementary filter analyses are traditionally done in the frequency domain. After the discovery and successful implementation of the EKF, CFs became less popular due to the potential advantages of the EKF. However, recently, likely motivated by simplicity for small unmanned systems, CFs are being revisited and are producing promising results [17][18][19].

1.3.2.2.2.2. *Extended Kalman Filter*

The Extended Kalman Filter gained massive popularity after its use on the Apollo program in 1960s [20]. The Kalman Filter, the EKF's predecessor, has been proven to be an optimal estimator from multiple criteria [2]. The KF, though, was limited to linear applications. The EKF is the evolution of the KF for non-

linear systems. Though the optimal estimation proofs do not hold true for the EKF, it remains a widely used filter in aerospace and other industries.

Kalman Filters are essentially a combination of measured and predicted values. These predicted values come from the propagation of the states of interest through a system model. In order for states to be propagated through a non-linear system model using a KF, the equations must be linearized. This linearization step is what differentiates the KF from the EKF.

EKFs have been implemented in many estimation solutions with success. Though, multiple problems have been reported with EKFs. Some of these problems have been solved, but were typically application (or formulation) specific solutions [2]. It is worth noting, w.r.t. attitude estimation, that the application that gained the EKF its fame included a direct measurement of the state being estimated—attitude. There are pseudo attitude calculations from accelerometers or GPS that can be used, but these are not always used by the estimators that utilize EKFs. Also, these are estimated attitudes themselves. This is all to say that the formulation supporting the estimator that gained the EKF its fame is not the same as the formulation being used with EKFs for small unmanned systems. Additionally, the EKF assumes a normal Gaussian distribution for noise. These are not guaranteed properties of MEMS sensors. Furthermore, the noise properties of an input to a filter that is not a direct measurement, are not the same as the noise properties of the sensors. That is, the sensors and their noise have been propagated through formulations prior to input to the filter. This is a fundamental architectural difference between typical attitude estimators for small unmanned systems, and the original implementation of the EKF for attitude estimation on the Apollo.

1.3.2.2.2.3. Unscented Kalman Filter

In 1997, the Unscented Kalman Filter was introduced as a new non-linear estimator. In order to predict states and covariance, the EKF approximates the non-linear system by linearizing the system model. The

UKF, instead, approximates the Gaussian distribution of the estimate and covariance, then propagates the sigma points through the nonlinear system model to predict states and covariance [21].

There are many theoretical advantages to the UKF over the EKF. Particularly, the UKF does not require linearization of the system model, which becomes worse of an approximation as the system dynamics become more nonlinear. Additionally, the UKF does not make assumptions about the sensor or process noise, as it calculates mean and covariance based on statistical distributions.

Some have reported superior results with the UKF compared to the EKF, but the opposite is also true. This is likely due to differences in the formulations that were combined with the filters for the estimators. When all else is held constant, the filters have been shown to perform similarly [3].

2. Theory

Firstly, a distinction of terminology should be made with respect to "Filter" vs. "Formulation". The different filter theories exist on their own without regard to attitude estimation. These same filter theories are also used for estimation of other parameters in fields such as engineering, medicine, and finance. "Formulation", in this text will refer to the equations of motion (EOM), assumptions, and implementation of the chosen sensor inputs for the attitude estimation problem. "Estimator", in this text, will refer to the filter/formulation fusion solution.

2.1. Coordinate Frames and Rotational Kinematics

The formulations in this document primarily use three coordinate systems: Inertial Frame, Vehicle Frame, and Body Frame. A Wind frame is used in one of the formulations (Airspeed Aided EKF); This will be discussed in Section 3.2. All coordinate frames used are right hand orthogonal frames.

Inertial (Earth) Frame:

The inertial frame is an Earth-fixed frame with an origin at the point at which the flight begins. The coordinate frame axes are such that the x-axis points North, the y-axis points East, and the z-axis points "down" toward the center of the Earth. This system is commonly referred to as NED (North, East, Down). This frame will enable measurement of the vehicle position, velocity, and acceleration w.r.t. Earth. It is possible to use this frame, without another frame whose origin is w.r.t. the center of the earth, longitude, and/or latitude because the Airlib simulation environment model (see Section 4.1) is defined in this inertial frame.

Vehicle Frame:

The vehicle frame maintains the same orientation, or axis-alignment, as the inertial frame, but its origin is at the center of gravity of the vehicle. This frame enables measurement of vehicle attitude angles w.r.t. Earth (since the vehicle frame remains aligned with the inertial frame).

Body Frame:

The body frame's origin, like the vehicle frame, is at the center of gravity of the vehicle. Though, its axes are aligned with the vehicle's body. The x-axis points from c.g. to the aircraft nose, the y-axis points from the c.g. to the right wingtip, and the z-axis points from the c.g. down (90deg from the x and y axes, as to maintain a right handed coordinate system). This frame enables measurement of accelerations and rotations from on-board the vehicle.

It should be noted that, in other analyses, researchers can align the body frame such that the x-axis points aft and the z-axis points up. The body axes relative to the accelerometer alignment is an important relationship to keep in mind. This affects the majority of transformation matrices used in attitude estimation problems.

Wind Frame:

The wind frame is oriented along the airspeed vector as it interacts with the body. For an aircraft, forces on the body (and acceleration of the body) are solely a function of the body's interaction with the air around it (i.e. aerodynamic lift). The previous statement neglects buoyancy, assuming the aircraft density is significantly denser than air.

Interactions of Frames:

The inertial, vehicle, and body frames are depicted in Figure 2-1, below. The vehicle to body relationship is shown more clearly and with more detail in Figure 2-2, below. Figures depicting this relationship have been generated by many people—some much better quality and more intuitive than others. One of the

more intuitive ones is reused for Figure 2-2. In Figure 2-2, $x|y|z$ are the vehicle frame and $x''|y''|z''$ are the body frame. The wind frame is defined only relative to the body. The wind and body frames are depicted in Figure 2-3, below. Table 2-1 and Figure 2-4 "Relation of Coordinate Frames", below, show the parameters that relate each frame to the others.

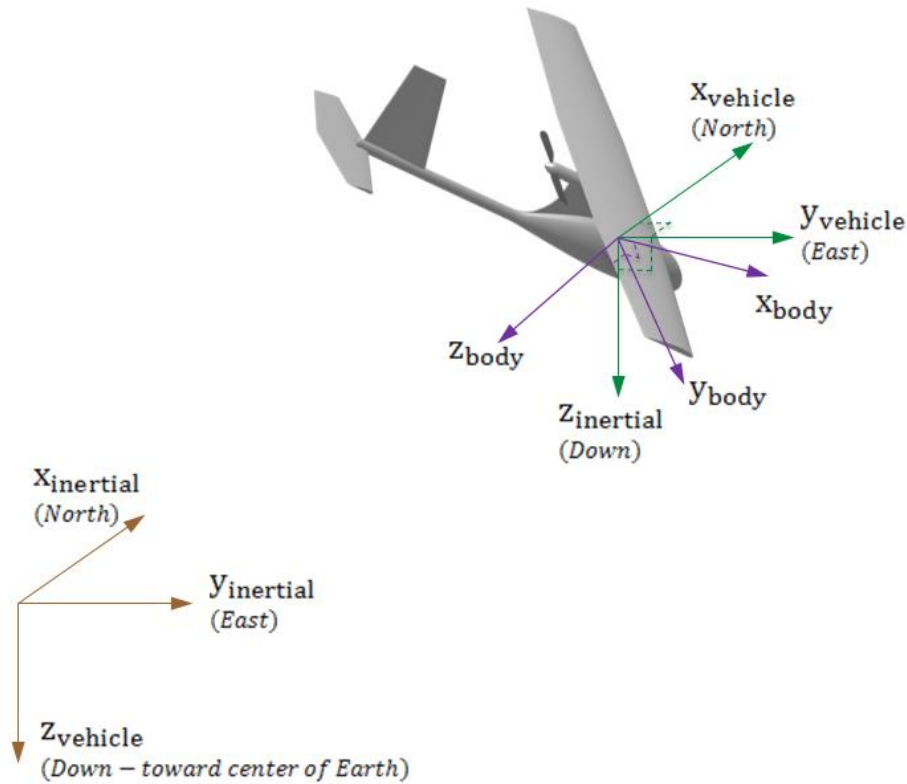
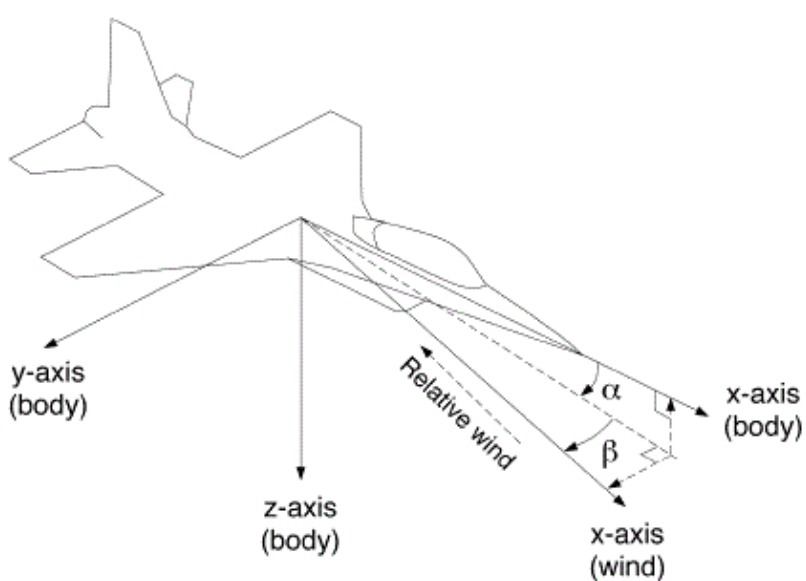
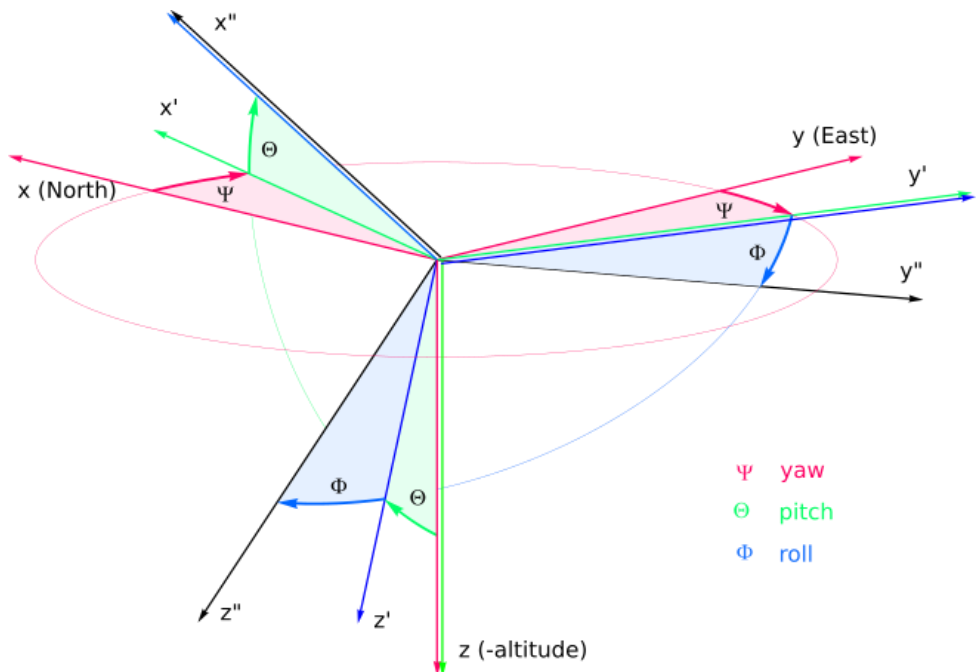


Figure 2-1: Inertial, Vehicle, and Body Frames; Source: (Modified from) [14]



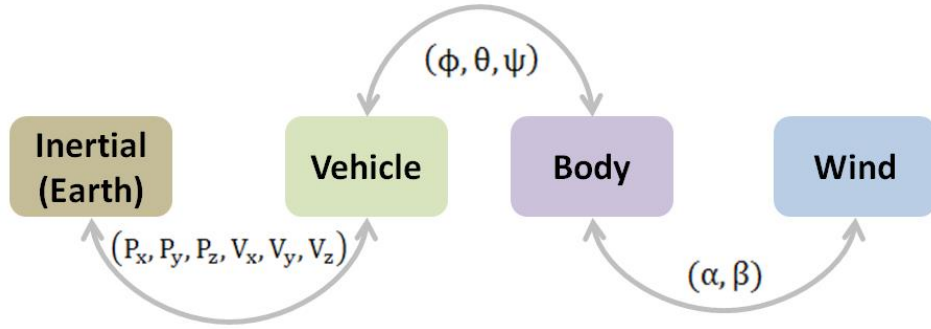


Figure 2-4: Relation of Coordinate Frames

Table 2-1: Relation of Coordinate Frames

Frame	Parameters Defined in Frame	Parameter Description
Inertial	position and velocity of vehicle	Position of vehicle relative starting point (origin of inertial frame)
Vehicle	yaw (ψ), pitch (θ), and roll (ϕ)	Orientation angles (attitude) of body frame relative vehicle frame
Body	p, q, and r	Rotation rate of body, in body frame
	ax, ay, and az	Acceleration of body, in body frame
Wind	Airspeed (V_a)	Vector along which the body moves through the air
	Angle of attack (α) and angle of sideslip (β)	Angles of V_a w.r.t. body x-y plane and y-z plane, respectively

Measurements, for the most part, are made in the body frame, as that is where the sensors and computations are made. Though, parameters such as attitude and position, which are measured in the vehicle and inertial frames respectively, are desired for inertial navigation. GPS measurements can provide inertial measurements irrespective of body and vehicle frames and parameters-- for the most part (i.e. if vehicle attitude blocks satellite line of site). Still, though, attitude measurement/estimation is an important part of an INS. Therefore, in order to fuse measurements, transformations must be possible between the coordinate frames.

Transforming between inertial and vehicle frames is a direct translation, as the coordinate systems are aligned. Translating between the vehicle/body and body/wind, though are dependent on rotations between frames. These relationships are described below.

Vehicle to Body:

As shown above in Figure 2-2, there are three independent rotations translating a vector from vehicle to body, or vice versa. These three rotations can be performed mathematically using three rotation matrices. These rotation matrices are combined to form the Direct Cosine Matrix (DCM) as shown in Equation 1, below.

$$\begin{aligned} \text{DCM} &= \begin{bmatrix} 1 & 0 & 0 \\ 0 & \cos \phi & \sin \phi \\ 0 & -\sin \phi & \cos \phi \end{bmatrix} \begin{bmatrix} \cos \theta & 0 & -\sin \theta \\ 0 & 1 & 0 \\ \sin \theta & 0 & \cos \theta \end{bmatrix} \begin{bmatrix} \cos \psi & \sin \psi & 0 \\ -\sin \psi & \cos \psi & 0 \\ 0 & 0 & 1 \end{bmatrix} \\ &= \begin{bmatrix} c(\psi)c(\theta) & s(\psi)c(\theta) & -s(\theta) \\ -s(\psi)c(\phi) + c(\psi)s(\theta)s(\phi) & c(\psi)c(\phi) + s(\psi)s(\theta)s(\phi) & c(\theta)s(\phi) \\ s(\psi)s(\phi) + c(\psi)s(\theta)c(\phi) & -c(\psi)s(\phi) + s(\psi)s(\theta)c(\phi) & c(\theta)c(\phi) \end{bmatrix} \end{aligned} \quad (1)$$

A common implementation is the one that transforms body accelerations to accelerations in the vehicle frame. Since the vehicle frame is aligned with the inertial frame, one can use the vehicle acceleration to determine inertial translation and velocity. Equations 2 and 3 show how the DCM is applied to transform the acceleration measured in the body frame into the vehicle frame and vice versa.

$$\begin{bmatrix} a_x \\ a_y \\ a_z \end{bmatrix}_{\text{body}} = \text{DCM} \begin{bmatrix} a_x \\ a_y \\ a_z \end{bmatrix}_{\text{vehicle}} \quad (2)$$

$$\begin{bmatrix} a_x \\ a_y \\ a_z \end{bmatrix}_{\text{vehicle}} = \text{DCM}^T \begin{bmatrix} a_x \\ a_y \\ a_z \end{bmatrix}_{\text{body}} \quad (3)$$

where the inverse of the DCM is equal to its transpose due to the DCM being orthogonal: $\text{DCM}^{-1} = \text{DCM}^T$.

Another vehicle to body translation of great importance for attitude estimation and INS is the translation of body rotations (p, q, r) to Euler angle rates. Attitude, in Euler angles, could then be calculated from the integration of Euler angle rates. Intuitively, one might infer that the DCM can be used for this purpose. This is not the case. The author has identified two "quick" and more intuitive, respectively, rationales as to why this is not the case. The first rationale comes from [14], who define a separate coordinate frame for each Euler rotation, stating that each Euler angle is represented in a different coordinate frame. The second rationale comes from the fact that the DCM translates vectors from one frame to another and the proof that rotations (i.e. p , q , and r) are not vectors because they are not commutative [24]. Regardless, a different set of equations is used to transform body rotations to vehicle rotations. Equation 4 (below) shows how the rotation matrices from Equation 1 (above) are used to relate body and Euler rotation rates. Equation 5 inverts the transformation matrix of Equation 4. This form transforms body rotation rates (as would be measured by a gyroscope) into Euler rotation rates, which can be easily integrated to Euler angles.

$$\begin{bmatrix} p \\ q \\ r \end{bmatrix} = \begin{bmatrix} \dot{\phi} \\ 0 \\ 0 \end{bmatrix} + \begin{bmatrix} 1 & 0 & 0 \\ 0 & \cos \phi & \sin \phi \\ 0 & -\sin \phi & \cos \phi \end{bmatrix} \begin{bmatrix} 0 \\ \dot{\theta} \\ 0 \end{bmatrix} + \begin{bmatrix} 1 & 0 & 0 \\ 0 & \cos \phi & \sin \phi \\ 0 & -\sin \phi & \cos \phi \end{bmatrix} \begin{bmatrix} \cos \theta & 0 & \sin \theta \\ 0 & 1 & 0 \\ -\sin \theta & 0 & \cos \theta \end{bmatrix} \begin{bmatrix} 0 \\ 0 \\ \dot{\psi} \end{bmatrix} \quad (4)$$

$$= \begin{bmatrix} 1 & 0 & -\sin \theta \\ 0 & \cos \phi & \sin \phi \cos \theta \\ 0 & -\sin \phi & \cos \phi \cos \theta \end{bmatrix} \begin{bmatrix} \dot{\phi} \\ \dot{\theta} \\ \dot{\psi} \end{bmatrix}$$

$$\begin{bmatrix} \dot{\phi} \\ \dot{\theta} \\ \dot{\psi} \end{bmatrix} = \begin{bmatrix} 1 & \sin \phi \tan \theta & \cos \phi \tan \theta \\ 0 & \cos \phi & -\sin \phi \\ 0 & \sin \phi \sec \theta & \cos \phi \sec \theta \end{bmatrix} \begin{bmatrix} p \\ q \\ r \end{bmatrix} \quad (5)$$

Wind to Body:

Similar to body/vehicle transformations, wind/body transformations can be made using rotation matrices. Equation 6, below, shows the individual rotation matrices for α and β , as well as the final rotation matrix for transforming wind to body. A typical implementation of the wind to body transformation is airspeed translated into body x, y, and z coordinates. These individual body components of airspeed are typically expressed as u , v , and w , respectively. This transformation is shown below in Equation (7).

$$\begin{aligned} R_w^b &= \begin{bmatrix} \cos \alpha & 0 & -\sin \alpha \\ 0 & 1 & 0 \\ \sin \alpha & 0 & \cos \alpha \end{bmatrix} \begin{bmatrix} \cos \beta & -\sin \beta & 0 \\ \sin \beta & \cos \beta & 0 \\ 0 & 0 & 1 \end{bmatrix} \\ &= \begin{bmatrix} \cos \alpha \cos \beta & -\cos \alpha \sin \beta & -\sin \alpha \\ \sin \beta & \cos \beta & 0 \\ \sin \alpha \cos \beta & \sin \alpha \sin \beta & \cos \alpha \end{bmatrix} \end{aligned} \quad (6)$$

$$\begin{aligned} \begin{bmatrix} u \\ v \\ w \end{bmatrix} &= \begin{bmatrix} \cos \alpha \cos \beta & -\cos \alpha \sin \beta & -\sin \alpha \\ \sin \beta & \cos \beta & 0 \\ \sin \alpha \cos \beta & \sin \alpha \sin \beta & \cos \alpha \end{bmatrix} \begin{bmatrix} V_a \\ 0 \\ 0 \end{bmatrix} \\ &= V_a \begin{bmatrix} \cos \alpha \cos \beta \\ \sin \beta \\ \sin \alpha \cos \beta \end{bmatrix} \end{aligned} \quad (7)$$

where airspeed is represented as $\begin{bmatrix} V_a \\ 0 \\ 0 \end{bmatrix}$, because airspeed is defined as the airflow along the wind axis.

2.1.1. Quaternion Rotations

Euler angles are typically used to represent attitude, as they are intuitive and relatively easy to represent visually. Euler angles, though, have a singularity condition when the x-y and y-z planes align (when pitch is 90 degrees). At this point, the system loses observability of one degree of freedom (yaw). For example, if an aircraft is pitched 90 degrees, then rotates 90 degrees about its x-axis, then pitches back down to 0 degrees pitch, the airplane will have rotated 90 degrees in yaw. Following such a

condition mentally makes sense, but cannot be achieved by Euler angle transformations. Referring back to Equation 5, above, the $\sec \theta$ terms are undefined at $\theta = 90$, driving $\dot{\psi}$ undefined.

The concept of gimbal lock is another good way of visualizing the loss of observability of an axis.

Recalling the concept of how gimbaled INS determine attitude, from Section 1.3.1.2 "Inertial Navigation", a stabilized platform would remain stationary within the gimbal with the gimbal mounted to an aircraft. When the aircraft attitude changed, the rings of the gimbal would move about the stabilized platform (right image of Figure 2-5, below). When the rings line up, they form a plane (left image of Figure 2-5, below). Any rotation in that plane is not observable by the gimbal.

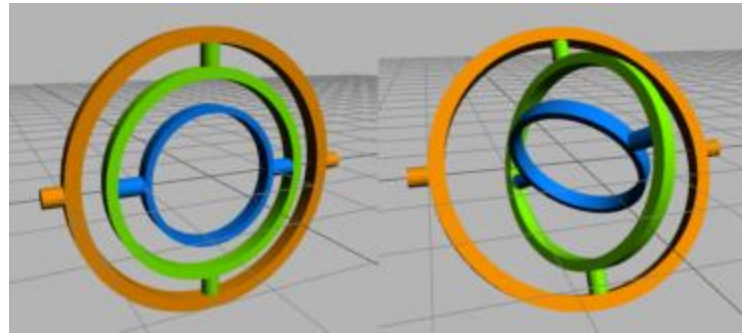


Figure 2-5: Gimbal Lock Example; Source:[25]

A four axis gimbal can overcome gimbal lock as long as the outermost ring's rotation axis is constantly driven 90 degrees from the inner most ring [9]. Figure 2-6, below, shows a 4 axis gimbal in gimbal lock because the 4th axis is not driven 90 degrees from the innermost ring. Though this does not directly translate to quaternion kinematics, it is a visual example of how the addition a 4th degree of freedom resolves the problem that a 3 axis gimbal has observing 3 degrees of freedom at all angles. Quaternions utilize a 4th degree of freedom to represent the 3 degrees of freedom of attitude.



Figure 2-6: 4 Axis Gimbal; Source: [26]

A quaternion rotation, most simply, is a single rotation (ε) about a vector ($\vec{\eta}$). If the vector, ($\vec{\eta}$) is not parallel to any of the body/vehicle axes, this single rotation, (ε), can rotate the body/vehicle about multiple body/vehicle axes. A quaternion, in its most general form, is as shown in Equation 8, below.

$$\hat{q} = \begin{bmatrix} q_0 \\ q_1 \\ q_2 \\ q_3 \end{bmatrix} = \begin{bmatrix} \cos(\varepsilon/2) \\ \sin(\varepsilon/2) \cdot \eta_1 \\ \sin(\varepsilon/2) \cdot \eta_2 \\ \sin(\varepsilon/2) \cdot \eta_3 \end{bmatrix} \quad (8)$$

where:

$$\vec{\eta} = \begin{bmatrix} \eta_1 \\ \eta_2 \\ \eta_3 \end{bmatrix} \quad (9)$$

$$\|\hat{q}\| = q_0^2 + q_1^2 + q_2^2 + q_3^2 = 1 \quad (10)$$

Due to the fact that $\|\hat{q}\|$ is a unit scalar, this property allows quaternion rotations to be normalized. This normalization can be used to remove calculation error—a known source of drift for INS. Quaternions can be converted to Euler angles using Equation 11, below.

$$\begin{aligned}\phi &= \tan^{-1} \left(\frac{2(q_0q_1 + q_2q_3)}{q_0^2 + q_3^2 - q_1^2 - q_2^2} \right) \\ \theta &= \sin^{-1}(2(q_0q_2 - q_1q_3)) \\ \psi &= \tan^{-1} \left(\frac{2(q_0q_3 + q_1q_2)}{q_0^2 + q_1^2 - q_2^2 - q_3^2} \right)\end{aligned}\tag{11}$$

Equation 3 and 5, in quaternion form, are represented in Equations 12 and 13, respectively below.

$$\begin{bmatrix} a_x \\ a_y \\ a_z \end{bmatrix}_{\text{vehicle}} = \begin{bmatrix} q_1^2 + q_0^2 - q_2^2 - q_3^2 & 2(q_1q_2 - q_3q_0) & 2(q_1q_3 - q_2q_0) \\ 2(q_1q_2 + q_3q_0) & q_2^2 + q_0^2 - q_1^2 - q_3^2 & 2(q_2q_3 - q_1q_0) \\ 2(q_1q_3 + q_2q_0) & 2(q_2q_3 + q_1q_0) & q_3^2 + q_0^2 - q_1^2 - q_2^2 \end{bmatrix} \begin{bmatrix} a_x \\ a_y \\ a_z \end{bmatrix}_{\text{body}}\tag{12}$$

$$\begin{bmatrix} \dot{q}_0 \\ \dot{q}_1 \\ \dot{q}_2 \\ \dot{q}_3 \end{bmatrix} = \frac{1}{2} \begin{bmatrix} 0 & -p & -q & -r \\ p & 0 & r & -q \\ q & -r & 0 & p \\ r & q & -p & 0 \end{bmatrix} \begin{bmatrix} q_0 \\ q_1 \\ q_2 \\ q_3 \end{bmatrix}\tag{13}$$

2.2. Non-Linear Estimation Filters

This section will describe each type of filter used in an estimator in the analyses to follow. This section will intentionally not dive into the fundamental relationships between the filters, as it is not directly applicable to these analyses. However, this information is likely a helpful source of intuition for the estimator designer. This type of fundamental comparison and understanding was of much interest prior to the final choice of attitude estimation for the Apollo mission. Higgins and Brown [16][27] provide thorough references.

2.2.1. Complementary Filter

A standard simple complementary filter is shown in Figure 2-7, where "τ" (Tau) is the time constant of the filter. In this figure, two direct measurements of signal "a" are combined to form an estimation of "a". If one measurement has high frequency noise, and the other has low frequency noise, they can be filtered using a low pass filter and high pass filter, respectively. The ideal complementary filter is such

that its two components complement each other. Stated otherwise, the two frequency domain filter equations add up to 1. The CF, as shown below, tracks the higher frequencies more as Tau increases and the lower frequencies more as Tau decreases.

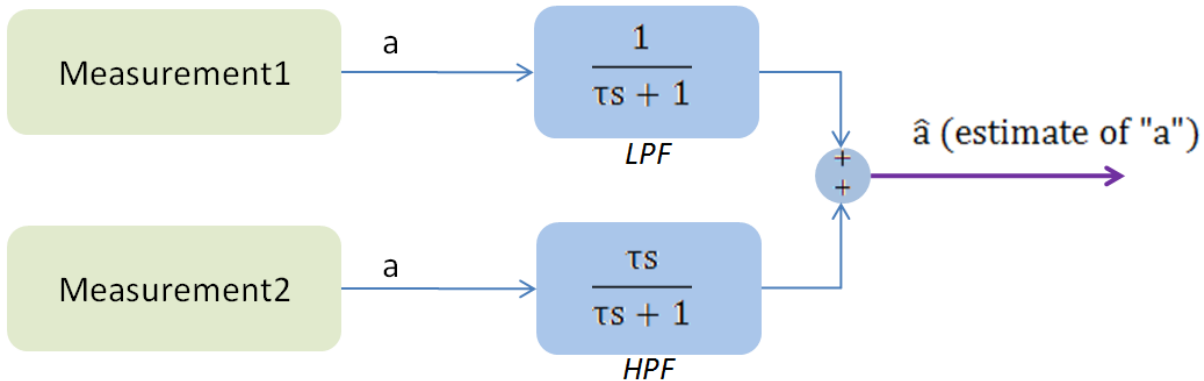


Figure 2-7: Standard Simple Complementary Filter

A typical application of a complementary filter is shown in Figure 2-8, below. This figure shows two measurements; one a direct measurement of state "a", and the other a measurement of the rate of change of "a". A typical application would be where "a" is vertical speed, as measured by a static port on an aircraft and "a_dot" is the acceleration as measured by an accelerometer. The static port is accurate over a long period of time, but cannot detect rapid changes. The accelerometer is able to detect rapid changes (high frequency), but will be subject to random walk over time, as its signal must be integrated in order to compute a velocity. This typical application applies a low pass filter to the static pressure vertical speed measurement, since it is accurate over a long period of time (low frequency), and a high pass filter to the accelerometer to filter out the low frequency random walk.

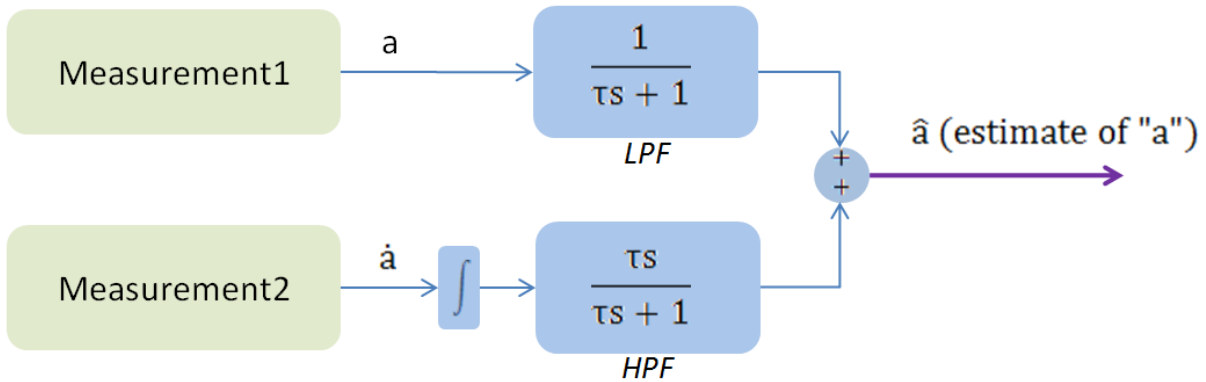


Figure 2-8: Complementary Filter Typical Application

Note that in Figure 2-8 the high pass filter is applied after the integrator. That is to say that the filter is not applied directly to the measurement. There are implementations, especially in the open source community, that apply filters directly to the measurement as to "[filter the noise of the sensor]". This kind of implementation may work after tuning, but does not preserve the observability of all frequencies. Careful consideration would be needed if implementing a filter this way with the intent of creating a complementary filter.

2.2.2. Extended Kalman Filter

The Extended Kalman Filter theory presented in this text, unlike traditionally presented, will start at the filter output equation and work backward. Typical presentations of this theory start with linear systems and probability theory, then introduce the Kalman Filter. The author's intent is to start with the application as it is likely the most familiar subject to a reader.

The EKF estimate (output of interest of EKF: \hat{x}^+), that is to be compared to truth, is calculated as shown in Equation 14, below.

$$\hat{x}^+ = \hat{x}^- + K(z - h(\hat{x}^-, u)) \quad (14)$$

Where z and u are measurements

Equation 14 described in pseudo equation form is:

$$\text{current estimate} = \text{previous estimate} + \frac{\text{gain} * (\text{error})}{\text{correction}}$$

$$\text{current estimate} = \text{previous estimate} + \text{gain} * \frac{(\text{measurement1} - h(\hat{x}^-, \text{measurement2}))}{\text{error}}$$

The pseudo equation explains that the EKF estimate being sought can be most simply thought of as the previous estimate plus some correction. The correction is an error multiplied by a gain. The error is the difference between a direct measurement (measurement 1) of states (z) and a calculation of those same states (h). "h" is a function of the estimate (\hat{x}^-) and measurement2 (u).

Now that the essence of the EKF output is explained, the full EKF algorithm will be presented in Figure 2-9, where equation "4)" (within the figure) is the equation just described above.

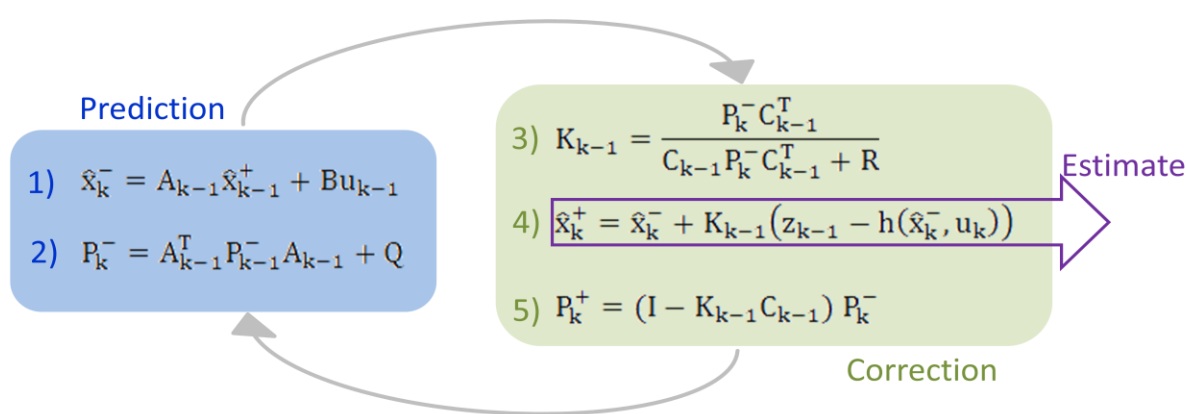


Figure 2-9: EKF Equations

Thus far \hat{x}^+ , \hat{x}^- , z , y , and K have been introduced from the EKF input/output perspective of, generally, what they are how they create an estimate. Now, how to calculate each of these variables

must be explained. Equation "1)" (within Figure 2-9) is the standard equation for a linear system expressed in discrete form. Systems, though, are often non-linear, and the EKF was designed for use with non linear systems; therefore for non-linear systems:

$$\dot{x} = f(x, u) \rightarrow \underbrace{Ax + Bu}_{\text{linearized}} \quad (15)$$

$$y = h(x, u) \rightarrow \underbrace{Cx + Du}_{\text{linearized}} \quad (16)$$

where:

$$A = \frac{\partial f}{\partial x} \quad (17)$$

$$C = \frac{\partial h}{\partial x} \quad (18)$$

It should be noted that "h" in Equation "4)" (within Figure 2-9 above) can be calculated directly or calculated as:

$$h = Cx \quad (19)$$

Q and R are the process and measurement noises, respectively. R is traditionally chosen to be an identity matrix multiplied by the covariance of the sensor noise. Q requires tuning. Many different methods and approaches exist for choosing Q depending on the application.

Both P and \hat{x} are calculated using the above defined variables. They do, though, require initial values for the first timestep of the algorithm. If the initial states to be estimated (\hat{x}_0) are well known, P_0 can be an n by n zero matrix.

2.2.3. Unscented Kalman Filter

The Unscented Kalman Filter equations are known for being less intuitive than those of the EKF, especially from a perspective of direct application to attitude estimation. Equating the UKF equations to that of the more intuitive EKF equations, the UKF equations are presented in a comparable pictorial below in Figure 2-10.

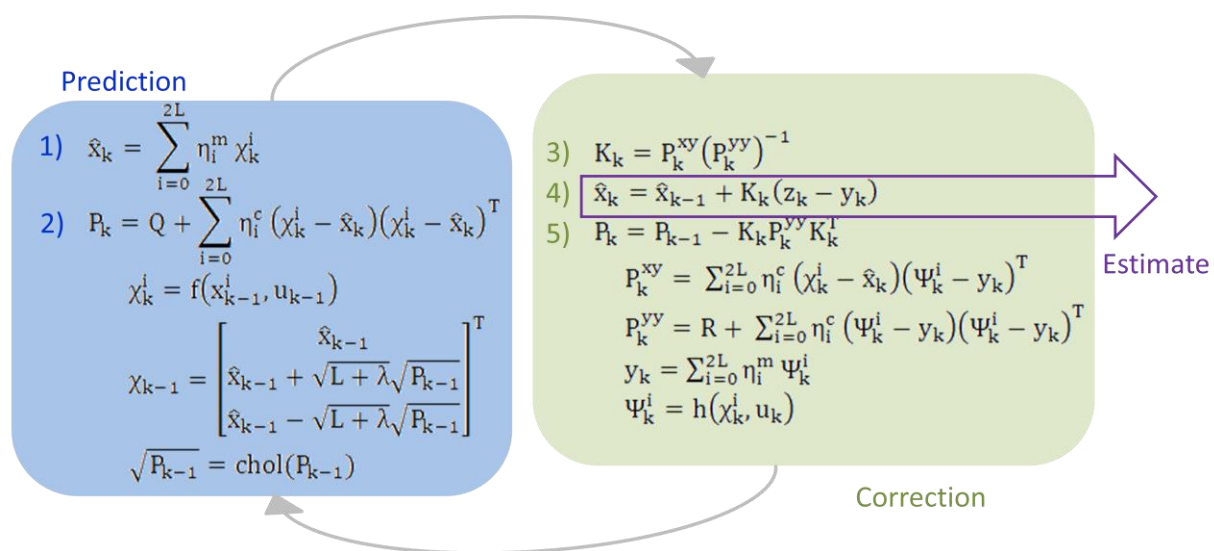


Figure 2-10: UKF Equations

where:

$$\eta_i^m = \eta_i^c = \frac{1}{[2(L + \lambda)]} \quad (20)$$

$$\eta_0^m = \frac{\lambda}{L + \lambda} \quad (21)$$

$$\eta_0^c = \frac{\lambda}{L + \lambda} + 1 - \alpha^2 + \beta \quad (22)$$

$$\lambda = \alpha^2(L + \kappa)^2 \quad (23)$$

“L” is the number of states in the estimate (i.e. length of \hat{x}). α , β , and κ are tuning parameters. Per [28], the values of these parameters are:

$$0.001 < \alpha < 1 \quad \beta = 2 \text{ is optimal for Gaussian noise} \quad \kappa = 0 \text{ for most applications}$$

Like for the EKF, Q and R are the process and measurement noises, respectively. They are traditionally chosen in the same manner as for the EKF.

3. Attitude Estimation Formulations

The following subsections will provide descriptions of implementations. Each Filter/Formulation will be presented as explicitly as possible. This is done to help achieve reproducibility of the experiments herein.

3.1. Complementary Filter ("Method 1")

The Complementary Filter Solution is fundamentally a combination of two different estimates of Euler angles from the IMU only. The most fundamental CF application would be one in which two direct measurements of a desired parameter are combined. However, aside from spacecraft or indoor limited systems, typically systems do not have a direct measurement of Euler angles; Therefore, estimates must be used in place of direct measurements.

The complementary solution implementation is most simply depicted in block diagram form, as shown in Figure 3-1. The first estimate of Euler angles comes from the integration of the gyro rotation rates (top path in figure). The second estimate comes from the trigonometric angles between a pseudo gravity vector and the aircraft body z-axis (bottom path in figure). The integration of the gyro rates is prone to random walk as well as drift (low frequency noise). The pseudo gravity vector based estimate only provides an estimate of Euler angles in unaccelerated flight. In accelerated flight, the pseudo gravity vector that is computed will also contain the body's acceleration. It is well understood that a fixed wing aircraft is often in accelerated flight. Though, if it is assumed that the body tends to return to unaccelerated flight or does not maintain long steady accelerated flight, the body accelerations would be mostly higher frequency (i.e. quick longitudinal adjustment that spikes body acceleration momentarily followed by constant velocity altitude change).

The complementary filter blends these two estimates by attenuating the frequencies that contain the error component, or only observing the frequencies in which the estimate is accurate. For the

integration of the gyros estimate input, the complementary filter will contain a high pass filter as to attenuate the low frequency random walk and drift. For the pseudo gravity vector based estimate input, the complementary filter will contain a low pass filter as to only allow the lower frequencies into the complementary filtered solution estimate.

While this solution contains assumptions that cannot be 100% guaranteed, it is a simple solution that was often used in the early development of open source autopilots, and did not perform as poorly as one might imagine. This solution is being included in this analysis as a simple and solid baseline by which to compare more advanced and complicated solutions.

There are a few particularities about this implementation to note. The first is that yaw angle is not part of this formulation, as only pitch and roll can be solved for using the pseudo gravity vector based method. It would be possible to estimate yaw using other means, including just integration of the gyros. Since there is no second estimate for yaw, and yaw is not required to be fed back to estimate pitch or roll, the signals of interest, yaw was not estimated. The second, and probably most important note for reproducibility, is that the sign convention of the inputs to the trigonometric solution for the angles between the body z axis and gravity vector are dependent upon accelerometer orientation with respect to the aircraft body. The final note about this implementation is that the High and Low-Pass Filters are such that their complement is 1, as described in the Complementary Filter Theory (Section 2.2.1), above. It is possible to choose Tau such that this filter performs as a band stop, but one would have to be sure that no actual body rotation existed at that frequency. This would require a high fidelity model of the aircraft dynamics.

Also, an important consideration for this formulation, and sensor fusion in general, is what is fed into the filter/fusion. In this implementation, both the low and high pass filters are fed with estimates of the Euler angles. The author has seen implementations, in code repositories for open source autopilots as

well as in published papers that directly filter the sensor input. While this is an acceptable means by which to filter sensor noise, it does not guarantee that there are not band-stop filter-like frequency attenuation(s) in the Euler solution. In this configuration, one would have to be sure that the filters applied directly to the sensors only filter sensor noise, and do not filter out frequencies from both estimates that contain actual airplane dynamics.

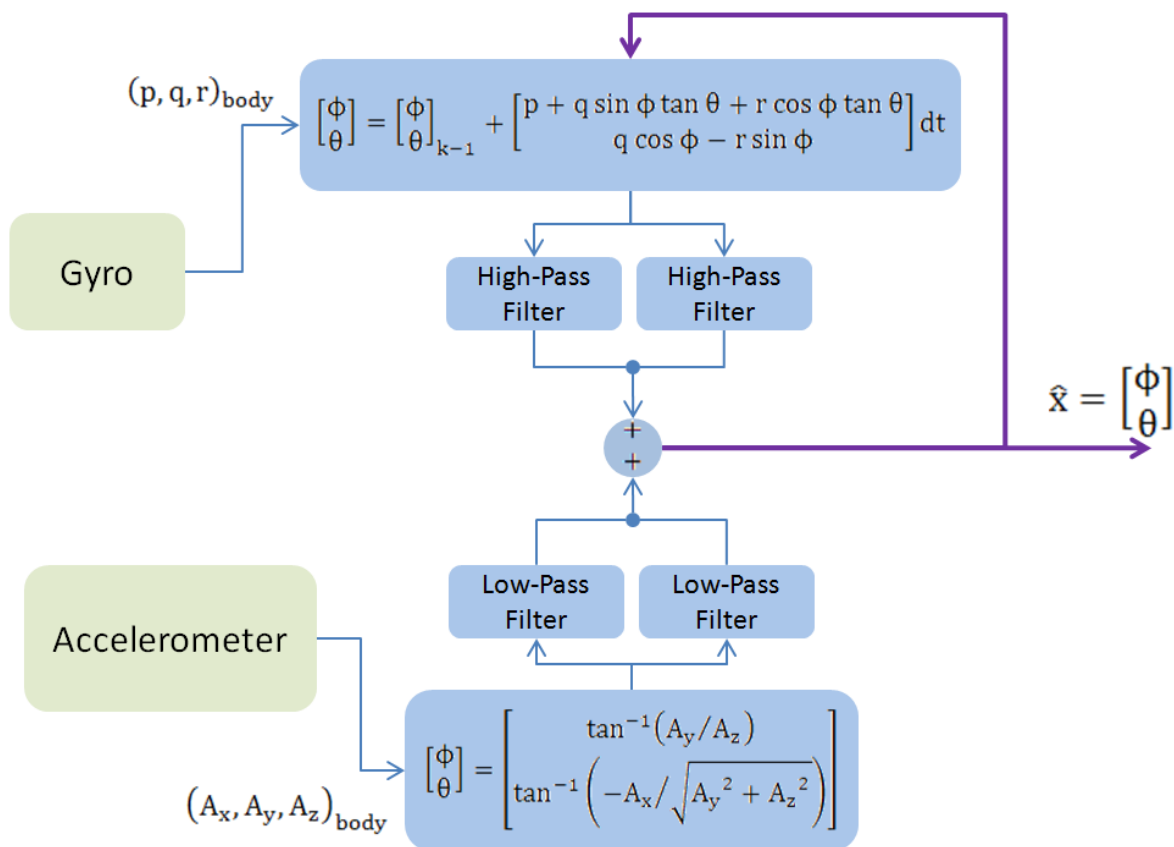


Figure 3-1: Complementary Filter/Formulation for Attitude Estimation

3.2. Airspeed Aided Inertial Attitude Extended Kalman Filter ("Method 2")

The following EKF formulation was created from "Algorithm 2" in [14]. This estimator utilizes the formulation of a strapdown INS corrected by a derived measurement of body acceleration aided by airspeed. To be as explicit as possible, the equations that are actually represented in the code that implements the EKF will be in bold font. A block diagram and a condensed form of the equations below will be presented at the end of this subsection.

To begin, the system equations $\dot{x} = f(x, u) \rightarrow \underbrace{Ax + Bu}_{\text{linearized}}$ and $y = h(x, u) \rightarrow \underbrace{Cx + Du}_{\text{linearized}}$ must be identified.

The following non-linear equations relating roll and pitch to body rates will represent $\dot{x} = f(x, u)$:

$$\begin{aligned}\dot{\phi} &= p + q \sin \phi \tan \theta + r \cos \phi \tan \theta \\ \dot{\theta} &= q \cos \phi - r \sin \phi\end{aligned}\tag{24}$$

In discrete form:

$$\begin{aligned}\phi_k &= \phi_{k-1} + (p + q \sin \phi \tan \theta + r \cos \phi \tan \theta)_{k-1} dt \\ \theta_k &= \theta_{k-1} + (q \cos \phi - r \sin \phi)_{k-1} dt\end{aligned}\tag{25}$$

The above equations are used to formulate "f" and "A" for the EKF in Equations 26 and 27 below:

$$f(\mathbf{x}, \mathbf{u}) = \begin{bmatrix} \dot{\phi} + (p + q \sin \phi \tan \theta + r \cos \phi \tan \theta)dt \\ \dot{\theta} + (q \cos \phi - r \sin \phi)dt \end{bmatrix}\tag{26}$$

$$A = \frac{\partial f}{\partial x} = \begin{bmatrix} 1 + (q \cos \phi \tan \theta - r \sin \phi \tan \theta)dt & \left(\frac{q \sin \phi + r \cos \phi}{\cos^2 \theta} \right) dt \\ (-q \sin \phi - r \cos \phi)dt & 1 \end{bmatrix}\tag{27}$$

The following non-linear equations relating body rates to body accelerations will represent $y = h(x, u)$:

$$A_x = \dot{u} + qw - rv + g \sin \theta \quad (28)$$

$$A_y = \dot{v} + ru - pw - g \cos \theta \sin \phi \quad (29)$$

$$A_z = \dot{w} + pv - qu - g \cos \theta \cos \phi \quad (30)$$

*note that $A_{x,y,z}$ are not at all related to the A matrix: $A = \frac{\partial f}{\partial x}$

Assuming,

$$\begin{bmatrix} u \\ v \\ w \end{bmatrix} \approx V_a \begin{bmatrix} \cos \alpha \cos \beta \\ \sin \beta \\ \sin \alpha \cos \beta \end{bmatrix}, \alpha \approx \theta, \text{ and } \beta \approx 0$$

These equations are used to create Equations 31 and 32, below, for use in the EKF (for creating h and C):

$$h(x, u) = \begin{bmatrix} qV_a \sin \theta + g \sin \theta \\ rV_a \cos \theta - pV_a \sin \theta - g \cos \theta \sin \phi \\ -qV_a \cos \theta - g \cos \theta \cos \phi \end{bmatrix} \quad (31)$$

$$C = \frac{\partial h}{\partial x} = \begin{bmatrix} 0 & qV_a \cos \theta + g \cos \theta \\ -g \cos \theta \cos \phi & -rV_a \sin \theta - pV_a \cos \theta + g \sin \theta \sin \phi \\ g \cos \theta \sin \phi & (qV_a + g \cos \phi) \sin \theta \end{bmatrix} \quad (32)$$

$h(x, u)$ will be compared to z . The error between h and z will be multiplied by the Kalman gain and added to the previous estimate as explained in Equation 14 in Section 2.2.2., where z is the vector of the body acceleration measurements from the accelerometer:

$$z = \begin{bmatrix} A_x \\ A_y \\ A_z \end{bmatrix}_{\text{accelerometer}} \quad (33)$$

Alternative Formulations:

A few implementation choices for this formulation are available at this point. Those choices are alternative formulations and/or inputs for the h matrix. First, V_a , an input to the h matrix, could be calculated using the integration of the accelerations as shown in Equation 34. Second, the h matrix could be calculated using Equation 35. Calculating the h matrix as shown below adds two instances of additional recursion in this estimator, though. That is, "C" has more instances of the estimated states in it than the "h" that is calculated directly in Equation 31, and the state estimates (\hat{x}_k^+) are a parameter in this equation. Neither of these choices were used in the following analyses, but this alternative implementation should be a known source of potential differences when comparing results from multiple sources.

$$V_a = \sqrt{V_{ax}^2 + V_{ay}^2 + V_{az}^2} \quad \text{where: } V_{ax} = \int A_x \quad (34)$$

$$h(x, u) = \frac{\partial h}{\partial x} x = Cx \quad (35)$$

The tuning parameters for this formulation are in the form shown, below. "qk_c" and "rk_c" are constants. Their value will be varied in proceeding sections as to show how these parameters affect the estimator performance.

$$Q = \begin{bmatrix} 1 & 0 \\ 0 & 1 \end{bmatrix} * qk_c \quad (36)$$

$$R = \begin{bmatrix} 1 & 0 & 0 \\ 0 & 1 & 0 \\ 0 & 0 & 1 \end{bmatrix} * rk_c \quad (37)$$

A block diagram that depicts the pseudo code implementation of this estimator is shown in Figure 3-2: Airspeed Aided Inertial Attitude EKF. This block diagram is intended to demonstrate how each of the equations used in this formulation interact. Each equation, as it relates to the EKF, is detailed in Table 3-1 and Table 3-2, below. This table is replicated from [13], updated to utilize the notation of this document.

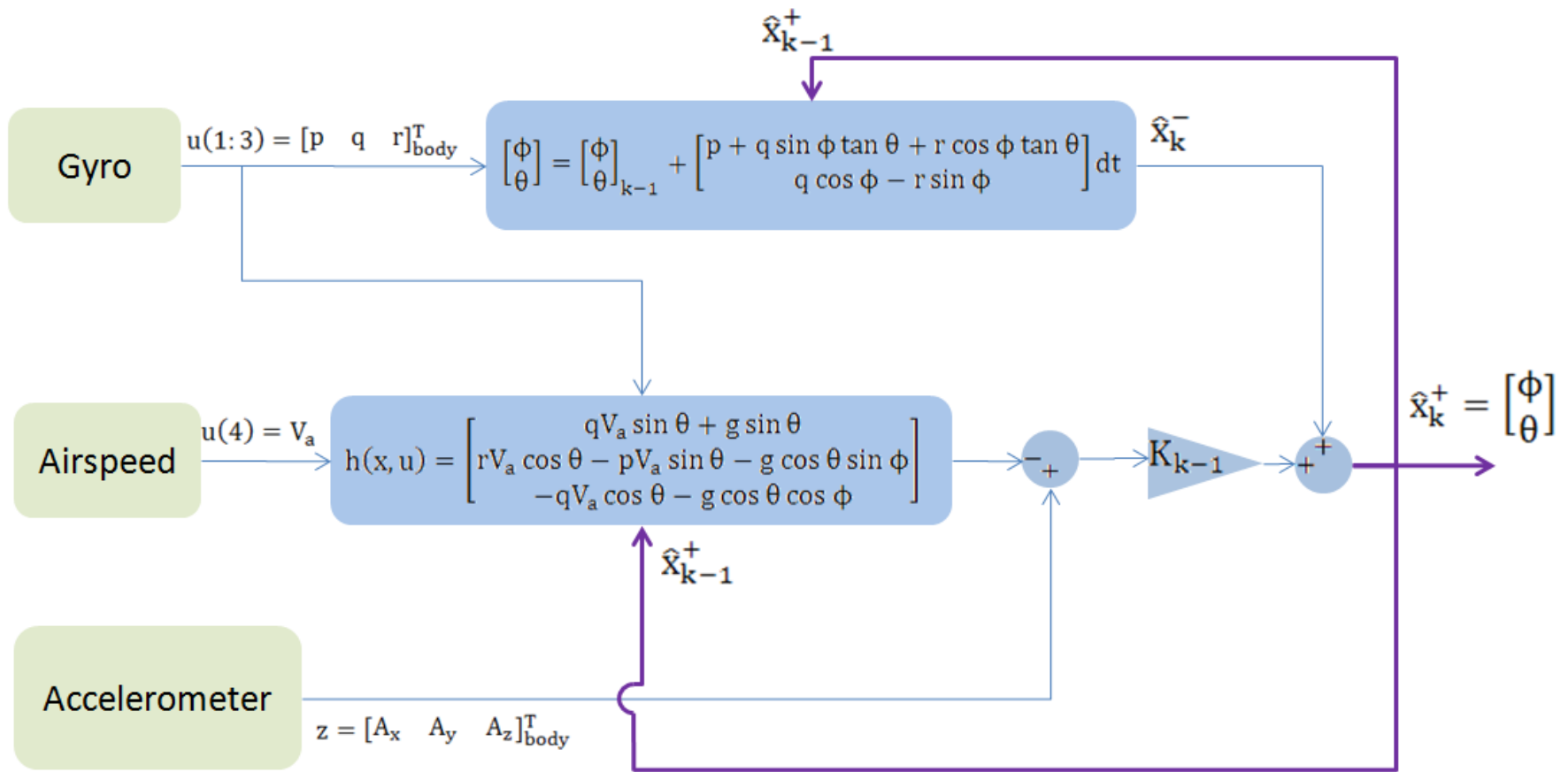


Figure 3-2: Airspeed Aided Inertial Attitude EKF

Table 3-1: Airspeed Aided Inertial Attitude EKF Prediction Equations

1) Project State:				
Equation	Nomenclature	Symbol	Matrix Size	Values
2) Project Error Covariance: $P_k^- = A_{k-1}^T P_{k-1}^- A_{k-1} + Q$	Error Covariance	P_k^- , P_{k-1}^-	2x2	$\begin{bmatrix} \# & \# \\ \# & \# \end{bmatrix}$
	State Transition Matrix	A_{k-1}	2x2	$\begin{bmatrix} 1 + (q \cos \phi \tan \theta - r \sin \phi \tan \theta)dt & \left(\frac{q \sin \phi + r \cos \phi}{\cos^2 \theta} \right) dt \\ (-q \sin \phi - r \cos \phi)dt & 1 \end{bmatrix}$
	Model/Input Covariance	Q	2x2	$\begin{bmatrix} qk_c & 0 \\ 0 & qk_c \end{bmatrix}$

Table 3-2: Airspeed Aided Inertial Attitude EKF Correction Equations

Equation	Nomenclature	Symbol	Matrix Size	Values
3) Compute the Kalman Gain: $K_{k-1} = \frac{P_k^- C_{k-1}^T}{C_{k-1} P_k^- C_{k-1}^T + R}$	Observation Matrix	C_{k-1}	3x2	$\begin{bmatrix} 0 & qV_a \cos \theta + g \cos \theta \\ -g \cos \theta \cos \phi & -rV_a \sin \theta - pV_a \cos \theta + g \sin \theta \sin \phi \\ g \cos \theta \sin \phi & (qV_a + g \cos \phi) \sin \theta \end{bmatrix}$
	Measurement Covariance Matrix	R	3x3	$\begin{bmatrix} rk_c & 0 & 0 \\ 0 & rk_c & 0 \\ 0 & 0 & rk_c \end{bmatrix}$
	Kalman Gain	K_{k-1}	2x3	$[\#_{2x3}]$
4) Update Estimate with Measurement: $\hat{x}_k^+ = \hat{x}_k^- + K_{k-1}(z_{k-1} - h(\hat{x}_k^-, u_k))$ Where: $h(\hat{x}_k^-, u_k) \neq C\hat{x}_k^-$	System States	\hat{x}_k^+, \hat{x}_k^-	2x1	$\begin{bmatrix} \phi \\ \theta \end{bmatrix}$
	Accelerometer Measurements	z_{k-1}	3x1	$\begin{bmatrix} A_x \\ A_y \\ A_z \end{bmatrix}_{\text{Body}}$
	Observation	$h(\hat{x}_k^-, u_k)$	3x1	$\begin{bmatrix} qV_a \sin \theta + g \sin \theta \\ rV_a \cos \theta - pV_a \sin \theta - g \cos \theta \sin \phi \\ -qV_a \cos \theta - g \cos \theta \cos \phi \end{bmatrix}$
5) Update the Error Covariance: $P_k^+ = (I - K_{k-1} C_{k-1}) P_k^-$	Identity Matrix	I	2x2	$\begin{bmatrix} 1 & 0 \\ 0 & 1 \end{bmatrix}$

3.3. GPS Aided Inertial Navigation Extended Kalman Filter ("Method 3")

The following EKF formulation for attitude estimation is based on that of the "Method 3" formulation in [13]. This estimator utilizes the formulation of a strapdown INS corrected by GPS measured position and velocity. This estimator will be referred to as "Method 3 EKF" within the text. A block diagram that depicts the pseudo code implementation of this estimator is shown below in Figure 3-3. This block diagram is intended to demonstrate how each of the equations used in this formulation interact. Each equation, as it relates to the EKF, is detailed in Table 3-3 and Table 3-4, below. This table is replicated from [13], updated to utilize the notation of this document. It should be noted that the equations depicted use Euler angles, though the actual implementation used in these analyses utilize quaternions. This depiction choice was made as to make the figure and table as intuitive as possible. The Euler angle equations are much more intuitive and are better known. Additionally, the Euler and Quaternion equations are "plug-n-play" interchangeable in the formulation. The quaternion equations used will be presented, as well, in the following subsection.

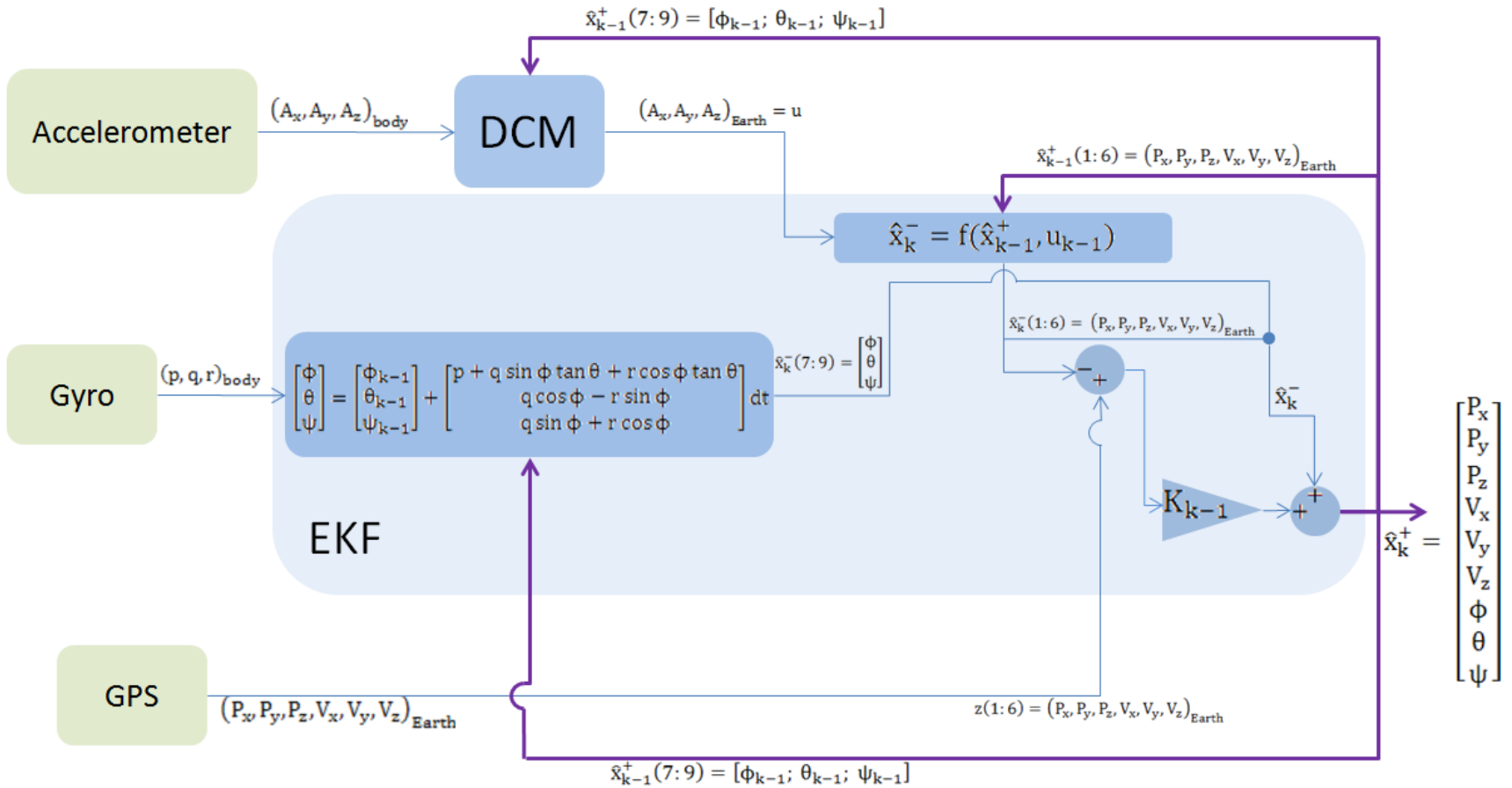


Figure 3-3: GPS Aided Inertial Navigation EKF Pseudo Code Block Diagram

Table 3-3: GPS Aided Inertial Navigation EKF Prediction Equations

1) Project State:

$$\hat{x}_k^- (1:6) = \begin{bmatrix} P_x \\ P_y \\ P_z \\ V_x \\ V_y \\ V_z \end{bmatrix}_k = \begin{bmatrix} 1 & 0 & 0 & dt & 0 & 0 \\ 0 & 1 & 0 & 0 & dt & 0 \\ 0 & 0 & 1 & 0 & 0 & dt \\ 0 & 0 & 0 & 1 & 0 & 0 \\ 0 & 0 & 0 & 0 & 1 & 0 \\ 0 & 0 & 0 & 0 & 0 & 1 \end{bmatrix} \begin{bmatrix} P_x \\ P_y \\ P_z \\ V_x \\ V_y \\ V_z \end{bmatrix}_{k-1} + \begin{bmatrix} 0 & 0 & 0 \\ 0 & 0 & 0 \\ 0 & 0 & 0 \\ dt & 0 & 0 \\ 0 & dt & 0 \\ 0 & 0 & dt \end{bmatrix} \begin{bmatrix} a_x \\ a_y \\ a_z \end{bmatrix}_{Earth,k-1}$$

$$\hat{x}_k^- (7:9) = \begin{bmatrix} \phi \\ \theta \\ \psi \end{bmatrix}_k = \begin{bmatrix} \phi \\ \theta \\ \psi \end{bmatrix}_{k-1} + \begin{bmatrix} p + q \sin \phi \tan \theta + r \cos \phi \tan \theta \\ q \cos \phi - r \sin \phi \\ q \sin \phi + r \cos \phi \end{bmatrix} dt$$

Equation	Nomenclature	Symbol	Matrix Size	Values
2) Project Error Covariance: $P_k^- = A_{k-1}^T P_{k-1}^- A_{k-1} + Q$	Error Covariance	P_k^- , P_{k-1}^-	9x9	$\begin{bmatrix} \text{diag}(\#_{3x3}) & 0_{3x3} & 0_{3x3} \\ 0_{3x3} & \text{diag}(\#_{3x3}) & 0_{3x3} \\ 0_{3x3} & 0_{3x3} & \#_{3x3} \end{bmatrix}$
	State Transition Matrix	A_{k-1}	9x9	$\begin{bmatrix} I_{3x3} & I_{3x3}dt & 0_{3x3} \\ 0_{3x3} & I_{3x3} & J_{3x3}^{\phi,\theta,\psi} \\ 0_{3x3} & 0_{3x3} & J_{3x3}^{\phi,\theta,\psi} \end{bmatrix}$
	Model/Input Covariance	Q	9x9	$\begin{bmatrix} \text{diag}(qkc1_{3x3}) & 0_{3x3} & 0_{3x3} \\ 0_{3x3} & \text{diag}(qkc1_{3x3}) & 0_{3x3} \\ 0_{3x3} & 0_{3x3} & \text{diag}(qkc2_{3x3}) \end{bmatrix}$

Table 3-4: GPS Aided Inertial Navigation EKF Corrections Equations

Equation	Nomenclature	Symbol	Matrix Size	Values
3) Compute the Kalman Gain: $K_{k-1} = \frac{P_k^- C_{k-1}^T}{C_{k-1} P_k^- C_{k-1}^T + R}$	Observation Matrix	C_{k-1}	6x9	$\begin{bmatrix} I_{3x3} & 0_{3x3} & 0_{3x3} \\ 0_{3x3} & I_{3x3} & 0_{3x3} \end{bmatrix}$
	Measurement Covariance Matrix	R	6x6	$\begin{bmatrix} \text{diag}(qkc1_{3x3}) & 0_{3x3} \\ 0_{3x3} & \text{diag}(qkc2_{3x3}) \end{bmatrix}$
	Kalman Gain	K_{k-1}	9x6	$[\#_{9x6}]$
4) Update Estimate with Measurement: $\hat{x}_k^+ = \hat{x}_k^- + K_{k-1}(z_{k-1} - h(\hat{x}_k^-, u_k))$ Where: $h(\hat{x}_k^-, u_k) = C\hat{x}_k^-$	System States	\hat{x}_k^+, \hat{x}_k^-	9x1	$[P_x \quad P_y \quad P_z \quad V_x \quad V_y \quad V_z \quad \phi \quad \theta \quad \psi]^T$
	GPS Measurements	z_{k-1}	6x1	$[P_x \quad P_y \quad P_z \quad V_x \quad V_y \quad V_z]^T$
5) Update the Error Covariance: $P_k^+ = (I - K_{k-1} C_{k-1}) P_k^-$	Identity Matrix	I	6x6	$\text{diag}(1_{6x6})$

Where "#" indicates a calculated value, and "diag(val)" indicates a diagonal matrix with the diagonal having values of "val". qkc1 and qkc2 are constants that are varied in the Monte Carlo analyses. Additionally, A(4:9,7:9) are defined in Equation 38, below.

$$A(4:9,7:9) = \begin{bmatrix} I_{3x3}^{\phi,\theta,\psi} & \begin{bmatrix} \partial V_x / \partial \phi & \partial V_x / \partial \theta & \partial V_x / \partial \psi \\ \partial V_y / \partial \phi & \partial V_y / \partial \theta & \partial V_y / \partial \psi \\ \partial V_z / \partial \phi & \partial V_z / \partial \theta & \partial V_z / \partial \psi \\ \partial \phi / \partial \phi & \partial \phi / \partial \theta & \partial \phi / \partial \psi \\ \partial \theta / \partial \phi & \partial \theta / \partial \theta & \partial \theta / \partial \psi \\ \partial \psi / \partial \phi & \partial \psi / \partial \theta & \partial \psi / \partial \psi \end{bmatrix} \end{bmatrix} \quad (38)$$

Where the following equations are used to obtain the partial derivatives of Equation 38, above. Note that Equation 41 is the discrete form of Equation 5:

$$V_{x|y|z} = V_{x|y|z_{k-1}} + A_{x|y|z_{k-1}, \text{Earth}} dt \quad (39)$$

Where:

$$A_{x|y|z_{k-1}, \text{Earth}} = \text{DCM} \cdot A_{x|y|z_{k-1}, \text{Body}} \quad (40)$$

$$\begin{aligned} \phi_k &= \phi_{k-1} + (p + q \sin \phi \tan \theta + r \cos \phi \tan \theta)_{k-1} dt \\ \theta_k &= \theta_{k-1} + (q \cos \phi - r \sin \phi)_{k-1} dt \\ \psi_k &= \psi_{k-1} + (q \sin \phi + r \cos \phi)_{k-1} dt \end{aligned} \quad (41)$$

*Note that Jarrell's original implementation does not include the partial derivatives of velocity w.r.t Euler angles. That is, his $A(4:6,7:9)$ are 0_{3x3} .

3.3.1. Quaternion Formulation

The description of the Method 3 EKF Formulation, thus far has been in Euler angles. This was done as Euler based rotational kinematics are more intuitive and familiar to most people. The Method 3 EKF that was evaluated in these analyses utilized quaternions. This subsection will present the quaternion equations that were used and describe how these new quaternion equations replace the previously described Euler equations in this EKF formulation. To make the differences quickly visually apparent, equations and dimensions that changed in the tables will be made blue font.

Table 3-5: GPS Aided Inertial Navigation EKF Prediction Equations - Quaternions

1) Project State:

$$\hat{x}_k^{-}(1:6) = \begin{bmatrix} P_x \\ P_y \\ P_z \\ V_x \\ V_y \\ V_z \end{bmatrix}_k = \begin{bmatrix} 1 & 0 & 0 & dt & 0 & 0 \\ 0 & 1 & 0 & 0 & dt & 0 \\ 0 & 0 & 1 & 0 & 0 & dt \\ 0 & 0 & 0 & 1 & 0 & 0 \\ 0 & 0 & 0 & 0 & 1 & 0 \\ 0 & 0 & 0 & 0 & 0 & 1 \end{bmatrix}_{k-1} \begin{bmatrix} P_x \\ P_y \\ P_z \\ V_x \\ V_y \\ V_z \end{bmatrix}_{k-1} + \begin{bmatrix} 0 & 0 & 0 \\ 0 & 0 & 0 \\ 0 & 0 & 0 \\ dt & 0 & 0 \\ 0 & dt & 0 \\ 0 & 0 & dt \end{bmatrix}_{Earth,k-1} \begin{bmatrix} a_x \\ a_y \\ a_z \end{bmatrix}$$

$$\hat{x}_k^{-}(7:10) = \begin{bmatrix} q_0 \\ q_1 \\ q_2 \\ q_3 \end{bmatrix}_k = \begin{bmatrix} q_0 \\ q_1 \\ q_2 \\ q_3 \end{bmatrix}_{k-1} + \frac{dt}{2} \begin{bmatrix} -pq_1 - qq_2 - rq_3 \\ pq_0 + rq_2 - qq_3 \\ qq_0 - rq_1 + pq_3 \\ rq_0 + qq_1 - pq_2 \end{bmatrix} + dt \begin{bmatrix} \lambda q_0 \\ \lambda q_1 \\ \lambda q_2 \\ \lambda q_3 \end{bmatrix} \text{ where: } \lambda = 1 - (q_0^2 + q_1^2 + q_2^2 + q_3^2)$$

Equation	Nomenclature	Symbol	Matrix Size	Values
2) Project Error Covariance: $P_k^- = A_{k-1}^T P_{k-1}^- A_{k-1} + Q$	Error Covariance	P_k^- , P_{k-1}^-	10x10	$\begin{bmatrix} \text{diag}(\#_{3x3}) & 0_{3x3} & 0_{3x4} \\ 0_{3x3} & \text{diag}(\#_{3x3}) & 0_{3x4} \\ 0_{3x3} & 0_{3x3} & \#_{4x4} \end{bmatrix}$
	State Transition Matrix	A_{k-1}	10x10	$\begin{bmatrix} I_{3x3} & I_{3x3}dt & 0_{3x4} \\ 0_{3x3} & I_{3x3} & J_{3x4}^{quat} \\ 0_{4x3} & 0_{4x3} & J_{4x4}^{quat} \end{bmatrix}$
	Model/Input Covariance	Q	10x10	$\begin{bmatrix} \text{diag}(qkc1_{3x3}) & 0_{3x3} & 0_{3x4} \\ 0_{3x3} & \text{diag}(qkc1_{3x3}) & 0_{3x4} \\ 0_{4x3} & 0_{4x3} & \text{diag}(qkc2_{4x4}) \end{bmatrix}$

Table 3-6: GPS Aided Inertial Navigation EKF Correction Equations - Quaternions

Equation	Nomenclature	Symbol	Matrix Size	Values
3) Compute the Kalman Gain: $K_{k-1} = \frac{P_k^- C_{k-1}^T}{C_{k-1} P_k^- C_{k-1}^T + R}$	Observation Matrix	C_{k-1}	6x10	$\begin{bmatrix} I_{3x3} & 0_{3x3} & 0_{3x4} \\ 0_{3x3} & I_{3x3} & 0_{3x4} \end{bmatrix}$
	Measurement Covariance Matrix	R	6x6	$\begin{bmatrix} \text{diag}(rkc1_{3x3}) & 0_{3x3} \\ 0_{3x3} & \text{diag}(rkc2_{3x3}) \end{bmatrix}$
	Kalman Gain	K_{k-1}	10x6	$[\#_{10x6}]$
4) Update Estimate with Measurement: $\hat{x}_k^+ = \hat{x}_k^- + K_{k-1}(z_{k-1} - h(\hat{x}_k^-, u_k))$ Where: $h(\hat{x}_k^-, u_k) = C\hat{x}_k^-$	System States	\hat{x}_k^+, \hat{x}_k^-	10x1	$[P_x \quad P_y \quad P_z \quad V_x \quad V_y \quad V_z \quad q_0 \quad q_1 \quad q_2 \quad q_3]^T$
	GPS Measurements	z_{k-1}	6x1	$[P_x \quad P_y \quad P_z \quad V_x \quad V_y \quad V_z]^T$
5) Update the Error Covariance: $P_k^+ = (I - K_{k-1} C_{k-1}) P_k^-$	Identity Matrix	I	6x6	$\text{diag}(1_{6x6})$

$$A(4:10,7:10) = J_{\text{quat}}^{\text{quat}} = \begin{bmatrix} \frac{\partial V_x}{\partial q_0} & \frac{\partial V_x}{\partial q_1} & \frac{\partial V_x}{\partial q_2} & \frac{\partial V_x}{\partial q_3} \\ \frac{\partial V_y}{\partial q_0} & \frac{\partial V_y}{\partial q_1} & \frac{\partial V_y}{\partial q_2} & \frac{\partial V_y}{\partial q_3} \\ \frac{\partial V_z}{\partial q_0} & \frac{\partial V_z}{\partial q_1} & \frac{\partial V_z}{\partial q_2} & \frac{\partial V_z}{\partial q_3} \\ \frac{\partial q_0}{\partial q_0} & \frac{\partial q_0}{\partial q_1} & \frac{\partial q_0}{\partial q_2} & \frac{\partial q_0}{\partial q_3} \\ \frac{\partial q_1}{\partial q_0} & \frac{\partial q_1}{\partial q_1} & \frac{\partial q_1}{\partial q_2} & \frac{\partial q_1}{\partial q_3} \\ \frac{\partial q_2}{\partial q_0} & \frac{\partial q_2}{\partial q_1} & \frac{\partial q_2}{\partial q_2} & \frac{\partial q_2}{\partial q_3} \\ \frac{\partial q_3}{\partial q_0} & \frac{\partial q_3}{\partial q_1} & \frac{\partial q_3}{\partial q_2} & \frac{\partial q_3}{\partial q_3} \end{bmatrix} \quad (42)$$

where: The following equations and Equations 39 and 40 are used to obtain the partial derivatives of Equation 42, above. The following quaternion equations are the discrete form of Equation 11 in the quaternion theory section (2.1.1).

$$\begin{aligned} q_0 &= q_{0k-1} + \frac{dt}{2}(-pq_1 - qq_2 - rq_3) + dt \cdot \lambda q_0 \\ q_1 &= q_{1k-1} + \frac{dt}{2}(pq_0 + rq_2 - qq_3) + dt \cdot \lambda q_1 \\ q_2 &= q_{2k-1} + \frac{dt}{2}(qq_0 - rq_1 + pq_3) + dt \cdot \lambda q_2 \\ q_3 &= q_{3k-1} + \frac{dt}{2}(rq_0 + qq_1 - pq_2) + dt \cdot \lambda q_3 \end{aligned} \quad (43)$$

where

$$\lambda = 1 - (q_0^2 + q_1^2 + q_2^2 + q_3^2) \quad (44)$$

3.4. GPS Aided Inertial Navigation Unscented Kalman Filter ("Method 4")

This section will describe the UKF version of the "Method 3" formulation in [13]. This estimator will be referred to as "Method 4 UKF" throughout this text. Table 3-7 and Table 3-8, below, show the equations for the Method 4 UKF implementation. The equations will utilize the Euler representations, as to present the more intuitive implementation. However, the following analyses are performed on the Method 4 UKF that utilizes the quaternion formulations. The previous subsection provides a thorough example of how to replace the Euler equations with quaternion equations for the Method 3 EKF and Method 4 UKF estimators.

Table 3-7: GPS Aided Inertial Navigation UKF Prediction Equations

1) Project State:

$$\hat{x}_k^- = \sum_{i=0}^{2L} \eta_i^m x_k^i$$

$$x_k^i(1:6) = \begin{bmatrix} P_x \\ P_y \\ P_z \\ V_x \\ V_y \\ V_z \end{bmatrix}_k = \begin{bmatrix} 1 & 0 & 0 & dt & 0 & 0 \\ 0 & 1 & 0 & 0 & dt & 0 \\ 0 & 0 & 1 & 0 & 0 & dt \\ 0 & 0 & 0 & 1 & 0 & 0 \\ 0 & 0 & 0 & 0 & 1 & 0 \\ 0 & 0 & 0 & 0 & 0 & 1 \end{bmatrix} \underbrace{\begin{bmatrix} P_x \pm \# \\ P_y \pm \# \\ P_z \pm \# \\ V_x \pm \# \\ V_y \pm \# \\ V_z \pm \# \end{bmatrix}}_{x_{k-1}^i(1:6)} + \begin{bmatrix} 0 & 0 & 0 \\ 0 & 0 & 0 \\ 0 & 0 & 0 \\ dt & 0 & 0 \\ 0 & dt & 0 \\ 0 & 0 & dt \end{bmatrix} \underbrace{\begin{bmatrix} a_x \\ a_y \\ a_z \end{bmatrix}}_{\text{Earth}, k-1} u(1:3)$$

$$x_k^i(7:9) = \begin{bmatrix} \phi \\ \theta \\ \psi \end{bmatrix}_k = \underbrace{\begin{bmatrix} \phi \\ \theta \\ \psi \end{bmatrix}}_{x_{k-1}^i(7:9)} + \begin{bmatrix} p + q \sin \phi \tan \theta + r \cos \phi \tan \theta \\ q \cos \phi - r \sin \phi \\ q \sin \phi + r \cos \phi \end{bmatrix} dt \quad \text{where } u(4:6) = p, q, r$$

Equation	Nomenclature	Symbol	Matrix Size	Values
2) Project Error Covariance:	Error Covariance	P_k^-	9x9	$[\#_{9x9}]$
	Sigma Points	X_{k-1}	9x19	$\begin{bmatrix} \hat{x}_{k-1}^+ \\ \vdots \\ \hat{x}_{k-1}^+ + \sqrt{L + \lambda} \sqrt{P_{k-1}} \\ \vdots \\ \hat{x}_{k-1}^+ + \sqrt{L + \lambda} \sqrt{P_{k-1}} \end{bmatrix}_{[9x1]}$
	Model/Input Covariance	Q	9x9	$\begin{bmatrix} \text{diag}(qkc1_{3x3}) & 0_{3x3} & 0_{3x3} \\ 0_{3x3} & \text{diag}(qkc1_{3x3}) & 0_{3x3} \\ 0_{3x3} & 0_{3x3} & \text{diag}(qkc2_{3x3}) \end{bmatrix}$

Table 3-8: GPS Aided Inertial Navigation UKF Correction Equations

Equation	Nomenclature	Symbol	Matrix Size	Values
3) Compute the Kalman Gain: $K = \frac{P_{xy}}{P_{yy}}$ $= \frac{\sum_{i=0}^{2L} \eta_i^c (\chi_k^i - \hat{x}_k)(\Psi_k^i - y_k)^T}{R + \sum_{i=0}^{2L} \eta_i^c (\Psi_k^i - y_k)(\Psi_k^i - y_k)^T}$	Observation	Ψ_k^i	6x1	$\chi_k^i(1:6)$
	Mean of Observations	y_k	6x1	$y_k = \sum_{i=0}^{2L} \eta_i^m \Psi_k^i$
	Measurement Covariance Matrix	R	6x6	$\begin{bmatrix} \text{diag}(rkc1_{3x3}) & 0_{3x3} \\ 0_{3x3} & \text{diag}(rkc2_{3x3}) \end{bmatrix}$
	Kalman Gain	K	9x6	$[\#_{9x6}]$
4) Update Estimate with Measurement: $\hat{x}_k^+ = \hat{x}_k^- + K(z_k - y_k)$	System States	\hat{x}_k^+, \hat{x}_k^-	9x1	$[P_x \ P_y \ P_z \ V_x \ V_y \ V_z \ \phi \ \theta \ \psi]^T$
	GPS Measurements	z_k	6x1	$[P_x \ P_y \ P_z \ V_x \ V_y \ V_z]^T$
5) Update the Error Covariance: $P_k^+ = P_k^- - K P_{yy} K^T$	Error Covariance	P_k^+	9x9	$[\#_{9x9}]$

Where: $\eta_i^m, \eta_i^c, \eta_0^m, \eta_0^c, \lambda, L, \alpha, \beta$, and κ are as defined in the UKF Theory Section and the UKF specific tuning parameters, based on [28], where chosen as:

$$\alpha = 1 \quad \beta = 2 \quad \kappa = 0$$

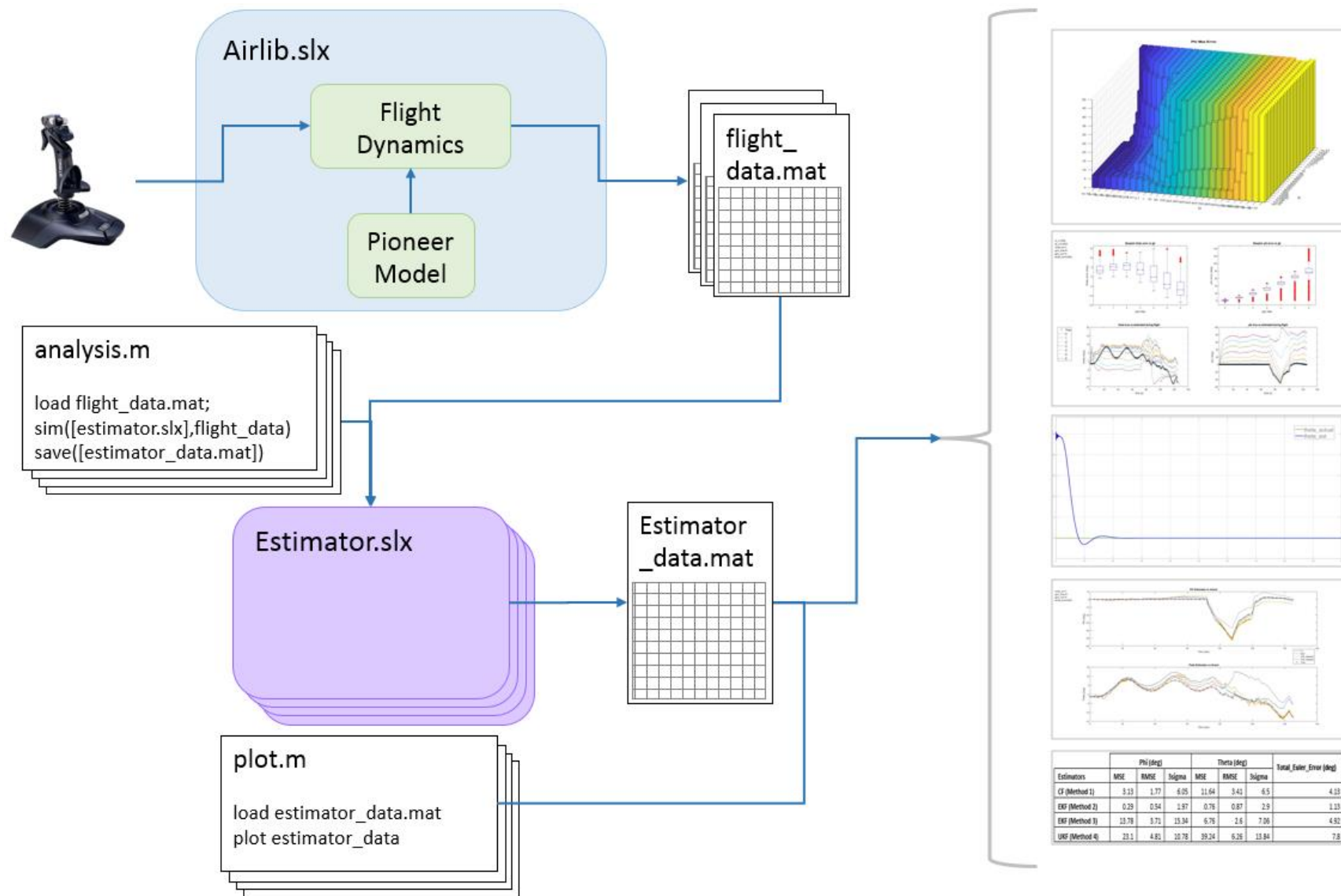
4. Experimental Setup

4.1. Simulation Environment

This analysis was conducted entirely using Matlab/Simulink. “Airlib”, an open source aero environment model built in Simulink, was used to simulate the aircraft equations of motion. Airlib offers multiple aircraft models; The Pioneer UAV aircraft model was chosen for this analysis, as its dynamics are most representative of the kind of platform on which the estimators being evaluated would likely be implemented. While many have created their own aerodynamic models and simulation environments, this open source model has been around since 1993, is able to be adapted by the user, and is thoroughly documented [29]. In order to achieve a consistent baseline on which to evaluate estimators between multiple research groups, a common environment should be used. Airlib is being recommended by the author.

Initially, the Estimators were prototyped and developed in-the-loop with the Airlib model. In order to guarantee repeatability and consistent inputs across all analyses, a few flights were performed while recording all applicable inputs and outputs of the Airlib environment (i.e. True Euler angles and other parameters required as inputs to estimators). These data would then be loaded and run through the estimator models. These data were recorded as timeseries in struct form. Using structs reduced the likelihood of error in simulation wiring, ensured scripts would be more easily readable, and reduced the need for significant downstream re-wiring for any upstream model changes. Structures were used for recording the outputs of the estimator models to aid plotting scripts that would plot data from analyses. Such structures and scripts were helpful to be able to repeat analyses quickly when changes were made. The simulation environment setup described above is depicted in Figure 4-1.

Figure 4-1: Simulation Environment Block Diagram



4.2. Flights

The analyses are performed on a set of three flights. The first flight is a trim condition, where all attitude states, rotation rates, and accelerations are approximately 0. The second flight is an elevator pulse condition, driving pitch attitudes of approximately +2 to -18 degrees damping over 100s with 0 variation in roll. The third flight is a 120s "short steady flight"—"steady" meaning lack of force jerks and rapid changes in rotation rate. This last flight condition contained a takeoff, short flight (~100s) with a large roll condition (circling back around to the runway), and landing. The attitudes of these conditions are plotted in the left halves of Figure 5-1 through Figure 5-3, respectively.

4.3. Noise Models

Where noise is included, throughout this work, it will have consistent magnitude and properties as described in this section. In order to evaluate the Extended Kalman Filter Formulations with the Unscented Kalman Filter and Complementary Filter Formulations, white Gaussian noise will be used. Based on real sensor hardware data, the sensors will have the covariance and calculation rates as shown in Table 4-1, below. The estimators are calculated at 50Hz. It is not uncommon that gyro/accelerometers are processed on a different piece of hardware than the estimator. If an experiment were to be set up with the IMU being sampled at a different rate than the estimator computations, the noise characteristics could vary.

Table 4-1: Sensor Noise Properties

Sensor	Covariance	Calculation Rate
Gyro	5 deg/s	50 Hz
Accelerometer	0.003 g's	50 Hz
GPS Position	3m*	10 Hz
GPS Velocity	6m/s*	10 Hz
Airspeed	6m/s*	50 Hz

*Note: GPS position and GPS/Airspeed velocity covariances used in these analyses are large compared to the best (still low-cost) sensors available at the time of the authoring of this thesis. The values in the table are more representative of the lower quality sensors available at this time. Higher performing low-cost sensors are closer to 1m, 0.6m/s, and 1m/s. Due to the rapid increases in low-cost sensor performance, it is recommended for researchers to do a quick scan of available low cost sensors at the time of their research to determine more accurate covariances.

4.4. Monte Carlo Setup

The Monte Carlo Analyses that are discussed in the “Analyses, Results, and Observations”, are described below. The Monte Carlo analyses range from one degree of freedom to 4 degrees of freedom. An example of a 1 DoF Monte Carlo would be the analysis that determined the experimentally optimum single tuning parameter for the Complementary Filter Solution (Tau). An example of a 4 DoF Monte Carlo would be the analysis that determined the 4 experimentally optimum tuning parameters (qkc1, qkc2, rkc1, and rkc2) for the Method 3 EKF and Method4 UKF solutions, where the top and bottom halves of their "Q" and "R" matrices were independently varied.

The Monte Carlo method is implemented in a Matlab .m script that uses the “sim()” command to call the estimator .slx models. The mfile defines a list of values for each parameter that was part of the Monte Carlo analysis. Nested for() loops, in the mfile, iterate through all possible combinations of each value in each list. The sim() command lies in the deepest nested for() loop. This is shown in the pseudo code block diagram in Figure 4-2, below.

Figure 4-2: Monte Carlo Setup Pseudo Code Block Diagram

```
rkc1list = [1E-9,1E-8, ... 1E8, 1E9]
...
qkc2list = [1E-9,1E-8, ... 1E8, 1E9]
```

```
a = 1;
for a = 1:size(rkc1list)
{
    b = 1;
    for b = 1:size(qkc2list)
    {
        c = 1;
        for c = 1:size(qkc1list)
        {
            d = 1;
            for d = 1:size(qkc2list)
            {
                qkc2 = qkc2list(d);
                qkc1 = qkc1list(c);
                rkc2 = rkc2list(b);
                rkc1 = rkc1list(a);

                R(1:3) = eye()*rkc1; R(4:6) = eye()*rkc2;
                Q(1:3) = eye()*qkc1; Q(4:9) = eye()*qkc2;
                sim(); %run flight data thru estimators
            }
            d++
        }
        c++
    }
    b++
}
a++
```

5. Analyses, Results, and Observations

In current research comparing attitude estimators, comparisons are typically done with only, or with respect to only, one set of tuning parameters per estimator. For example, Estimator A (with $Q=X$ and $R=Y$) will be compared to Estimator B (with $Q=J$ and $R=K$); or Estimator A/Bs' sensitivity to tuning parameters will be compared, comparing multiples of the chosen Q/R matrices. The Q/R choices will have rationale behind them; however, they are typically not proven to be optimal for the tested estimator for the given conditions, or test cases.

This analysis, first, takes a broad look at the many Q/R choices that produce Euler estimates for each filter/formulation (Section 5.1 "Optimal Tuning Parameters"). This provides an additional measure of how optimal each filter/formulation is compared to the others. Given that other analyses choose the Q/R for each estimator without proving, experimentally, that the Q/R choices are optimal, it is possible that one estimator is inherently more optimal than the other-- by tuning alone. That is, a comparison between an EKF and UKF, without knowing how optimally tuned each is, is likely to lead to inconclusive and/or conflicting results, as observed by Rhudy et al. [3].

5.1. Optimal Tuning Parameters

5.1.1. Complementary Filter ("Method 1")

5.1.1.1. *Without Noise*

Figure 5-1, Figure 5-2, and Figure 5-3 contain plots for 3 different flight conditions: trim, elevator pulse, and a short steady flight, respectively. Each figure contains box plots of Euler error (top) and plots of actual Euler vs estimated Euler for multiple time constants (Tau) (bottom). The left half of the figures corresponds to pitch, and the right half corresponds to roll.

Figure 5-1 and Figure 5-2 have 0 error in roll as these conditions are trim and elevator pulse, respectively. The other plots show, definitively though, that this complementary filter formulation (with no noise) is optimal at a high time constant. A large time constant forces the estimate toward the integration of the gyros, for Euler angle estimate, rather than the trigonometric solution of the gravity vector from the accelerometer.

With the optimal (no noise) solution strongly favoring the integration of the gyros, it is apparent that the assumption of a non-accelerated body, that is required by the trigonometric solution of the pseudo gravity vector from the accelerometer, is invalid for a significant amount of the flight conditions. Though less pronounced in the trim and elevator pulse conditions, it is still apparent.

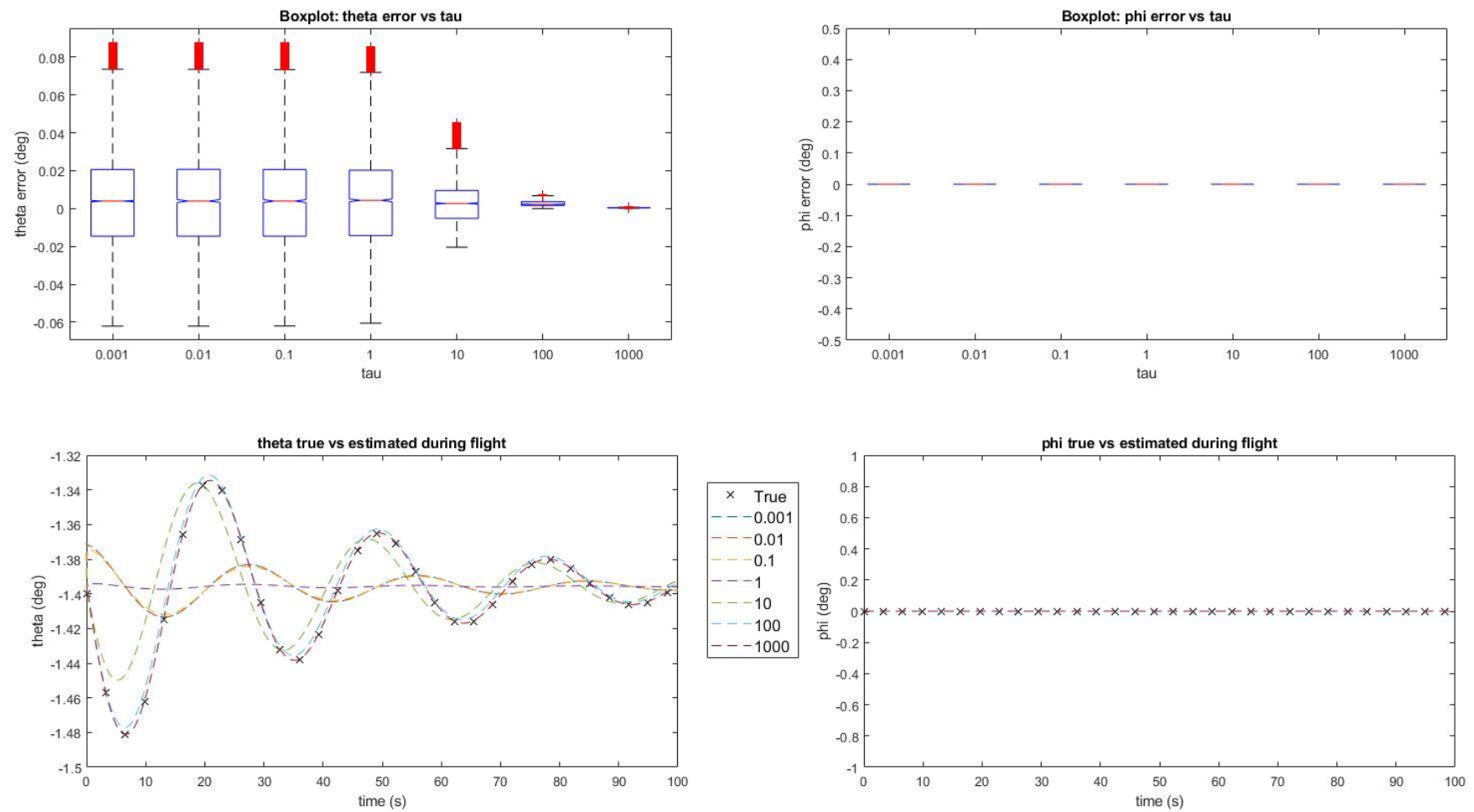


Figure 5-1: CF - Without Noise - Flight: Trim

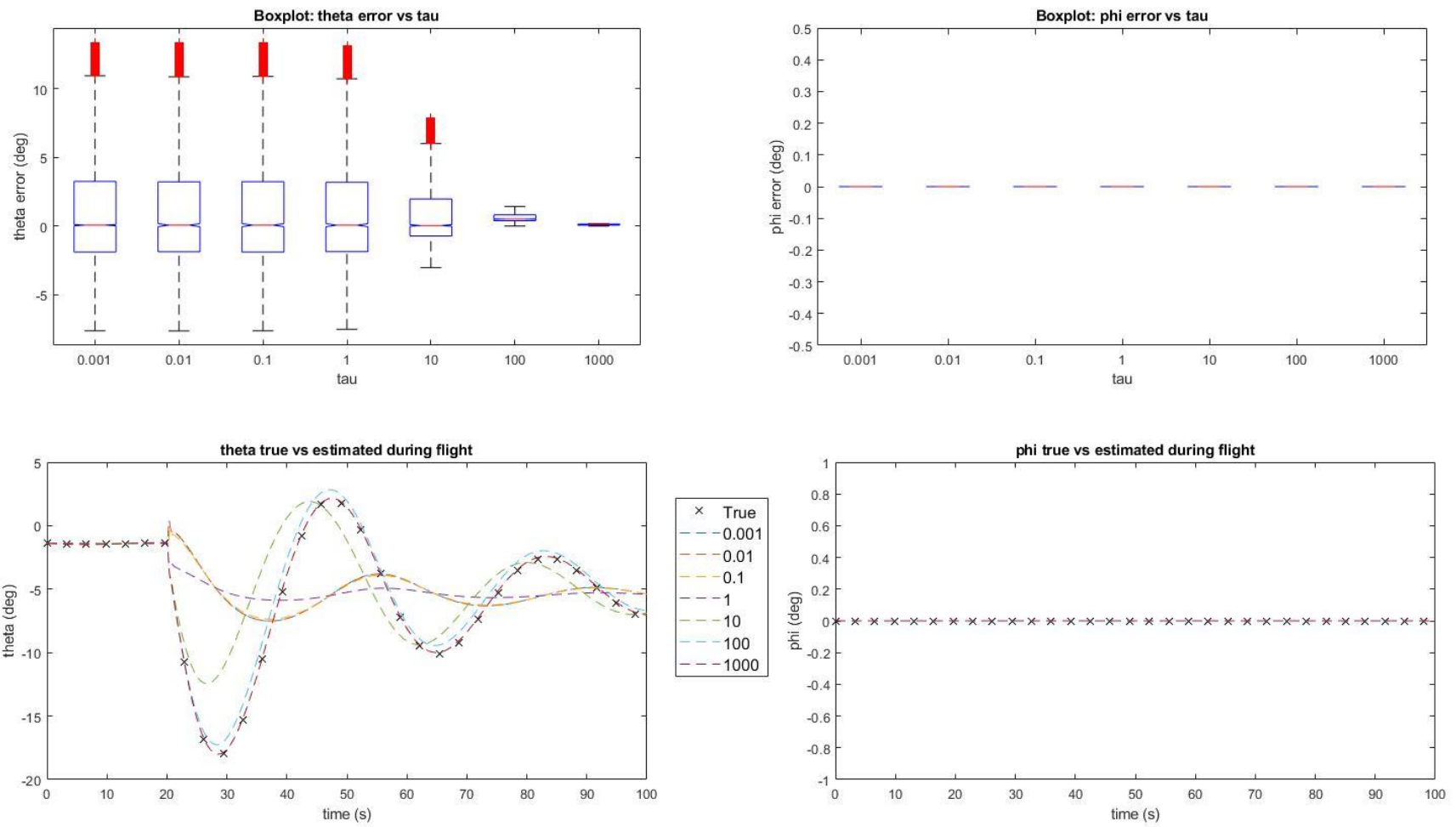


Figure 5-2: CF - Without Noise - Flight: Elevator Pulse Input

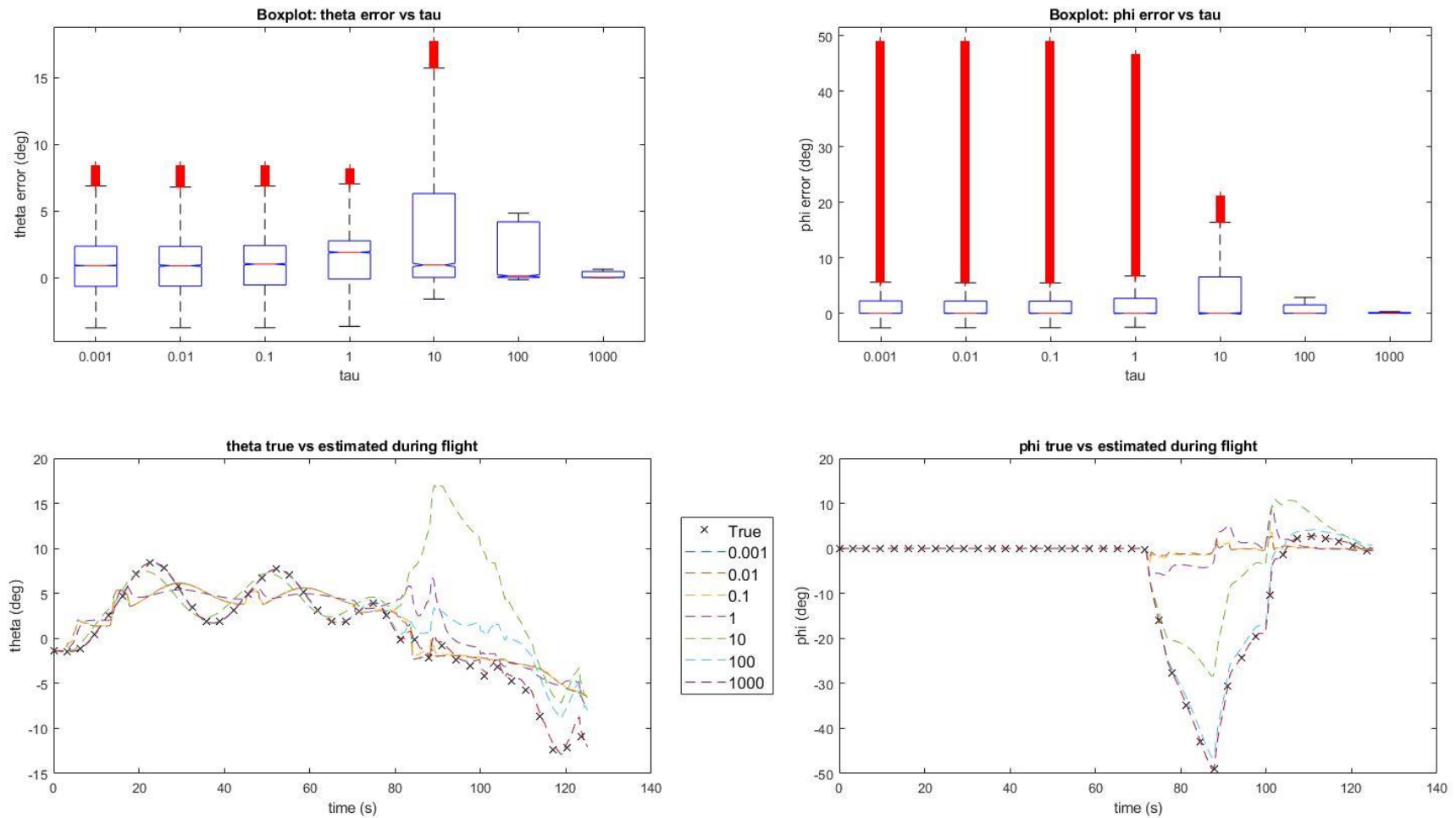


Figure 5-3: CF - Without Noise - Flight: Short Steady Flight

5.1.1.2. With Noise

Figure 5-4, Figure 5-5, and Figure 5-6 contain plots for 3 different flight conditions: trim, elevator pulse, and a short steady flight, respectively. Each figure contains box plots of Euler error (top) and plots of actual Euler vs estimated Euler for multiple Taus (bottom). The left half of the figures corresponds to pitch, and the right half corresponds to roll.

From these plots it can be seen that the optimal tau for each estimated parameter for a particular flight is not necessarily the same. For example, the optimal tau for estimating theta for the trim condition ($\text{Tau} = 1$) is not the same as the optimal tau for estimating phi for that same trim condition ($\text{Tau} = 10$); Also, the optimal tau for estimating theta for the trim condition ($\text{Tau} = 1$) is not the same as the optimal tau for estimating theta for the short steady flight case ($\text{Tau} = 1000$). Note that $\text{Tau} = 1000$ was chosen as optimal Tau for estimating pitch for the short steady flight condition as it has the lowest median and maximum error.

These results show that for the given filter/formulation and flight conditions tested, that a Tau between 1 and 100 should be chosen, assuming only one value of Tau must be chosen for all states. If outliers, or maximum error is a concern, for even one timestep, $\text{Tau} = 100$ would be a better choice as it has low median errors, and no maximum errors greater than $|5|$ degrees.

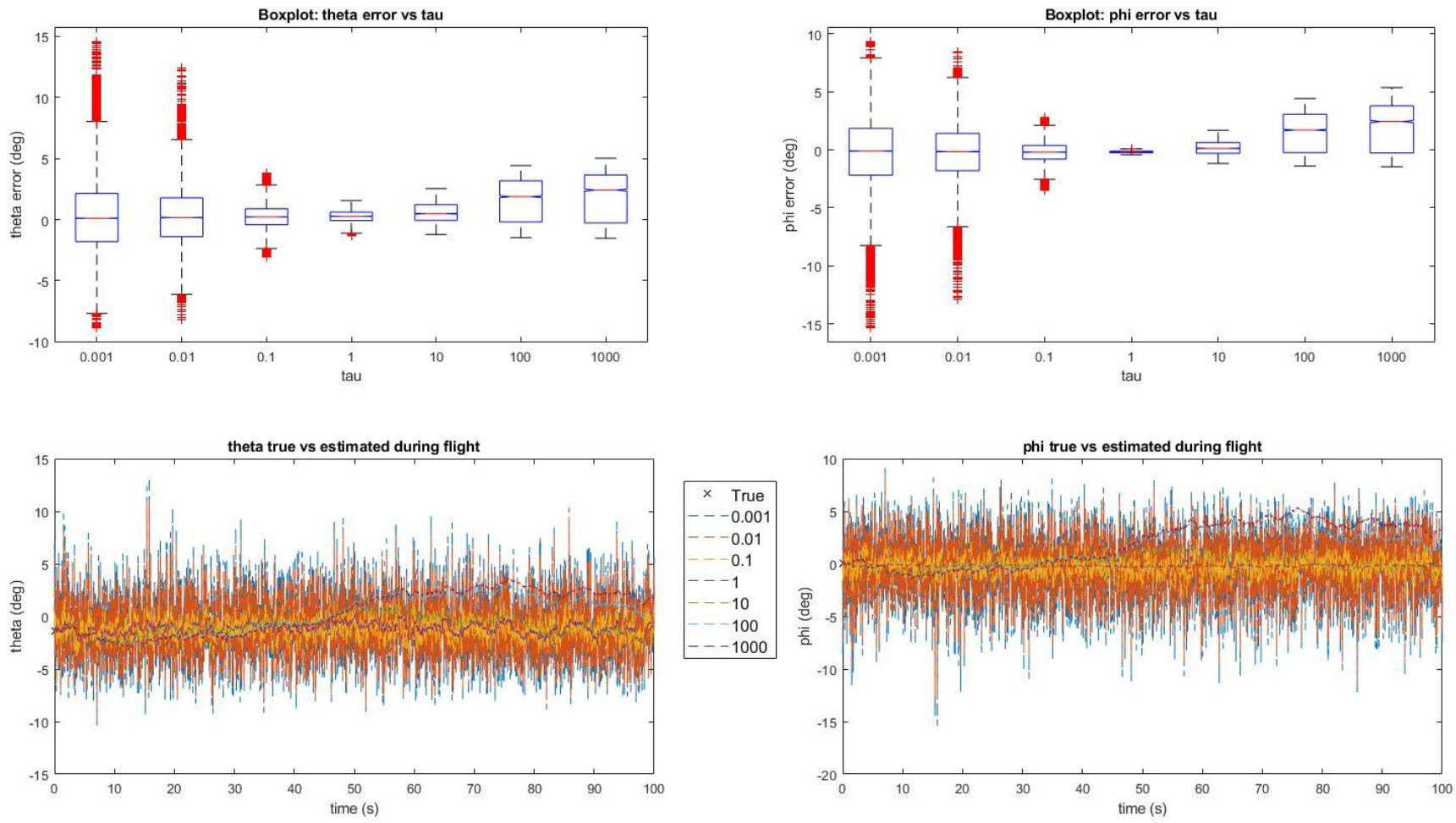


Figure 5-4: CF - With Noise - Flight: Trim

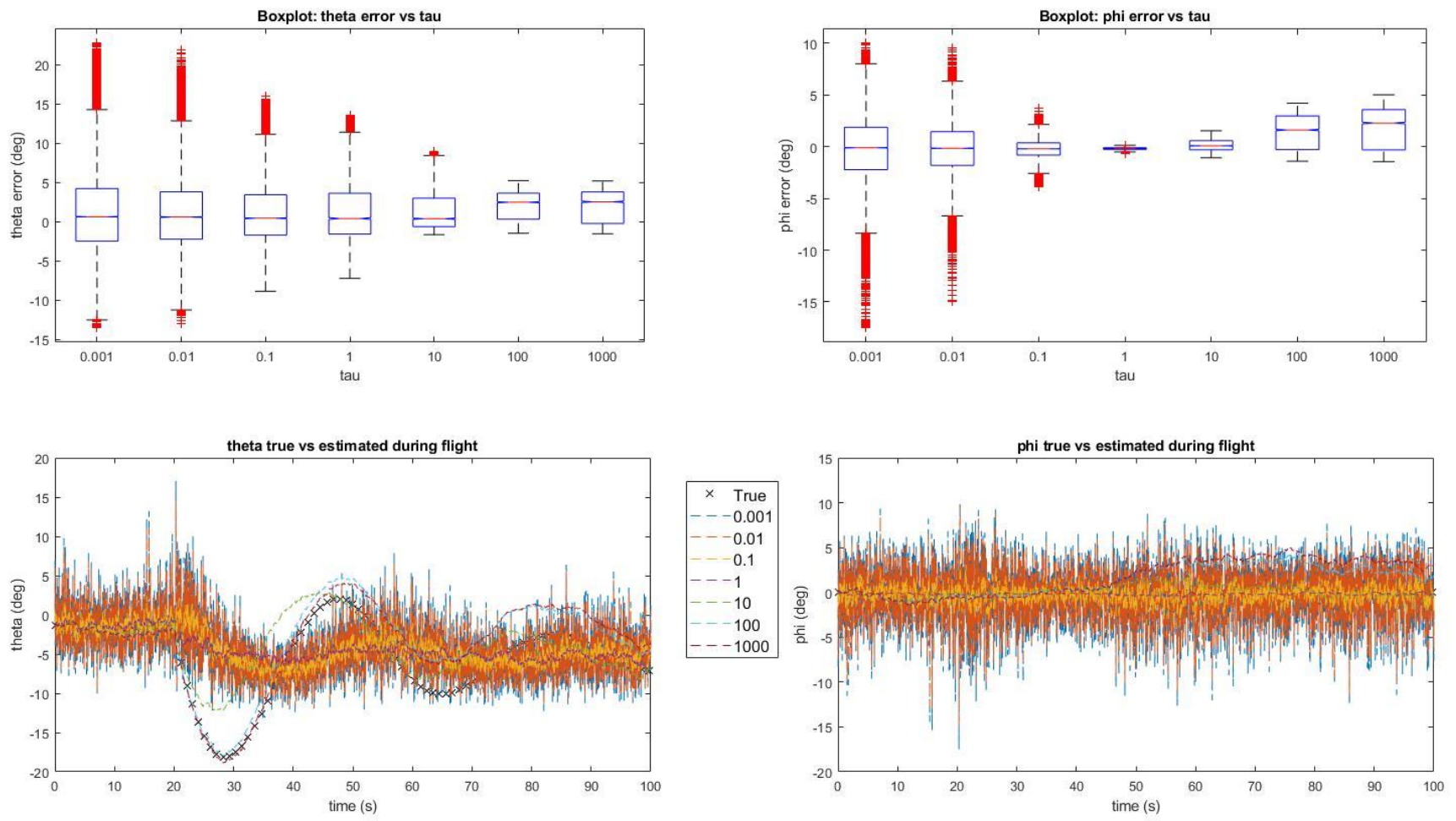


Figure 5-5: CF - With Noise - Flight: Elevator Pulse Input

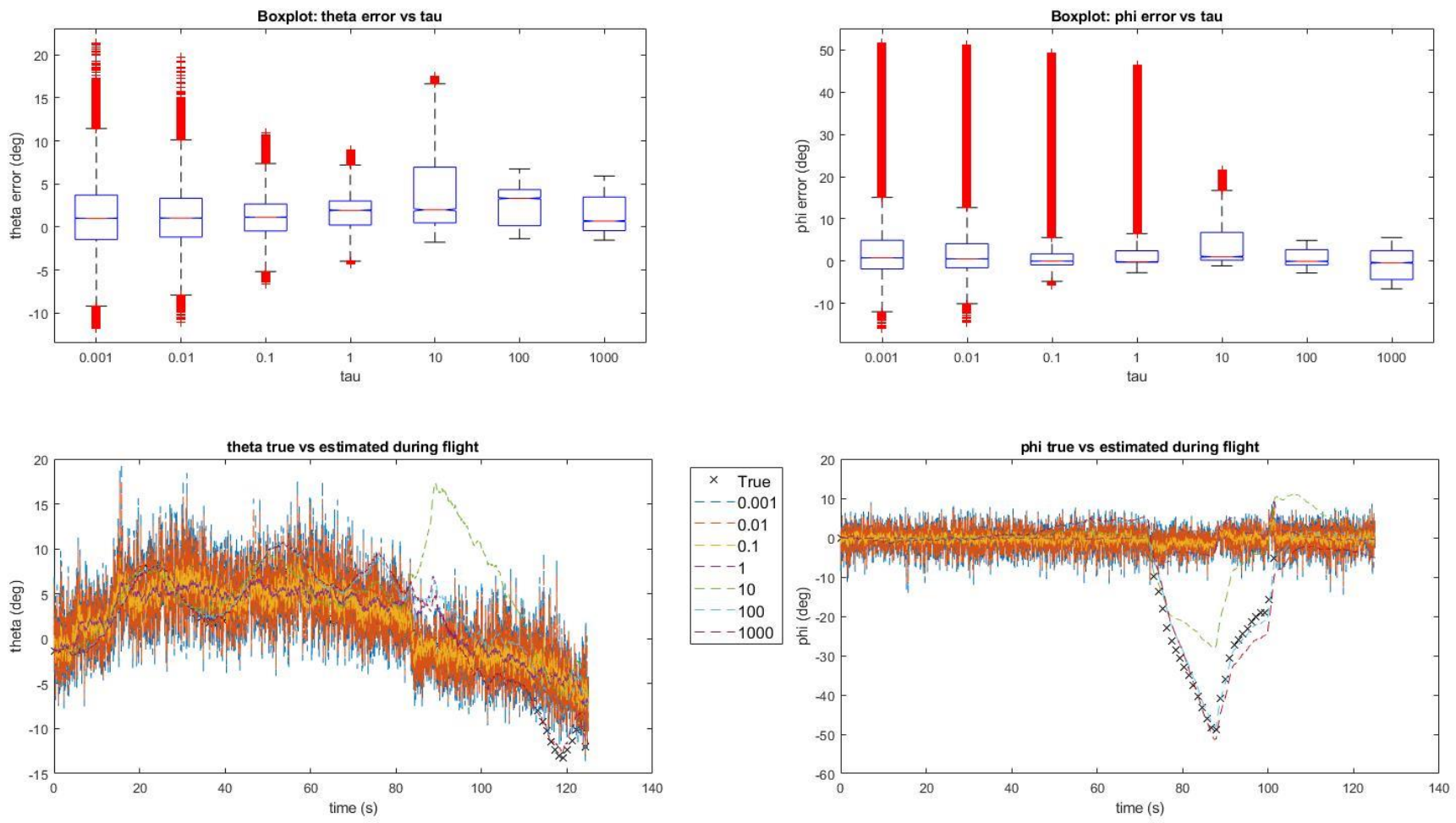


Figure 5-6: CF - With Noise - Flight: Short Steady Flight

Figure 5-7 through Figure 5-9 are higher resolution runs with $1 < \text{Tau} < 1000$, as that is where the optimal with-noise solution occurs. It is clear that for the steady state scenario (trim conditions and roll angle in elevator pulse flight), $\text{Tau} = 1$ is optimal. For the more dynamic scenarios, though, it is less apparent which Tau is optimal for both axes. $\text{Tau} = 1000$ is optimal for pitch for the short steady flight, while $50 \leq \text{Tau} \leq 80$ is optimal for phi in that condition. A Tau between 50 and 80 also produces adequate estimates in the pitch axis for the short steady flight, and both axes for the other flight conditions. Additionally, $\text{Tau} = 10$ produces low median and 75th percentile errors compared with $20 \leq \text{Tau} < 50$, and comparable to that of $50 \leq \text{Tau} \leq 80$. $\text{Tau} = 10$, though has higher maximum errors.

The chosen experimentally optimal Tau to be used as the baseline for the sensitivity analyses of this estimator will be 20. The rationale is that larger Taus will track the integration of the gyros closely, which is known to be a flawed solution. Additionally, as Tau decreases, the short steady flight conditions results in exponentially increasing error.

Discussion:

These results suggest that utilizing a sliding tuning parameter for each estimated state, as a function of the current conditions (magnitude of acceleration/rotation) may be able to produce a more optimal and robust solution. For example: making Tau a function of gyro rate over acceleration with respect to each Euler angle being estimated.

```

noise_on=1;
gyro_bias=0;
gyro_cov=5;
accel_cov=0.003;

```

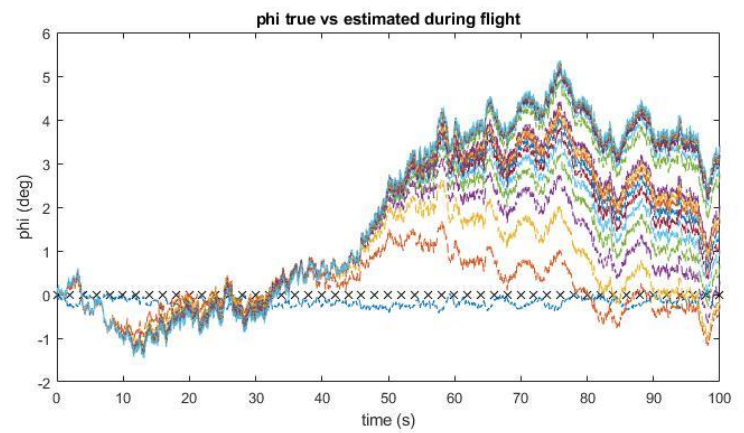
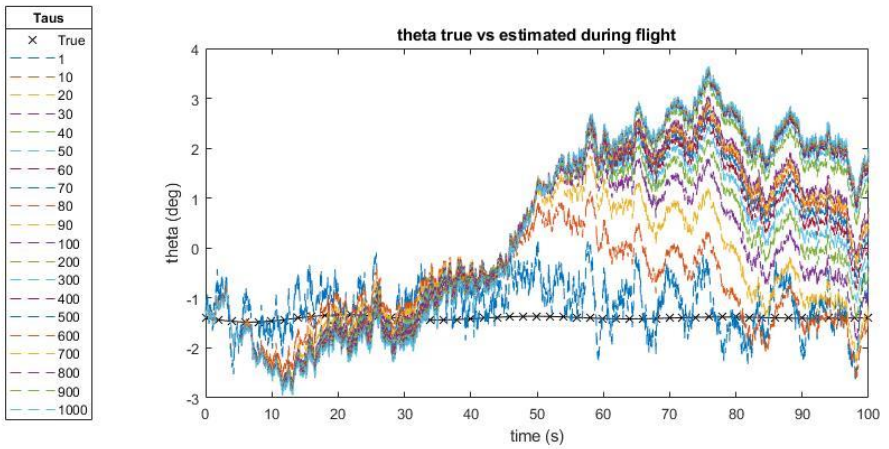
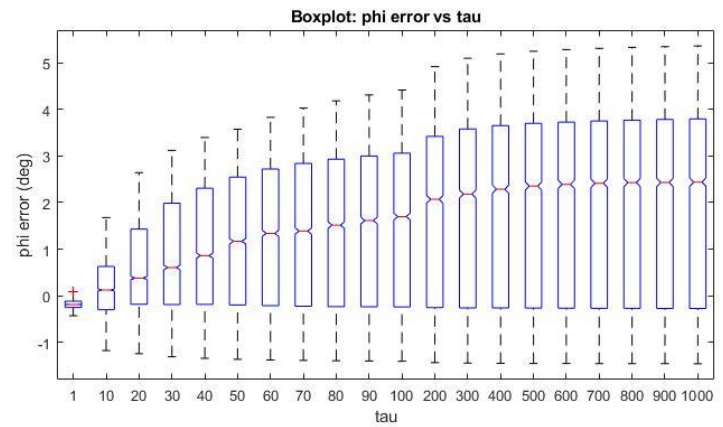
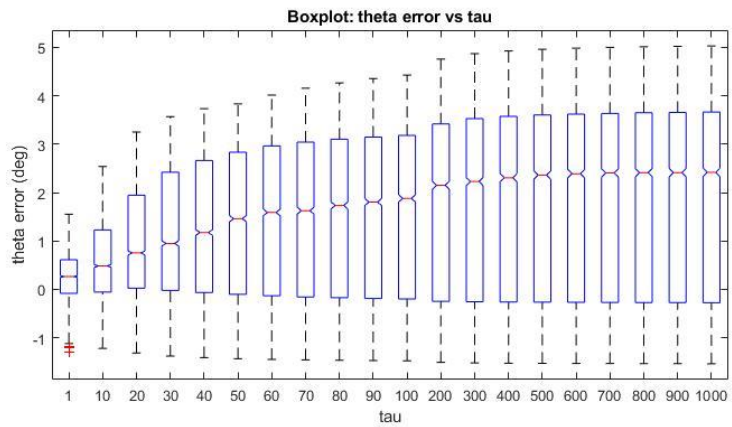


Figure 5-7: CF - With Noise - Flight: Trim - Refined Tau

```

noise_on=1;
gyro_bias=0;
gyro_cov=5;
accel_cov=0.003;

```

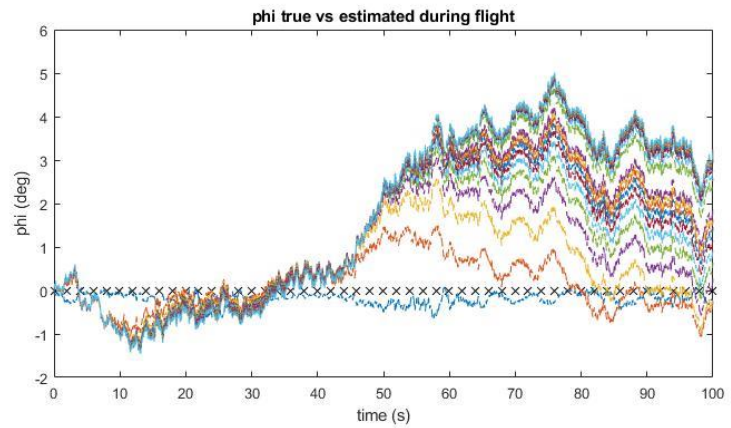
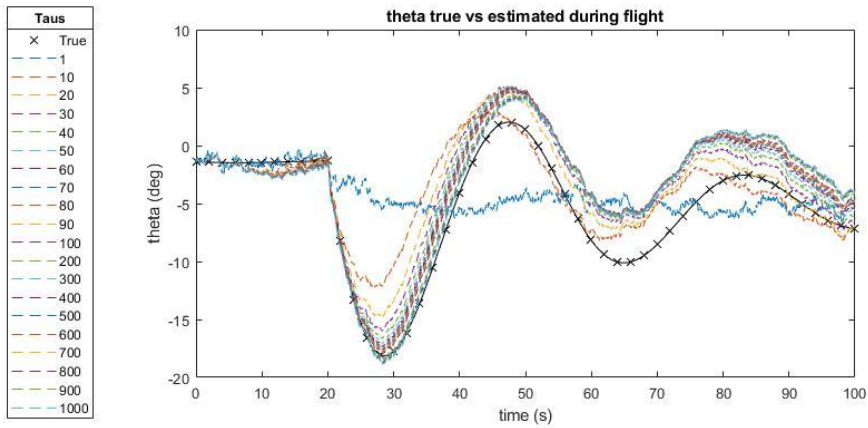
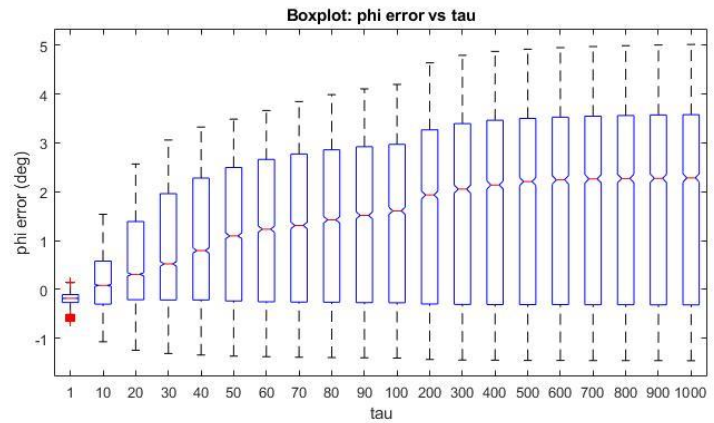
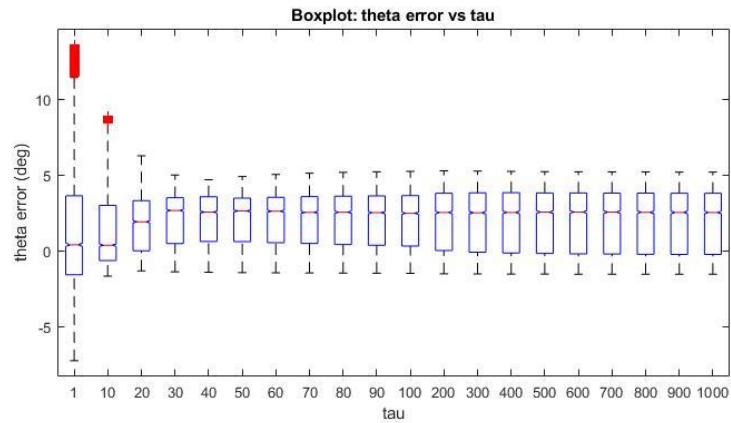


Figure 5-8: CF - With Noise - Flight: Elevator Pulse Input - Refined Tau

```

noise_on=1;
gyro_bias=0;
gyro_cov=5;
accel_cov=0.003;

```

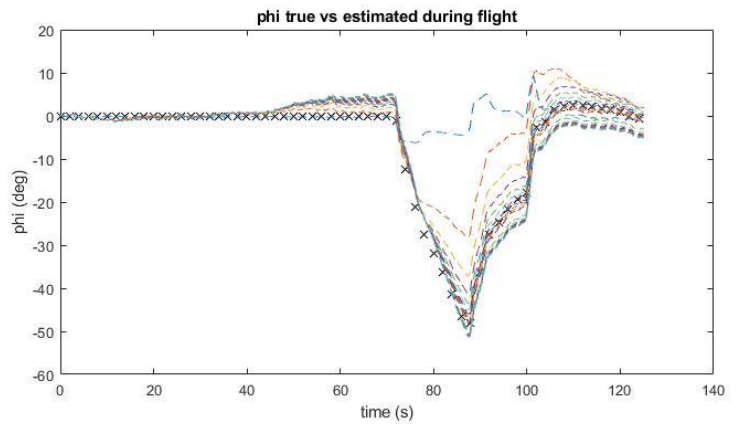
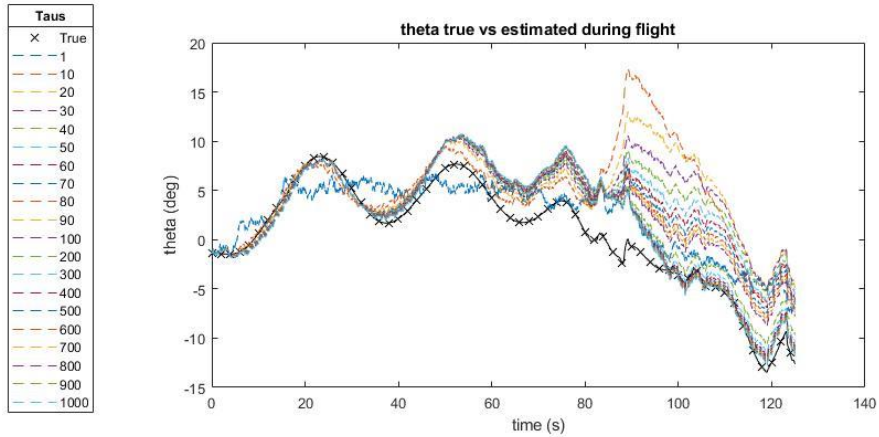
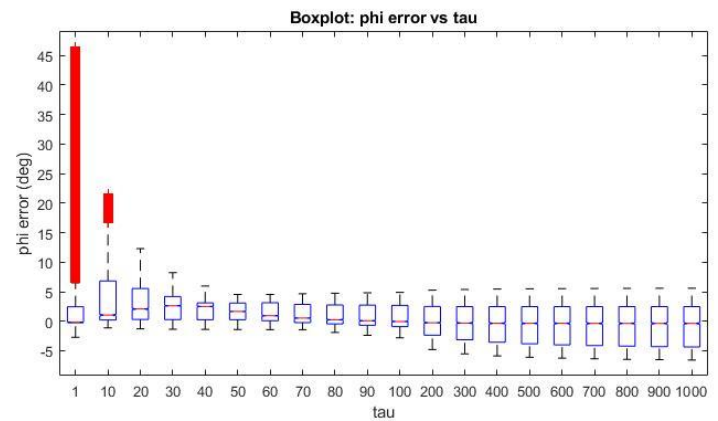
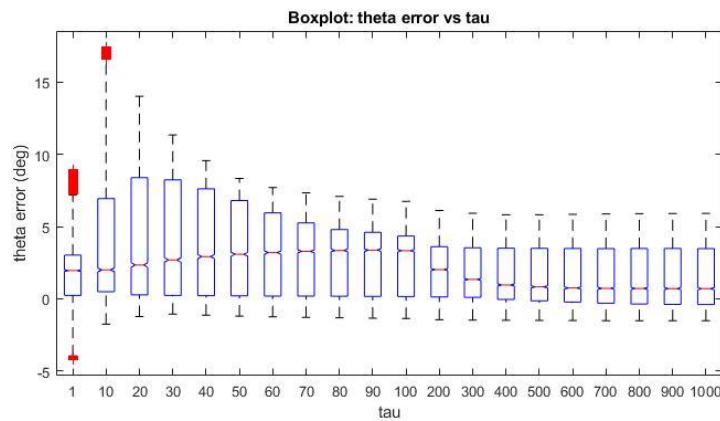


Figure 5-9: CF - With Noise - Flight: Short Steady Flight - Refined Tau

5.1.2. Airspeed Aided Inertial Attitude Extended Kalman Filter ("Method 2")

5.1.2.1. Without Noise

Figure 5-10 through Figure 5-14 show the results of a Monte Carlo analysis of the no-noise Method 2 EKF solution for a short steady flight. The error (z-axis) is the max or mean of the absolute values of the error at each timestep for the pitch and roll axes. This measure of error serves as a simple and intuitive metric for comparing estimators. Whether the plot represents max or mean and pitch or roll, is specified in each figure.

These two figures show that, for the EKF solution that uses only the IMU, the ideal solution uses a Q and R matrix that are as shown in Equations 45 and 46. Note that 1E-10 and 1E10 were chosen arbitrarily as large and small numbers. These figures show that for this EKF configuration, the best solution comes from a small Q and large R such that the solution closely follows the input (u) rather than the measurement (y). With this EKF configuration, that means that the solution closely follows the integration of the gyros.

Note that in these figures, there are smaller errors, relatively, in the corners that represent large Q and small R combinations. This is misleading. This is a downfall to the automated method that was used to collect the Monte Carlo data. If an estimator diverged completely such that the Simulink model stopped producing an estimate, the error that was recorded from then on was 0. This results in apparently low error for divergent solutions. Those solutions, though, all fall near other high error estimates, and the errors follow trends; therefore, it is obvious where this is occurring.

$$Q = \begin{bmatrix} 1 & 0 & 0 \\ 0 & 1 & 0 \\ 0 & 0 & 1 \end{bmatrix} \cdot 1^{-10} \quad (45)$$

$$R = \begin{bmatrix} 1 & 0 & 0 \\ 0 & 1 & 0 \\ 0 & 0 & 1 \end{bmatrix} \cdot 1^{10} \quad (46)$$

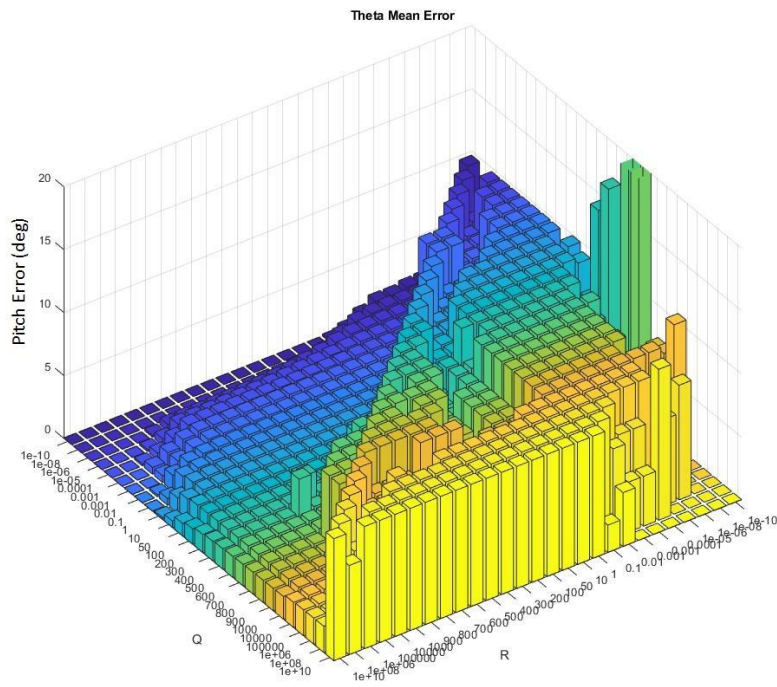


Figure 5-10: Airspeed Aided Attitude EKF - Theta Mean Error - Without Noise

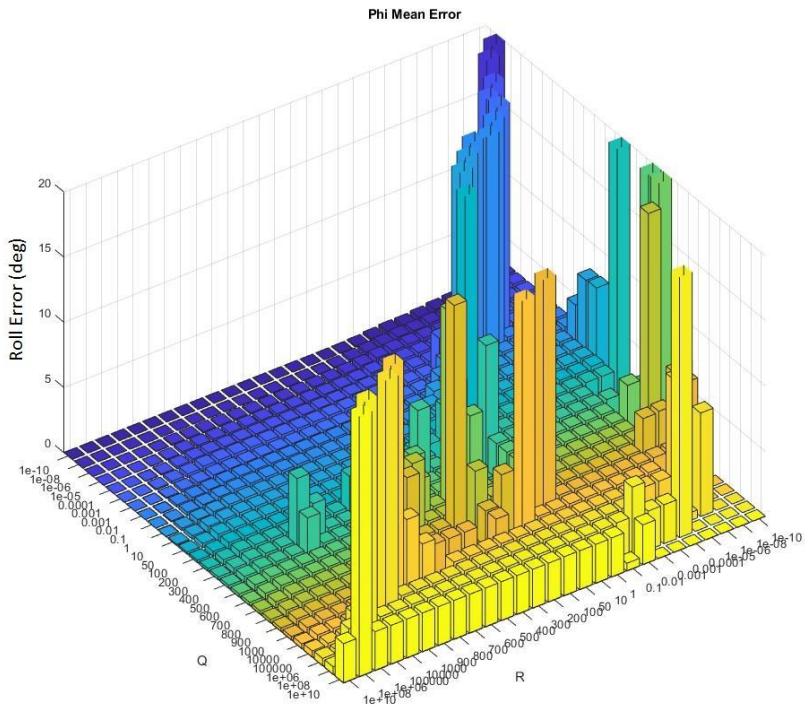


Figure 5-11: Airspeed Aided Attitude EKF - Phi Mean Error - Without Noise

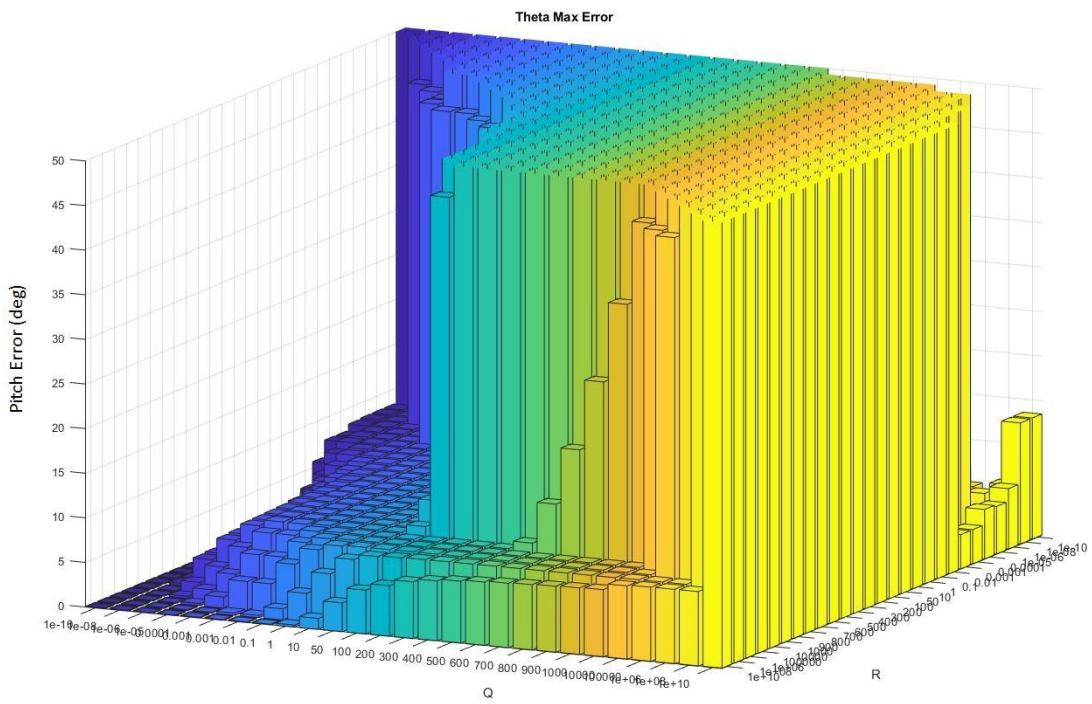


Figure 5-12: Airspeed Aided Attitude EKF - Theta Max Error - Without Noise

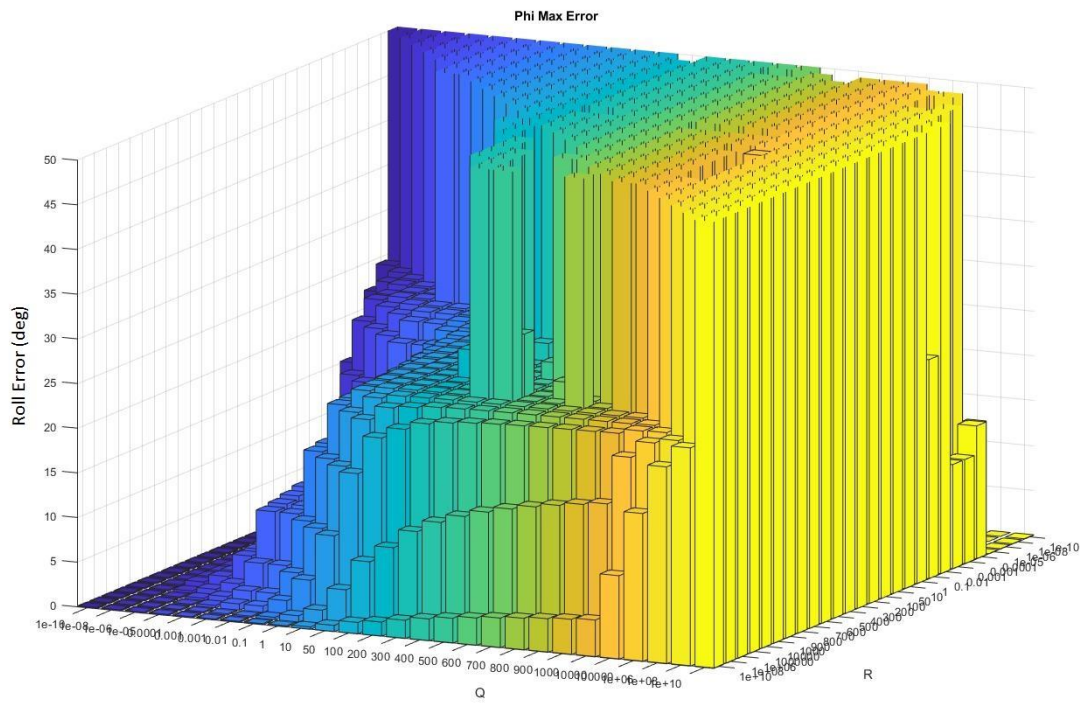


Figure 5-13: Airspeed Aided Attitude EKF - Phi Max Error - Without Noise

5.1.2.2. With Noise

Figure 5-14 through Figure 5-17, below, show the results of a Monte Carlo analysis of the with-noise Method 2 EKF solution for a short steady flight. The noise modeled is gyro covariance of 5 deg/s and accelerometer covariance of 0.003 g's. These noise values are also used for the other estimators' "with-noise" runs in the following subsections.

These figures show, like the complementary filter in the previous section, the optimal Q and R are not the same for both pitch and roll axes. For the pitch estimate, even with noise, the lowest max and mean errors come from the lowest Q and highest R combinations. The roll error estimate plots show a definitive valley of experimentally optimal Q and R matrices that do not include the lowest Q and highest R combinations. These results make sense as the pitch axis had higher frequency maneuvers, while the roll axis had lower frequency maneuvers. That is, maneuvers in the pitch axes were not as observable by the lower frequency component (accelerometer measurement) of the EKF; therefore, the better solution more closely follows the higher frequency component (gyro input). The opposite is true for the roll axes, as the higher frequency gyro input is subject to random walk over lower frequency maneuvers. Both axes show a similar trend for which Q and R combinations produce bad estimates. This observation refines the solution space to a smaller subset of Q and R combinations.

The most restrictive solution space is for the maximum roll error seen in Figure 5-17. For this estimate the most optimal Q and R combination is shown to a Q between 1E-5 and 1E-4 and an R between 1E3 and 1E5. Fortunately, for the short steady flight condition, these Q and R values also show to be within the most optimal solutions of the roll mean error and pitch max and mean error figures.

Note that in these figures, like the no-noise figures, there are small error values in the corners that represent the large Q and small R combinations. This is misleading. This is a downfall to the automated method that was used to collect the Monte Carlo data. If an estimator diverged completely such that the

Simulink model stopped producing an estimate, the error that was recorded from then on was 0. This results in apparently low error for divergent solutions. Those solutions, though, all fall near other high error estimates, and the errors follow trends; therefore, it is obvious where this is occurring.

The chosen experimentally optimal Q and R values to be used as the baseline for the sensitivity analyses of this estimator will come from the values $rk_c = 1000$ and $qk_c = 1E-4$. The rationale is that these values fall toward the middle of optimal "valleys". Additionally, these lean toward the lower R and higher Q, such that the estimator isn't driven so closely to the integration of the gyros—a known flawed solution.

Discussion:

From these results, it can be concluded that the optimal estimate does not use the "standard" method for choosing R as the covariances of the measurements. The results also show that the best choice for tuning parameters is dependent upon the flight conditions that will be observed.

These results, too, suggest that a better EKF estimator may be possible if the Q and R values are dynamic with respect to the current flight conditions. Additionally, since the dynamics of the pitch and roll axes are independent, these results suggest that a better EKF may be possible by estimating each axis with its own EKF estimator. While this sounds extreme, the EKFs would share a lot of the same components. The Jacobians, which constitute the majority of the computation expense, would only have to be computed once for use in multiple EKFs. Therefore, the suggestion of an EKF for each axis would not require 2 or more times the computation cost.

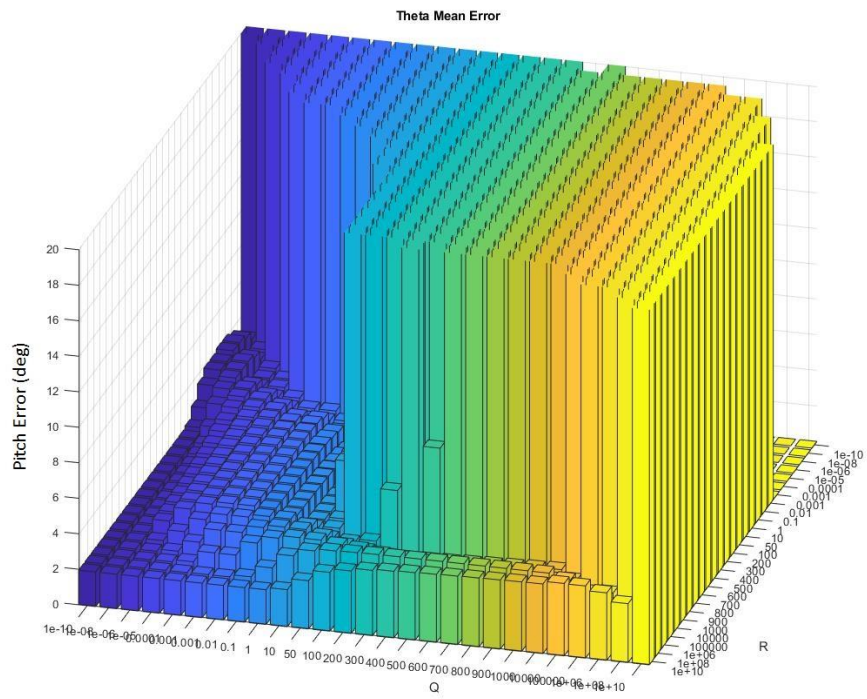


Figure 5-14: Airspeed Aided Attitude EKF - Theta Mean Error - With Noise

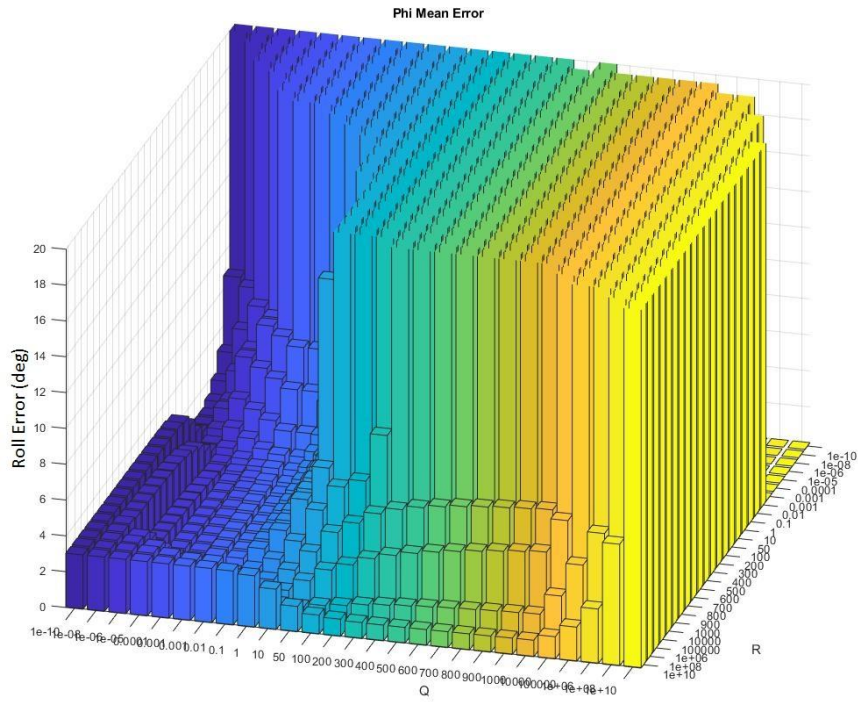


Figure 5-15: Airspeed Aided Attitude EKF - Phi Mean Error - With Noise

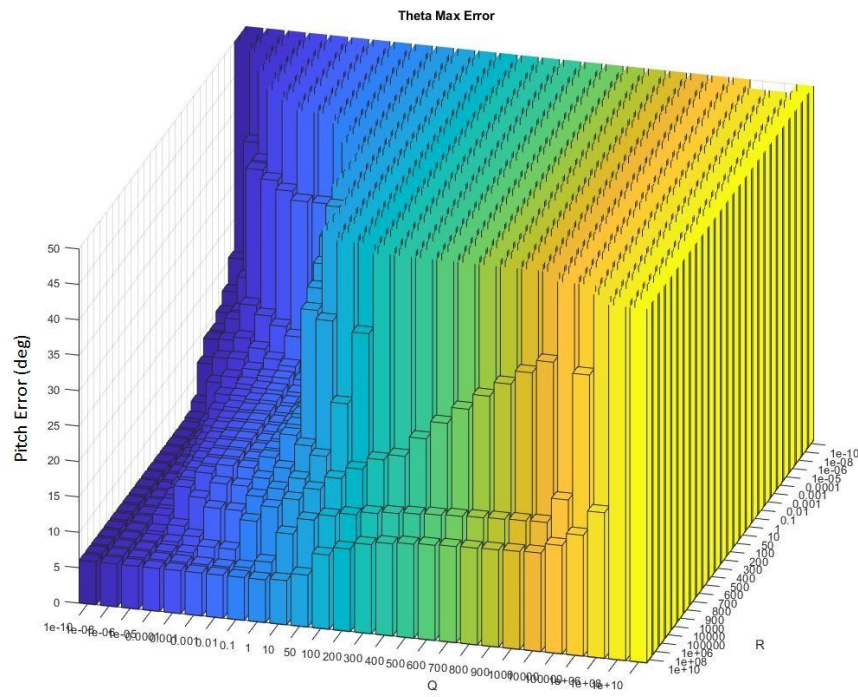


Figure 5-16: Airspeed Aided Attitude EKF - Theta Max Error - With Noise

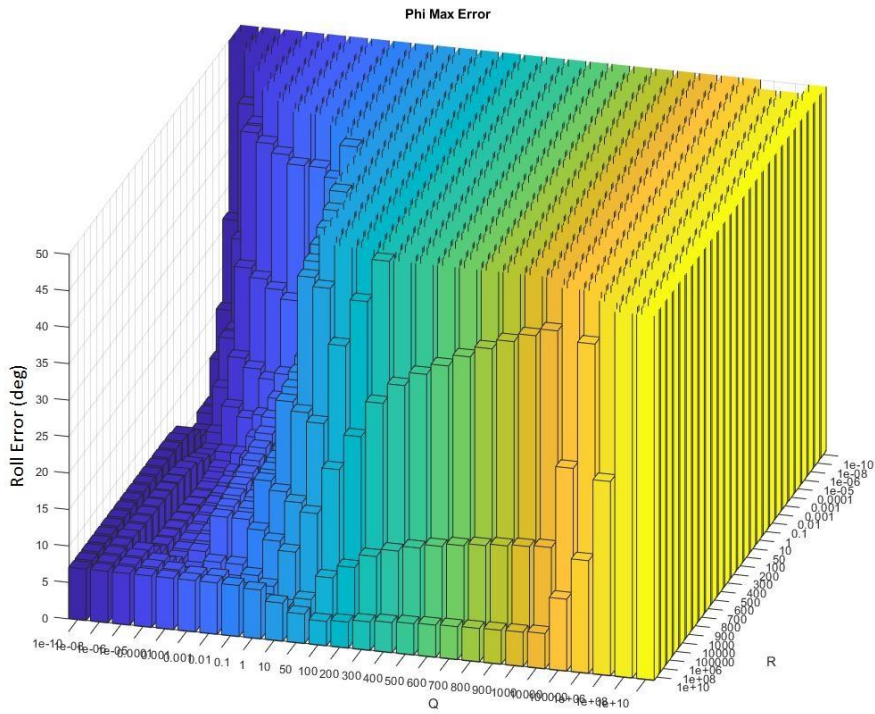


Figure 5-17: Airspeed Aided Attitude EKF - Phi Max Error - With Noise

5.1.3. GPS Aided Inertial Navigation Extended Kalman Filter ("Method 3")

5.1.3.1. Without Noise

Table 5-1 and Table 5-2 show the results of a noiseless 3^4 run Monte Carlo analysis of the no-noise EKF solution for a short steady flight with the specifications listed above the table. Table 5-1 shows the results from Q and R combinations that did not cause the estimator to diverge. Table 5-2 shows the results from Q and R combinations that caused the estimator to diverge. Table 5-2 is important as it can be useful to know what does not work as well as what does. The tuning parameters chosen for this Monte Carlo are representative of a very small number, very large number, and 1. These were chosen as a representative cross section of tuning parameter combinations based on the results from the prior section. The rows are sorted from lowest to highest Total Euler Error from the simulation runs. Total Euler Error is simply the sum of the means of the absolute values of the errors of the three Euler estimates (in degrees), as defined in Equation 47. Similarly, Total Position Error and Total Velocity Error are the sums of the means of the absolute values of the x, y, and z errors of position and velocity, in meters and meters per second, respectively. These serve as a simple, intuitive metrics for the initial evaluation of each Q/R combination. The errors are rounded to the nearest 100th. The last rows, that have no error columns, are the Q/R combinations that caused divergence of any of the state estimates.

$$\text{Total Euler Error} = |\phi_{\text{error}}^{\text{mean}}| + |\theta_{\text{error}}^{\text{mean}}| + |\Psi_{\text{error}}^{\text{mean}}| \quad (47)$$

Table 5-1: Monte Carlo Results from EKF ("Method 3") - Without Noise - Theoretical Q/R

Row #(/81)	rkc2	rkc1	qkc2	qkc1	Errors					
					Mean phi	Mean theta	Mean psi	Total Euler	Total Position	Total Velocity
1	1E-11	1E-11	1E-11	1	0.01	0.01	0.01	0.03	0	0.19
2	1E-11	1E-11	1E-11	99999999	0.01	0.01	0.01	0.03	0	0.19
3	1E-11	1E-11	1	99999999	0.01	0.01	0.01	0.03	0	0.19
4	1E-11	1	1E-11	1	0.01	0.01	0.01	0.03	0	0.19
5	1E-11	1	1E-11	99999999	0.01	0.01	0.01	0.03	0	0.19
6	1E-11	1	1	99999999	0.01	0.01	0.01	0.03	0	0.19
7	1E-11	99999999	1E-11	1	0.01	0.01	0.01	0.03	0	0.19
8	1E-11	99999999	1E-11	99999999	0.01	0.01	0.01	0.03	0	0.19
9	1E-11	99999999	1	99999999	0.01	0.01	0.01	0.03	0	0.19
10	1	1E-11	1E-11	1	0.01	0.01	0.01	0.03	0	0.18
11	1	1E-11	1E-11	99999999	0.01	0.01	0.01	0.03	0	0.19
12	1	1E-11	1	99999999	0.01	0.01	0.01	0.03	0	0.19
13	1	1	1E-11	1	0.01	0.01	0.01	0.03	0	0.18
14	1	1	1E-11	99999999	0.01	0.01	0.01	0.03	0	0.19
15	1	1	1	99999999	0.01	0.01	0.01	0.03	0	0.19
16	1	99999999	1E-11	1	0.01	0.01	0.01	0.03	0	0.18
17	1	99999999	1E-11	99999999	0.01	0.01	0.01	0.03	0	0.19
18	1	99999999	1	99999999	0.01	0.01	0.01	0.03	0	0.19
19	99999999	1E-11	1E-11	1	0.01	0.01	0.01	0.03	6.02	3.04
20	99999999	1E-11	1E-11	99999999	0.01	0.01	0.01	0.03	0	0.18
21	99999999	1E-11	1	99999999	0.01	0.01	0.01	0.03	0	0.18
22	99999999	1	1E-11	1	0.01	0.01	0.01	0.03	5.16	2.18
23	99999999	1	1E-11	99999999	0.01	0.01	0.01	0.03	0	0.18
24	99999999	1	1	99999999	0.01	0.01	0.01	0.03	0	0.18
25	99999999	99999999	1E-11	1E-11	0.01	0.01	0.01	0.03	3.19	0.24
26	99999999	99999999	1E-11	1	0.01	0.01	0.01	0.03	3.08	0.21
27	99999999	99999999	1E-11	99999999	0.01	0.01	0.01	0.03	0	0.18
28	99999999	99999999	1	99999999	0.01	0.01	0.01	0.03	0	0.18
29	1	99999999	1E-11	1E-11	0.01	0.01	0.02	0.04	0	0.2
30	1	1	1E-11	1E-11	0.01	0.08	0.07	0.16	4.1	0.3
31	99999999	1	1E-11	1E-11	0.01	0.08	0.07	0.16	4.13	0.31
32	99999999	99999999	1	1E-11	0.05	0.21	0.32	0.58	3.24	0.25
33	99999999	99999999	1	1	0.04	0.17	0.4	0.61	3.18	0.25
34	1E-11	1	1E-11	1E-11	39.89	3.34	46.45	89.68	5.99	0.32
35	1E-11	99999999	1E-11	1E-11	39.89	3.34	46.45	89.68	5.99	0.32
36	1	99999999	1	1	39.89	3.34	46.45	89.68	5.66	0.32
37	1	99999999	1	1E-11	40.17	3.66	47.89	91.72	6.08	0.33
38	1	1E-11	1	1	40.72	3.54	47.76	92.02	6	0.32
39	99999999	1E-11	99999999	99999999	40.72	3.54	47.76	92.02	6	0.32
40	99999999	1	99999999	99999999	40.72	3.54	47.76	92.02	6	0.32
41	1E-11	1E-11	1E-11	1E-11	40.24	3.81	48.7	92.75	5.12	0.32
42	1	1	1	1	40.24	3.81	48.7	92.75	5.12	0.32
43	99999999	99999999	99999999	99999999	40.24	3.81	48.7	92.75	5.12	0.32
44	1E-11	1E-11	99999999	99999999	68.36	4.11	49.16	121.63	6	0.29
45	1E-11	1	99999999	99999999	68.36	4.11	49.16	121.63	6	0.29
46	1E-11	1E-11	1	1	67.94	4.09	49.76	121.79	6	0.29
47	1E-11	99999999	1	1	68.24	4.11	49.67	122.02	5.71	0.29
48	1E-11	99999999	99999999	99999999	68.4	4.11	49.51	122.02	5.12	0.29
49	1E-11	1	1	1	68.07	4.09	49.96	122.12	5.12	0.29
50	1	99999999	99999999	99999999	68.5	4.09	49.72	122.31	5.12	0.29
51	1	1E-11	99999999	99999999	68.4	4.1	50.05	122.55	6	0.29
52	1	1	99999999	99999999	68.4	4.1	50.05	122.55	6	0.29

Table 5-2: Monte Carlo Results from EKF ("Method 3") - Without Noise - Theoretical Q/R – Divergent Q/R Combinations

Row #(/81)	rkc2	rkc1	qkc2	qkc1
53	1E-11	1E-11	1	1E-11
54	1E-11	1E-11	99999999	1E-11
55	1E-11	1E-11	99999999	1
56	1E-11	1	1	1E-11
57	1E-11	1	99999999	1E-11
58	1E-11	1	99999999	1
59	1E-11	99999999	1	1E-11
60	1E-11	99999999	99999999	1E-11
61	1E-11	99999999	99999999	1
62	1	1E-11	1E-11	1E-11
63	1	1E-11	1	1E-11
64	1	1E-11	99999999	1E-11
65	1	1E-11	99999999	1
66	1	1	1	1E-11
67	1	1	99999999	1E-11
68	1	1	99999999	1
69	1	99999999	99999999	1E-11
70	1	99999999	99999999	1
71	99999999	1E-11	1E-11	1E-11
72	99999999	1E-11	1	1E-11
73	99999999	1E-11	1	1
74	99999999	1E-11	99999999	1E-11
75	99999999	1E-11	99999999	1
76	99999999	1	1	1E-11
77	99999999	1	1	1
78	99999999	1	99999999	1E-11
79	99999999	1	99999999	1
80	99999999	99999999	99999999	1E-11
81	99999999	99999999	99999999	1

5.1.3.2. With Noise

Table 5-3 and Table 5-4 show two subsets of a Monte Carlo analysis of the with-noise EKF solution for a short steady flight with the specifications and Q/R combinations listed above the table. The value in the "Row #/(5184)" column is the rank from best (1) to worst (5184) of the estimators, based on Total Euler Error. Table 5-3 shows the Q/R combinations that produced the best 50 Euler estimates, based on lowest Total Euler Error. Table 5-4 shows all runs with the R matrix that would have been used if the R matrix was chosen to be a diagonal matrix of the covariance of the sensors. The covariances of the GPS position and velocity modeled in the GPS noise model are 3.048m and 6.096m/s, respectively.

Choosing the R matrix to be a diagonal matrix of the sensor covariance is a standard approach. The optimal estimation solution (by mathematical proof) for a pure Kalman Filter would have the R matrix formulated in this way. Keep in mind that the optimal estimation solution of a Kalman Filter also comes with assumptions about the noise, and does not account for the measurement occurring at a different frequency than the estimator, as the GPS does in these experiments (GPS: 10Hz; Estimator: 50Hz). Additionally, the optimal estimation proof is not valid for EKFs or UKFs, as they are not optimal estimators. Nonetheless, it is standard practice to use the sensor covariance directly for the choice of the R matrix.

Table 5-3 shows that the "standard" choice for the R matrix is not represented in the top 50 (out of 5184) Euler estimates. In fact, only 14 out of the top 50 are even multiples of the "standard" covariances (rows 11, 14, 15, 20-22, 24-28, 31, 32, and 33). The majority of the top 50 Euler estimates have, at least, one half of the covariances in the diagonal of the R matrix as 99999999, which is a non-intuitive (per theory) and different from the standard practice choice for the R matrix. Some of the top 50 estimators for estimating Euler angles, though, do not produce adequate position and velocity estimates (rows highlighted red).

Additionally, it appears that a low q_1/q_2 ratio appears to drive a good Euler estimate. This can be seen in Table 5-3, in that all of the top 50 estimates, less the rows with bad position or velocity estimates (highlighted red), have a low q_1/q_2 regardless of what the r_1 and r_2 values are. Though not directly analogous, this is similar to the results of the previous estimators in that the experimentally optimal solution comes from small covariances assigned to the gyro and larger assigned to the accelerometer.

Table 5-4 shows that, although not optimal (by experiment), the standard practice choice for the R matrix can be used to produce an adequate estimation of Euler angles, position, and velocity. The results produced below show that the optimal (by experiment) estimator produces a Total Euler Error of 2.5deg, while the best estimator that uses a standard practice R matrix produces a Total Euler Error of 4.42deg).

The chosen experimentally optimal Q and R values to be used as the baseline for the sensitivity analyses of this estimator will come from the values in row 1 (highlighted cyan).

Discussion:

Table 5-3 and Table 5-4 provide evidence that the standard practice method of determining the R matrix may not produce experimentally optimal results. However, computational performance could limit the ability to choose very large and very small numbers, as seen in the Q/R matrices of the best estimators.

Table 5-3: Monte Carlo Results from EKF ("Method 3") - With Noise

Row	rkc2	rkc1	qkc2	qkc1	Errors					
					Mean	Mean	Mean	Total	Total	Total
1	99999999	99999999	1	1000	0.44	0.69	1.37	2.5	3.38	0.71
2	99999999	99999999	0.1	100	0.51	0.66	1.43	2.6	3.75	0.88
3	99999999	99999999	0.1	1000	0.57	0.73	1.44	2.74	3.46	0.83
4	99999999	99999999	0.01	10	0.7	0.74	1.47	2.91	6	1.54
5	99999999	99999999	0.1	10	0.56	0.66	1.85	3.07	5.08	1.08
6	99999999	99999999	0.01	100	0.73	0.82	1.55	3.1	4.54	1.39
7	99999999	99999999	1	100	0.47	0.78	1.93	3.18	3.73	0.79
8	99999999	30.48	0.0001	1	0.81	1.32	1.39	3.52	4.99	3.08
9	0.006096	99999999	1E-11	1E-11	0.71	0.82	2	3.53	37.52	2.23
10	99999999	99999999	0.001	1	0.92	1.02	1.59	3.53	14.07	2.94
11	0.006096	30.48	1E-11	1E-11	0.7	0.81	2.03	3.54	36.51	2.18
12	0.06096	99999999	1E-11	1E-11	0.91	1.06	1.58	3.55	57.13	3.75
13	99999999	99999999	0.01	1	0.79	0.78	1.99	3.56	9.58	1.94
14	0.06096	30.48	1E-11	1E-11	0.89	1.06	1.66	3.61	47.6	3.53
15	0.006096	3.048	1E-11	1E-11	0.68	0.81	2.22	3.71	28.7	1.96
16	99999999	99999999	0.001	10	0.93	0.99	1.83	3.75	9.65	2.59
17	0.006096	1	1E-11	1E-11	0.66	0.82	2.4	3.88	21.37	1.74
18	60.96	99999999	0.0001	1	0.97	1.49	1.56	4.02	10.48	3.29
19	60.96	99999999	0.0001	10	0.86	1.41	1.76	4.03	9.79	5.34
20	60.96	30.48	0.0001	10	0.86	1.42	1.77	4.05	6.57	5.36
21	60.96	3.048	0.0001	10	0.86	1.41	1.8	4.07	7.71	5.35
22	60.96	1	0.0001	10	0.86	1.41	1.81	4.08	7.91	5.35
23	99999999	99999999	0.001	0.1	0.97	1.15	1.97	4.09	20.25	3.35
24	60.96	0.0003048	0.0001	10	0.86	1.41	1.82	4.09	8.03	5.35
25	60.96	0.003048	0.0001	10	0.86	1.41	1.82	4.09	8.03	5.35
26	60.96	0.03048	0.0001	10	0.86	1.41	1.82	4.09	8.02	5.35
27	60.96	0.3048	0.0001	10	0.86	1.41	1.82	4.09	7.99	5.35
28	60.96	30.48	0.0001	1	1	1.54	1.58	4.12	4.94	3.39
29	99999999	30.48	0.0001	10	0.97	1.27	1.9	4.14	6.6	4.51
30	99999999	99999999	0.01	1000	1.04	1.04	2.08	4.16	3.94	1.33
31	0.006096	0.3048	1E-11	1E-11	0.69	0.87	2.65	4.21	14.86	1.53
32	0.06096	3.048	1E-11	1E-11	0.87	1.1	2.26	4.23	30.22	3
33	60.96	3.048	0.0001	1	1.02	1.6	1.65	4.27	6.53	3.47
34	99999999	30.48	0.001	100	0.97	1.46	1.86	4.29	7.73	5.37
35	99999999	3.048	0.0001	10	0.97	1.47	1.86	4.3	7.73	5.39
36	99999999	1	0.0001	10	0.96	1.5	1.86	4.32	7.92	5.54
37	99999999	30.48	0.01	1000	0.96	1.51	1.86	4.33	8.01	5.54
38	99999999	1	0.001	100	0.96	1.52	1.87	4.35	8.03	5.62
39	99999999	1	0.01	1000	0.96	1.52	1.87	4.35	8.05	5.57
40	99999999	0.0003048	0.01	1000	0.96	1.52	1.87	4.35	8.05	5.57
41	99999999	0.003048	0.01	1000	0.96	1.52	1.87	4.35	8.05	5.57
42	99999999	0.03048	0.01	1000	0.96	1.52	1.87	4.35	8.05	5.57
43	99999999	0.3048	0.0001	10	0.96	1.52	1.87	4.35	8.01	5.6
44	99999999	0.3048	0.01	1000	0.96	1.52	1.87	4.35	8.05	5.57
45	99999999	3.048	0.001	100	0.96	1.52	1.87	4.35	8.01	5.6
46	99999999	3.048	0.01	1000	0.96	1.52	1.87	4.35	8.05	5.57
47	99999999	99999999	10	1000	0.73	1.13	2.5	4.36	3.49	0.93
48	99999999	0.0003048	0.0001	10	0.96	1.53	1.87	4.36	8.05	5.64
49	99999999	0.0003048	0.001	100	0.96	1.53	1.87	4.36	8.05	5.63
50	99999999	0.003048	0.0001	10	0.96	1.53	1.87	4.36	8.05	5.64

Table 5-4: Monte Carlo Results from EKF ("Method 3") - With Noise – Q/R Combinations with Traditional R Values

Row	rkc2	rkc1	qkc2	qkc1	Errors					
					Mean	Mean	Mean	Total	Total	Total
59	6.096	3.048	0.0001	10	0.93	1.89	1.6	4.42	7.73	6.13
125	6.096	3.048	0.001	100	1.09	2.45	1.54	5.08	8	6.15
177	6.096	3.048	0.01	1000	1.18	2.67	1.51	5.36	8.03	6.15
304	6.096	3.048	0.0001	100	1.88	1.59	2.68	6.15	8	6.15
392	6.096	3.048	0.001	1000	1.88	1.61	2.67	6.16	8.03	6.15
540	6.096	3.048	0.0001	1000	2.81	1.85	2.88	7.54	8.03	6.15
572	6.096	3.048	1E-11	0.0001	2.82	1.85	2.89	7.56	4.54	2.18
638	6.096	3.048	1E-11	0.001	3.01	1.91	2.9	7.82	3.66	1.5
976	6.096	3.048	1E-11	1	3.03	1.92	2.9	7.85	6.57	5.34
977	6.096	3.048	1E-11	0.01	3.03	1.92	2.9	7.85	3.96	1.89
978	6.096	3.048	1E-11	0.1	3.03	1.92	2.9	7.85	4.94	3.33
979	6.096	3.048	1E-11	10	3.03	1.92	2.9	7.85	7.73	6.12
980	6.096	3.048	1E-11	100	3.03	1.92	2.9	7.85	8	6.15
981	6.096	3.048	1E-11	1000	3.03	1.92	2.9	7.85	8.03	6.15
1036	6.096	3.048	0.0001	1	2.34	3.25	2.29	7.88	6.57	5.39
1085	6.096	3.048	0.001	10	4.74	5.58	3	13.32	7.73	6.16
1143	6.096	3.048	0.01	100	47.47	7.18	10.88	65.53	8	6.18
1191	6.096	3.048	0.1	1000	50.1	7.9	13.25	71.25	8.03	6.18
1298	6.096	3.048	0.0001	0.1	52.33	6.59	40.12	99.04	4.94	4.08
1331	6.096	3.048	0.0001	0.01	55.63	7.63	46.04	109.3	4.09	4
1369	6.096	3.048	0.0001	0.001	57.81	8.18	47.23	113.22	3.97	4.28
1373	6.096	3.048	0.01	10	64.66	13.95	34.75	113.36	7.73	6.22
1423	6.096	3.048	0.001	1	60.26	10.69	45.89	116.84	6.58	5.56
1434	6.096	3.048	0.0001	0.0001	59.79	8.61	48.78	117.18	4.46	4.78
1470	6.096	3.048	0.001	0.1	61.47	12.95	49.24	123.66	4.96	4.29
1491	6.096	3.048	0.0001	1E-11	61.5	10.06	55.55	127.11	5.04	5.23
1550	6.096	3.048	1	1000	67.97	17.76	45.16	130.89	8.03	6.2
1690	6.096	3.048	0.1	100	67.15	16.69	54.33	138.17	8	6.2
1731	6.096	3.048	0.1	10	105.68	22.32	103.56	231.56	7.73	6.25
1784	6.096	3.048	0.01	0.0001	124.86	24.32	96.18	245.36	3.86	5.14
1800	6.096	3.048	0.01	1E-11	127.31	25.15	95.26	247.72	3.85	5.16
1812	6.096	3.048	0.01	0.001	125.93	25.03	98.62	249.58	3.89	5.17
1825	6.096	3.048	0.01	0.1	130.16	22.94	98.51	251.61	5	5.14
1840	6.096	3.048	0.01	0.01	125.24	24.71	104.44	254.39	4.13	5.1
1885	6.096	3.048	0.001	0.01	147.41	15.03	96.29	258.73	4.17	5.29
1942	6.096	3.048	0.01	1	153.03	18.71	99.98	271.72	6.58	5.9
1952	6.096	3.048	0.001	0.001	158.33	15.02	100.22	273.57	3.98	5.6
1981	6.096	3.048	0.001	0.0001	160.68	15.75	100.83	277.26	3.96	5.61
1992	6.096	3.048	0.001	1E-11	160.97	15.74	101.2	277.91	3.97	5.6

5.1.4. GPS Aided Inertial Navigation Unscented Kalman Filter ("Method 4")

5.1.4.1. Without Noise

Table 5-5 and Table 5-6 show the results of a noiseless 3^4 run Monte Carlo analysis of the no-noise UKF solution for a short steady flight with the specifications listed above the table. The rows are sorted from lowest to highest Total Euler Error from the simulation runs. Table 5-6 has no error columns, as it contains only the Q/R combinations that caused divergence in any of the state estimates.

Comparing Table 5-5 with Table 5-1, provides useful insight for choosing between the EKF and UKF solutions. It should be noted that the best Euler estimate comes from the same Q/R combination in the EKF and UKF. This result is evidence that the solutions are both implemented correctly.

The Total Euler Error is lower for the EKF solution: 0.03deg error for the EKF vs. 0.28 deg error for the UKF. The Total Position and Velocity Errors, though are 0 for the UKF, while they are 6m and 0.19m/s for the EKF. This result indicates that the ideal no-noise EKF solution produces a more accurate Euler estimate, while the ideal no-noise UKF solution produces more accurate position and velocity estimates.

The most notable difference between the two results is that the EKF has more combinations of acceptable Q/R choices. This indicates that the EKF solution is more robust to a sub-optimal design, while the UKF solution may be more robust to computation rate and aliasing.

It may be worth noting that all of the Q/R combinations that produced adequate estimates in the UKF solution (rows 1-8), also produced adequate estimates in the EKF solution. The inverse scenario is not true, which agrees with the conclusions about robustness discussed in the previous paragraph.

Table 5-5: Monte Carlo Results from UKF ("Method 4") - Without Noise - Theoretical Q/R

Row #/(81)	rkc2	rkc1	qkc2	qkc1	Errors					
					Mean phi	Mean theta	Mean psi	Total Euler	Total Position	Total Velocity
1	1E-11	1E-11	1E-11	1	0.02	0.02	0.24	0.28	0	0
2	1E-11	1	1E-11	1	0.02	0.02	0.24	0.28	0.8	0
3	1	1E-11	1E-11	1	0.02	0.02	0.24	0.28	0	0.13
4	1	1	1E-11	1	0.02	0.02	0.24	0.28	0.79	0.13
5	1	99999999	1E-11	1	0.02	0.01	0.28	0.31	62.17	0.09
6	1E-11	99999999	1E-11	1	0.03	0.01	0.28	0.32	61.86	0
7	99999999	1	1E-11	1	0.13	0.04	0.96	1.13	0.79	27.14
8	99999999	1E-11	1E-11	1	0.17	0.05	1.09	1.31	0	30.56
9	1	99999999	1E-11	1E-11	15.07	10.59	6.01	31.67	2741.44	37.53
10	99999999	99999999	1E-11	1E-11	0.81	1.18	59.92	61.91	1092.84	97.2
11	99999999	1	1E-11	1E-11	26.13	13.58	49.53	89.24	113.09	43.2
12	1	1	1E-11	1E-11	25.78	16.24	52.16	94.18	107.96	39.82
13	99999999	99999999	1	1	15.73	15.93	83.76	115.42	1351.55	1517.46
14	99999999	99999999	1	99999999	6.91	4.38	105.34	116.63	2.35	54.81
15	99999999	99999999	1	1E-11	15.31	16.17	85.75	117.23	1356.87	1521.33
16	1E-11	99999999	1	99999999	6.91	4.38	107.58	118.87	2.75	0
17	1E-11	1E-11	1	99999999	6.91	4.39	107.6	118.9	0	0
18	99999999	1E-11	1	99999999	6.91	4.38	107.65	118.94	0	54.83
19	1	99999999	1	99999999	6.91	4.38	107.71	119	2.75	0
20	99999999	1	1	99999999	6.91	4.38	107.78	119.07	0	54.83
21	1	1E-11	1	99999999	6.91	4.38	107.87	119.16	0	0
22	1	1	1	99999999	6.91	4.38	108.53	119.82	0	0
23	1E-11	1	1	99999999	6.91	4.38	108.88	120.17	0	0
24	99999999	99999999	1E-11	1	1.14	3.83	139.51	144.48	468.13	77.58
25	1E-11	1E-11	1E-11	99999999	6.6	4.39	172.72	183.71	0	0
26	1	1E-11	1E-11	99999999	6.6	4.39	172.72	183.71	0	0
27	1E-11	1	1E-11	99999999	6.6	4.39	172.73	183.72	0	0
28	1	1	1E-11	99999999	6.6	4.39	172.73	183.72	0	0
29	99999999	1E-11	1E-11	99999999	6.6	4.39	172.73	183.72	0	0.49
30	99999999	1	1E-11	99999999	6.6	4.39	172.73	183.72	0	0.49
31	1E-11	99999999	1E-11	99999999	6.61	4.39	172.73	183.73	1.95	0
32	1	99999999	1E-11	99999999	6.61	4.39	172.73	183.73	1.95	0
33	99999999	99999999	1E-11	99999999	6.61	4.39	172.77	183.77	1.96	0.48

Table 5-6: Monte Carlo Results from UKF ("Method 4") - Without Noise - Theoretical Q/R – Divergent Q/R Combinations

Row #/(81)	rkc2	rkc1	qkc2	qkc1
34	1E-11	1E-11	1E-11	1E-11
35	1E-11	1E-11	1	1E-11
36	1E-11	1E-11	1	1
37	1E-11	1E-11	99999999	1E-11
38	1E-11	1E-11	99999999	1
39	1E-11	1E-11	99999999	99999999
40	1E-11	1	1E-11	1E-11
41	1E-11	1	1	1E-11
42	1E-11	1	1	1
43	1E-11	1	99999999	1E-11
44	1E-11	1	99999999	1
45	1E-11	1	99999999	99999999
46	1E-11	99999999	1E-11	1E-11
47	1E-11	99999999	1	1E-11
48	1E-11	99999999	1	1
49	1E-11	99999999	99999999	1E-11
50	1E-11	99999999	99999999	1
51	1E-11	99999999	99999999	99999999
52	1	1E-11	1E-11	1E-11
53	1	1E-11	1	1E-11
54	1	1E-11	1	1
55	1	1E-11	99999999	1E-11
56	1	1E-11	99999999	1
57	1	1E-11	99999999	99999999
58	1	1	1	1E-11
59	1	1	1	1
60	1	1	99999999	1E-11
61	1	1	99999999	1
62	1	1	99999999	99999999
63	1	99999999	1	1E-11
64	1	99999999	1	1
65	1	99999999	99999999	1E-11
66	1	99999999	99999999	1
67	1	99999999	99999999	99999999
68	99999999	1E-11	1E-11	1E-11
69	99999999	1E-11	1	1E-11
70	99999999	1E-11	1	1
71	99999999	1E-11	99999999	1E-11
72	99999999	1E-11	99999999	1
73	99999999	1E-11	99999999	99999999
74	99999999	1	1	1E-11
75	99999999	1	1	1
76	99999999	1	99999999	1E-11
77	99999999	1	99999999	1
78	99999999	1	99999999	99999999
79	99999999	99999999	99999999	1E-11
80	99999999	99999999	99999999	1
81	99999999	99999999	99999999	99999999

5.1.4.2. With Noise

Table 5-7 and Table 5-8 show two subsets of a Monte Carlo analysis of the with-noise UKF solution for a short steady flight with the specifications and Q/R combinations listed above the table. The value in the "Row #(/5184)" column is the rank from best (1) to worst (5184) of the estimators, based on Total Euler Error. The first 50 rows of the table are the best 50 Euler estimates (lowest Total Euler Error). The last portion of the table (separated by a slightly thicker borderline) represents all runs with the R matrix that would have been used if the R matrix was chosen to be a diagonal matrix of the covariance of the sensors. The covariances of the GPS position and velocity modeled in the GPS noise model are 3.048m and 6.096m/s, respectively.

Table 5-7 shows that, like the EKF solution, the "standard" choice for the R matrix is not represented in the top 50. Unlike the EKF solution, though, the majority of the top 50 are multiples of the covariances of the sensors.

The chosen experimentally optimal Q and R values to be used as the baseline for the sensitivity analyses of this estimator will come from the values in row 3 (highlighted cyan). This is the lowest total Euler error that correlates to reasonable velocity and position estimates.

Discussion:

Table 5-7 shows that there is one qkc2 value that produces the most accurate estimates regardless of qkc1, rkc1, and rkc2 values (1E-11). This is also evident in Table 5-5, though less obvious, as there are many less adequate Euler estimates (rows 1-8 only). This suggests that Q and R are more independent of each other for UKF solutions than they are for the EKF solutions. This is supported by the formulae of the two solutions, in that the Kalman gain of the EKF can be looked at as a scalar function of Q divided by R [13] while the Kalman gain of the UKF is less direct; The UKF Kalman gain is influenced by Q only through the UKF Kalman gain being a function of x_{k-1} , which is a function of Q.

The ratio of Q/R being more influential on the EKF solution than the UKF would provide rationale as to why the EKF had so many more combinations of Q/R that produced adequate estimates than the UKF. That is, since the qkc and rkc values were all multiples of each other, there were multiple instances in which the same Q/R ratio was achieved.

Table 5-7: Monte Carlo Results from UKF ("Method 4") - With Noise

Row #/(5184)	rkc2	rkc1	qkc2	qkc1	Errors					
					Mean phi	Mean theta	Mean psi	Total Euler	Total Position	Total Velocity
1	60.96	0.0003048	1E-11	0.001	3	2	2.36	7.36	4.57	38.83
2	6.096	0.0003048	1E-11	0.001	3.02	2.04	2.3	7.36	4.5	34.97
3	0.0006096	0.0003048	1E-11	0.0001	3	1.91	2.71	7.62	3.89	3.73
4	99999999	0.0003048	1E-11	0.001	3.08	2.02	2.54	7.64	4.51	41.69
5	1	0.0003048	1E-11	0.001	3.01	1.94	2.84	7.79	4.37	20.06
6	0.0006096	0.0003048	1E-11	0.001	3.01	1.92	3	7.93	4.33	4.79
7	0.6096	0.0003048	1E-11	0.001	3.03	1.92	3	7.95	4.26	14.98
8	0.06096	0.0003048	1E-11	0.001	3.08	1.96	2.92	7.96	4.27	3.82
9	0.06096	0.0003048	1E-11	0.0001	3.03	1.91	3.03	7.97	5.16	36.83
10	1	0.0003048	1E-11	0.0001	3.03	1.93	3.04	8	5.14	21.17
11	1	0.0003048	1E-11	0.0001	3.12	2.32	2.58	8.02	14.01	109.77
12	0.006096	0.0003048	1E-11	0.001	3	1.92	3.11	8.03	4.15	3.62
13	0.6096	0.0003048	1E-11	0.0001	3.03	1.93	3.07	8.03	4.78	17.49
14	60.96	0.0003048	1E-11	0.0001	3.03	1.92	3.08	8.03	5.22	27.9
15	0.0006096	0.0003048	1E-11	0.0001	3.03	1.93	3.08	8.04	3.88	3.84
16	0.06096	0.0003048	1E-11	0.0001	3.03	1.93	3.08	8.04	3.96	5.61
17	0.06096	0.3048	1E-11	0.01	3.04	1.92	3.08	8.04	3.82	3.96
18	0.6096	3.048	1E-11	0.1	3.04	1.92	3.08	8.04	3.82	3.96
19	6.096	0.0003048	1E-11	0.01	3.04	1.92	3.08	8.04	4.26	2.62
20	6.096	0.0003048	1E-11	0.0001	3.02	1.92	3.1	8.04	5.3	26.55
21	60.96	0.0003048	1E-11	0.1	3.04	1.92	3.08	8.04	4.34	2.65
22	60.96	0.0003048	1E-11	0.1	3.04	1.92	3.08	8.04	4.26	2.62
23	1	1	1E-11	0.1	3.04	1.92	3.09	8.05	3.82	3.83
24	1	0.0003048	1E-11	0.01	3.04	1.92	3.09	8.05	4.26	2.61
25	1	0.0003048	1E-11	0.1	3.04	1.92	3.09	8.05	4.34	3.77
26	1	0.003048	1E-11	0.1	3.04	1.92	3.09	8.05	4.26	3.77
27	1	0.03048	1E-11	0.1	3.04	1.92	3.09	8.05	3.88	3.79
28	1	0.3048	1E-11	0.1	3.04	1.92	3.09	8.05	3.78	3.83
29	1	3.048	1E-11	0.1	3.04	1.92	3.09	8.05	3.76	3.83
30	99999999	0.003048	1E-11	0.0001	3.04	1.92	3.09	8.05	5.52	28.54
31	0.006096	0.003048	1E-11	0.0001	3.03	1.93	3.09	8.05	3.73	3.06
32	0.006096	0.003048	1E-11	0.001	3.04	1.93	3.08	8.05	3.8	3.93
33	0.006096	0.03048	1E-11	0.001	3.04	1.93	3.08	8.05	3.82	3.96
34	0.06096	1	1E-11	0.01	3.04	1.93	3.08	8.05	4.05	3.96
35	0.06096	0.0003048	1E-11	0.01	3.04	1.92	3.09	8.05	4.26	3.93
36	0.06096	0.003048	1E-11	0.01	3.04	1.92	3.09	8.05	3.88	3.94
37	0.06096	0.03048	1E-11	0.01	3.04	1.92	3.09	8.05	3.78	3.96
38	0.6096	1	1E-11	0.1	3.04	1.92	3.09	8.05	3.85	3.96
39	0.6096	0.0003048	1E-11	0.01	3.04	1.92	3.09	8.05	4.26	2.84
40	0.6096	0.0003048	1E-11	0.1	3.04	1.92	3.09	8.05	4.34	3.93
41	0.6096	0.003048	1E-11	0.1	3.04	1.92	3.09	8.05	4.26	3.93
42	0.6096	0.03048	1E-11	0.1	3.04	1.92	3.09	8.05	3.88	3.94
43	0.6096	0.3048	1E-11	0.1	3.04	1.92	3.09	8.05	3.78	3.96
44	0.6096	3.048	1E-11	0.01	3.04	1.92	3.09	8.05	3.51	2.95
45	6.096	1	1E-11	1	3.04	1.92	3.09	8.05	3.73	3.94
46	6.096	0.0003048	1E-11	1	3.04	1.92	3.09	8.05	4.35	3.92
47	6.096	0.0003048	1E-11	0.1	3.04	1.92	3.09	8.05	4.34	2.84
48	6.096	0.003048	1E-11	1	3.04	1.92	3.09	8.05	4.34	3.93
49	6.096	0.03048	1E-11	0.001	3.04	1.93	3.08	8.05	3.78	7
50	6.096	0.003048	1E-11	0.01	3.04	1.92	3.09	8.05	3.88	2.46

Table 5-8: Monte Carlo Results from UKF ("Method 4") - With Noise – Q/R Combinations with Traditional R Values

Row #(/5184)	rkc2	rkc1	qkc2	qkc1	Errors					
					Mean phi	Mean theta	Mean psi	Total Euler	Total Position	Total Velocity
54	6.096	3.048	1E-11	1	3.04	1.92	3.09	8.05	3.78	3.96
103	6.096	3.048	1E-11	0.01	3.04	1.93	3.09	8.06	3.27	2.37
104	6.096	3.048	1E-11	0.1	3.04	1.93	3.09	8.06	3.63	2.98
173	6.096	3.048	1E-11	0.001	3.04	1.93	3.11	8.08	3.63	3.86
231	6.096	3.048	1E-11	10	3.05	1.93	3.13	8.11	3.89	4.58
281	6.096	3.048	1E-11	0.0001	3.07	1.93	3.19	8.19	6.92	8.57
335	6.096	3.048	1E-11	100	3.16	1.93	4.77	9.86	4.26	5.82
501	6.096	3.048	1E-11	1000	3.57	2.11	60.05	65.73	4.34	6.12
511	6.096	3.048	1E-11	1E-11	15.8	16.81	33.76	66.37	118.38	33.94
648	6.096	3.048	0.1	1000	9.44	6.42	135.51	151.37	4.34	6.12
664	6.096	3.048	0.01	100	7.77	5.26	140.56	153.59	4.26	5.82

5.2. Sensitivity to Tuning Parameters

This section is meant to show each estimator's sensitivity to its tuning parameters. The intent of this section is not to analyze accuracy of any estimator, but to compare the sensitivity of the estimators' errors with respect to the tuning parameters. In order to show which estimators are more or less sensitive, tuning parameters that produce adequate estimations will be chosen for each filter/formulation. Then, tuning parameter multipliers from 1E-3 to 1E3 will be applied to each estimator. Given that the multipliers will be the same for each estimator, the results will provide an experimental comparison how sensitive each estimator is to its given tuning parameters.

5.2.1. Complementary Filter ("Method 1")

Figure 5-18, below, shows that the Method 1 formulation using a complementary filter is not extremely sensitive to tuning parameters in lower dynamic situations such as the pitch condition for the short steady flight (-15 < pitch < 10). The more dynamic scenario of the roll axis in the short steady flight is much more sensitive to the tuning parameter than the less dynamic scenario of the pitch axis.

```

tau=60;
noise_on=1;
gyro_bias=0;
gyro_cov=5;
accel_cov=0.003;

```

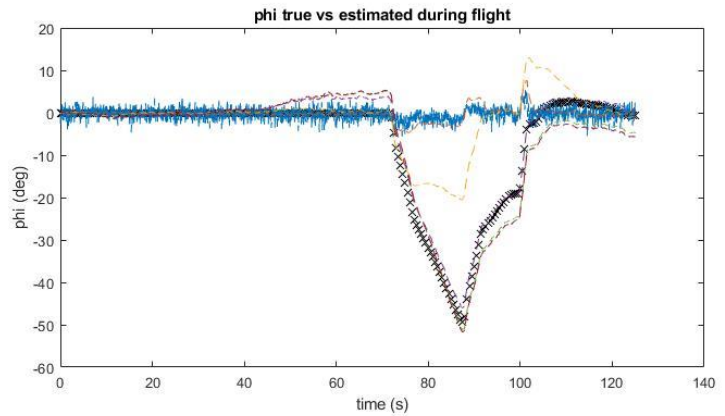
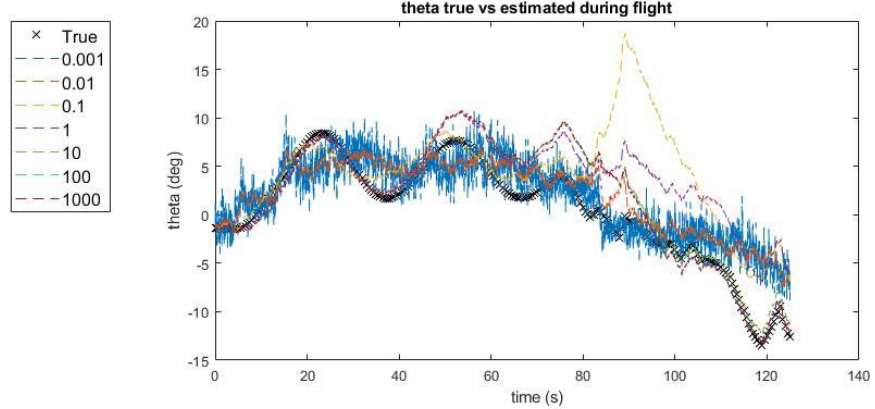
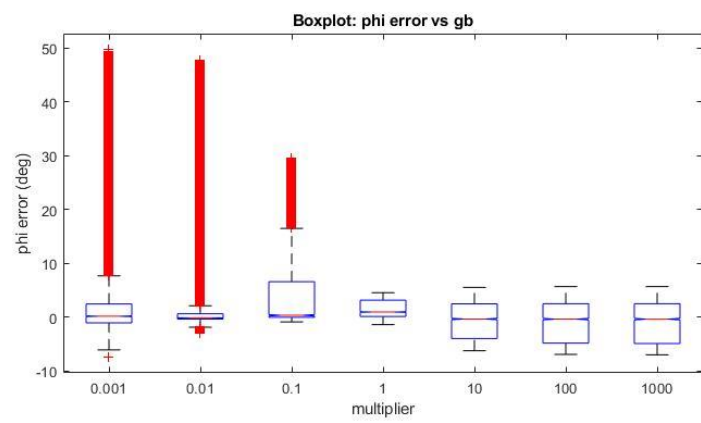
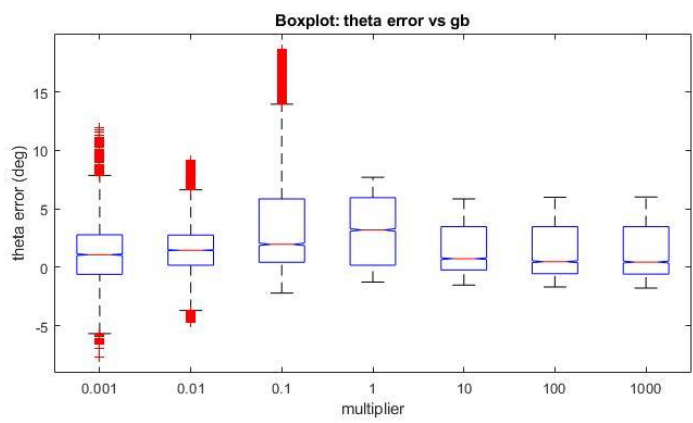


Figure 5-18: CF - Tuning Parameter Multiplier

5.2.2. Airspeed Aided Inertial Attitude Extended Kalman Filter ("Method 2")

Figure 5-19 is the result of multiplying *both* Q and R by the same multiplier for the Method 2 EKF solution. All of the solutions are exactly the same. This provides evidence in support of the discussion regarding the high importance of the ratio of Q/R for an EKF solution.

Figure 5-20 is the result of multiplying only Q by the multiplier. This alters the Q/R ratio, and therefore has an effect on the estimator. Comparing to Figure 5-18: CF - Tuning Parameter Multiplier, shows that the EKF is less sensitive to a change in tuning parameters than the CF. This is somewhat qualitative, but there is significantly less error associated with the multipliers that produce the worst estimates in Figure 5-20 than in Figure 5-18.

```

rk_c=100000;
qk_c=1e-05;
noise_on=1;
gyro_bias=0;
gyro_cov=5;
accel_cov=0.003;
Qonly=0;

```

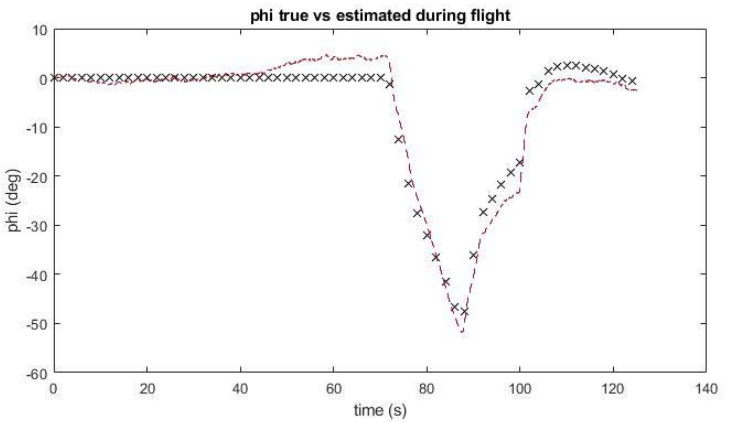
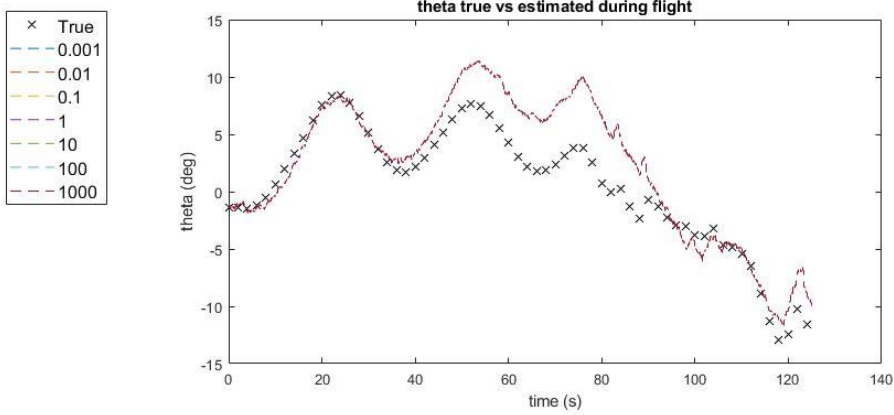
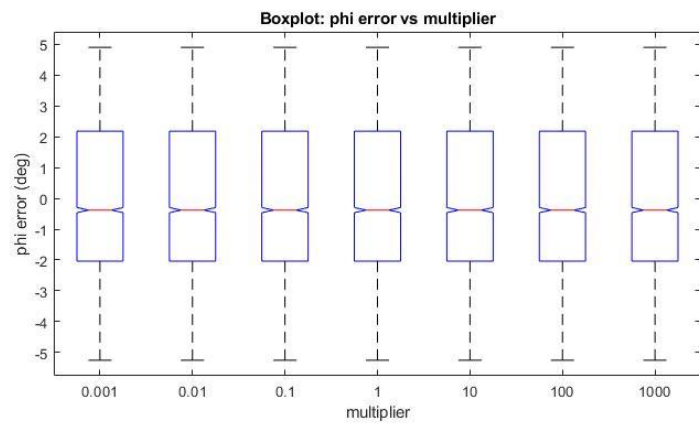
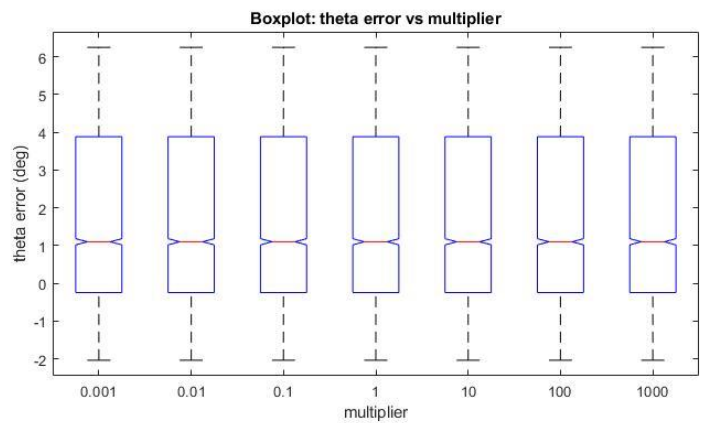


Figure 5-19: Airspeed Aided Inertial Attitude EKF - Tuning Parameter Multiplier (Q and R)

```

rk_c=100000;
qk_c=1e-05;
noise_on=1;
gyro_bias=0;
gyro_cov=5;
accel_cov=0.003;
Qonly=1;

```

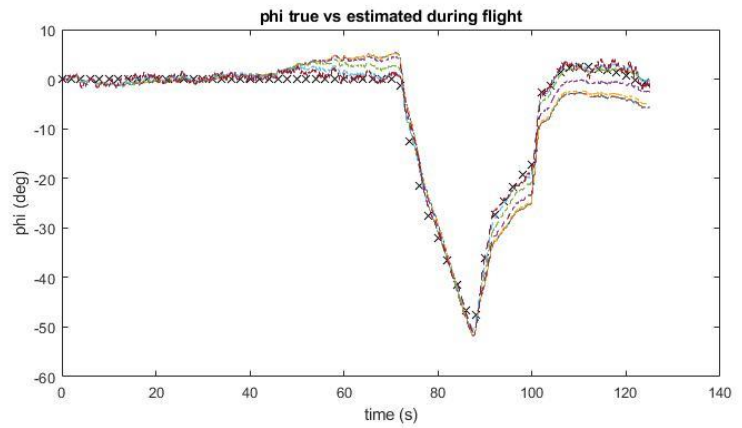
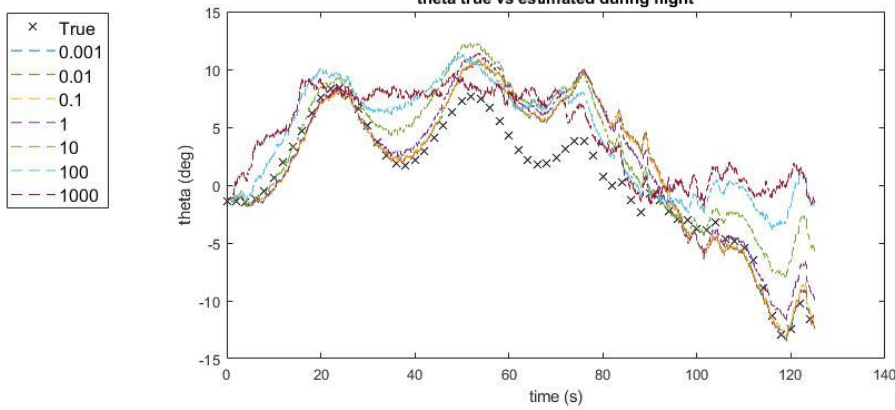
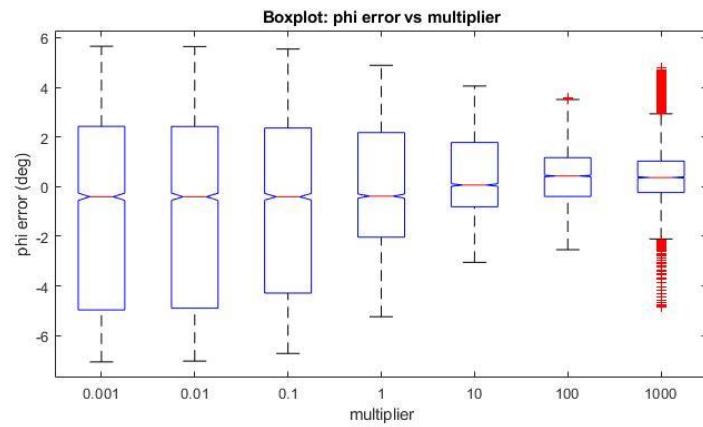
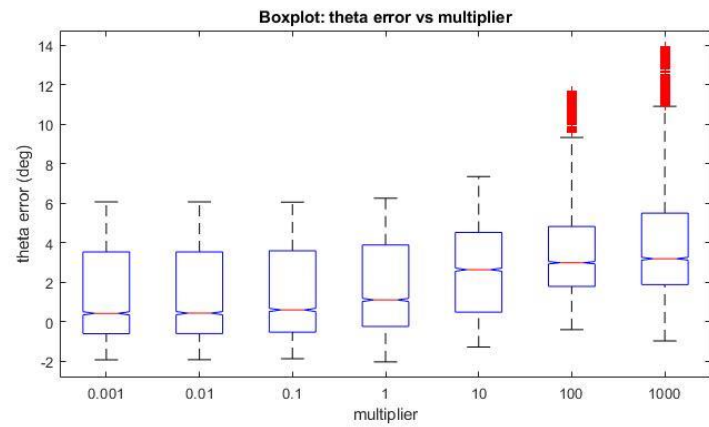


Figure 5-20: Airspeed Aided Inertial Attitude EKF - Tuning Parameter Multiplier (Q Only)

5.2.3. GPS Aided Inertial Navigation Extended Kalman Filter ("Method 3")

Similar to the previous EKF, multiplying Q and R by the same value does not alter the estimator results, as the Q/R ratio stays the same. Since there is no sensitivity of this filter/formulation to varying both Q and R at the same time, two additional sensitivity analyses will be presented. The first, in Figure 5-22, will show the sensitivity of this estimator to a multiplier applied to Q alone. The second, in Figure 5-23, will show the sensitivity of this estimator to a multiplier applied to the lower half of Q only. The lower portion of Q, is the portion that corresponds to the gyro inputs to the estimator. Figure 5-22 and Figure 5-23 show that applying a multiplier to the entire Q matrix does not affect the results as much as varying only the lower half of the Q matrix. That is, this filter/formulation is less sensitive to the Q/R ratio than it is to the qkc_1/qkc_2 ratio (where qkc_#'s are defined in Table 3-3, in the "Formulations" Section, above).

```

rkc1=99999999;
rkc2=99999999;
qkc1=1000;
qkc2=1;
noise_on=1;
gyro_bias=0;
gyro_cov=5;
accel_cov=0.003;
Qonly=0;
qkc2only=0;

```

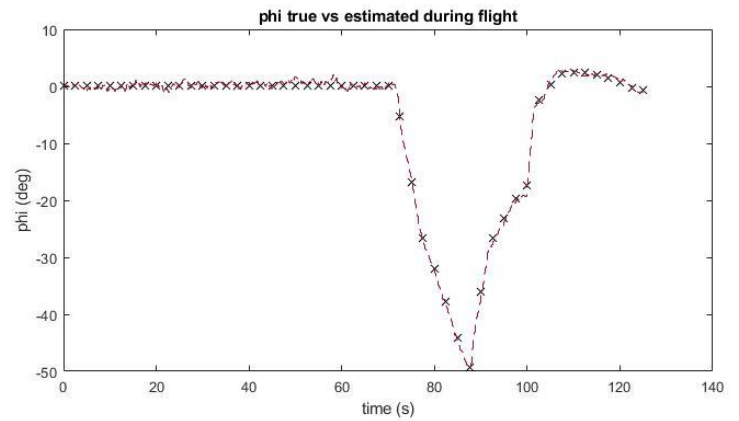
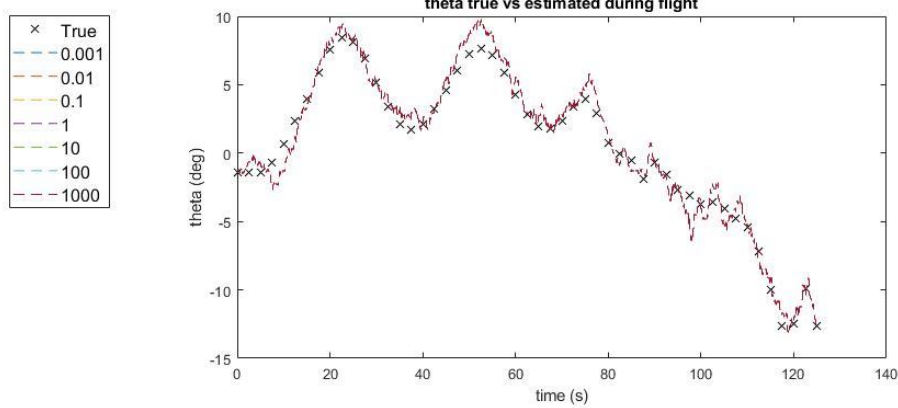
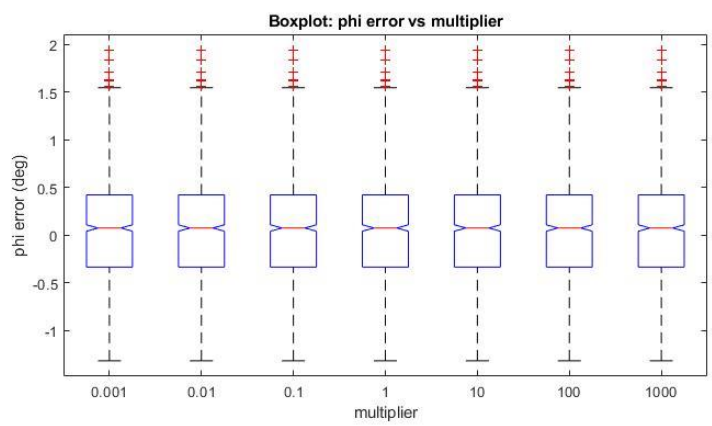
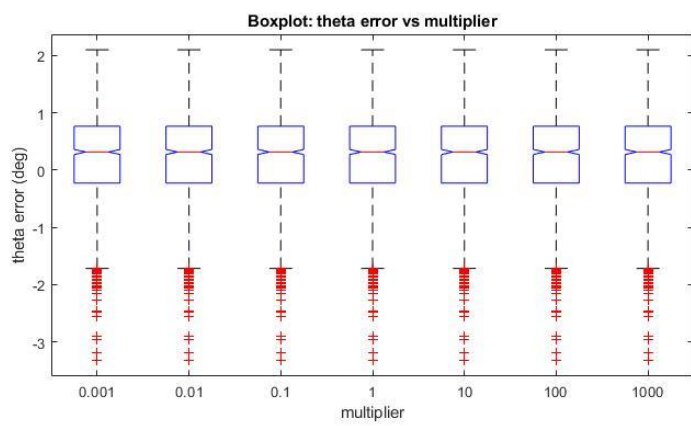


Figure 5-21: GPS Aided Inertial Navigation EKF - Tuning Parameter Multiplier (Q and R)

```

rkc1=99999999;
rkc2=99999999;
qkc1=1000;
qkc2=1;
noise_on=1;
gyro_bias=0;
gyro_cov=5;
accel_cov=0.003;
Qonly=1;
qkc2only=0;

```

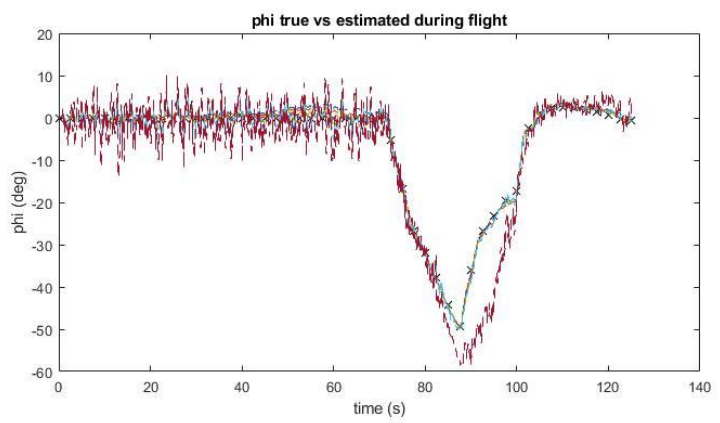
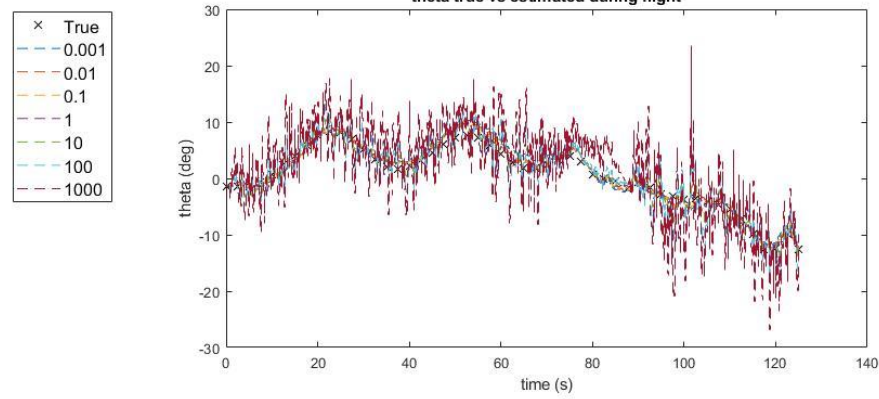
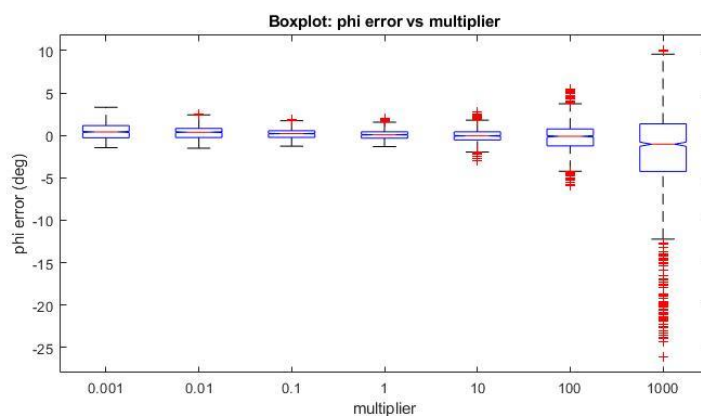
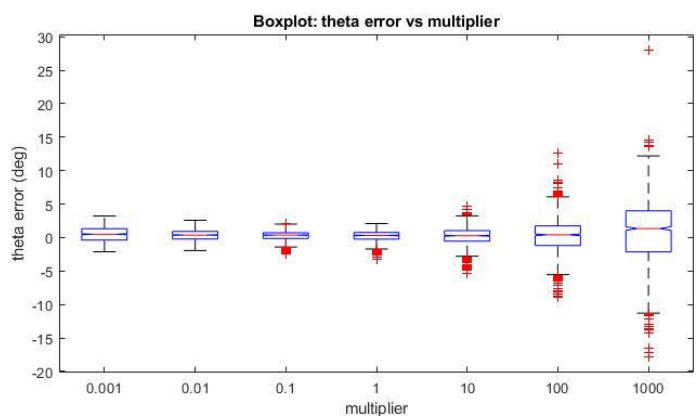


Figure 5-22: GPS Aided Inertial Navigation EKF - Tuning Parameter Multiplier (Q Only)

```

rkc1=99999999;
rkc2=99999999;
qkc1=1000;
qkc2=1;
noise_on=1;
gyro_bias=0;
gyro_cov=5;
accel_cov=0.003;
Qonly=1;
qkc2only=1;

```

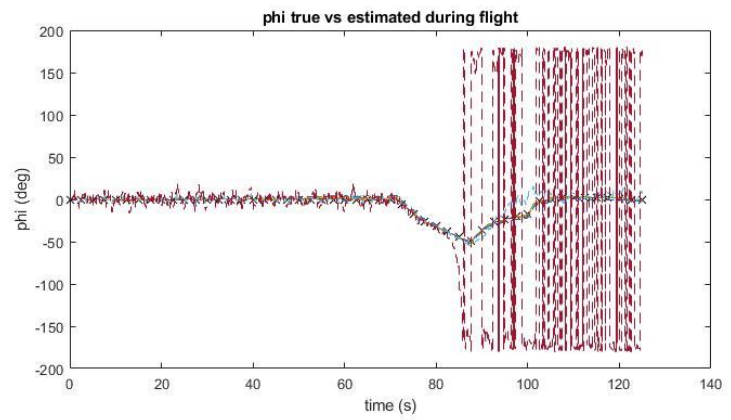
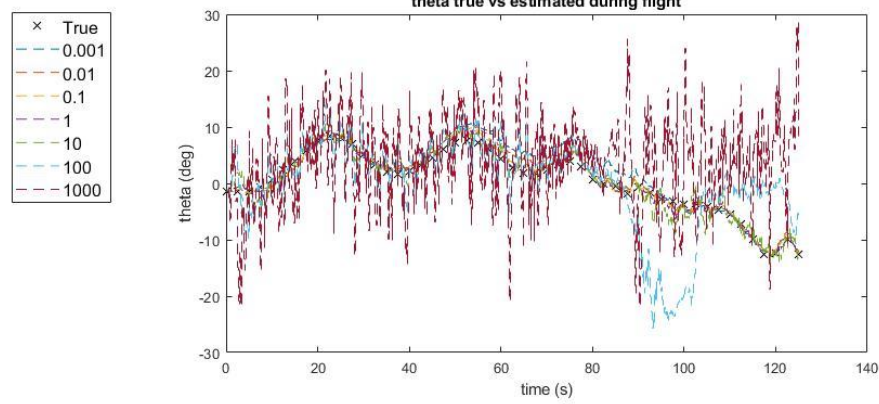
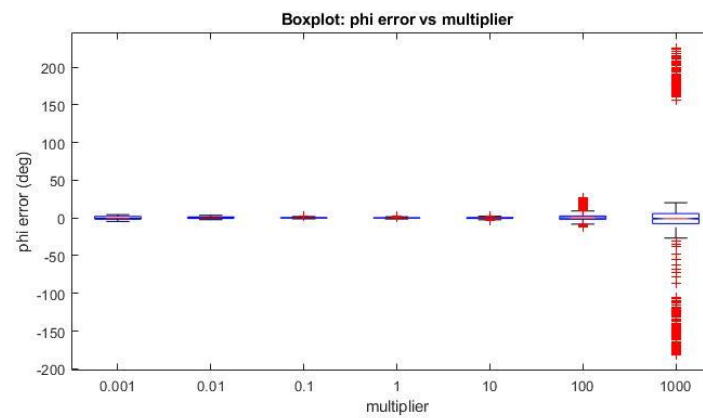
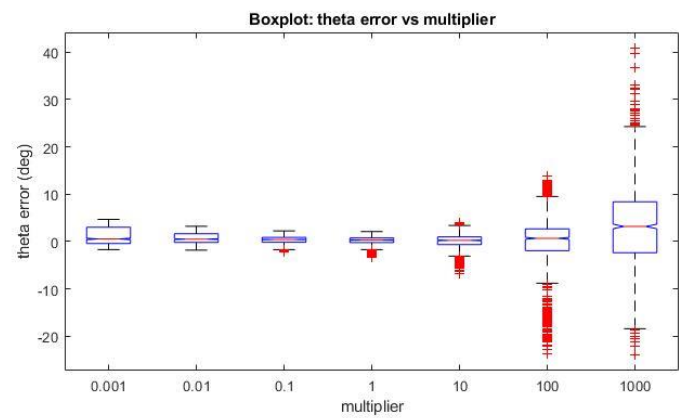


Figure 5-23: GPS Aided Inertial Navigation EKF - Tuning Parameter Multiplier (Lower Portion of Q Only)

5.2.4. GPS Aided Inertial Navigation Unscented Kalman Filter ("Method 4")

Figure 5-24 through Figure 5-26 were created using the same tuning parameter multipliers and method as those corresponding to the Method 3 EKF in the previous section. Unlike the EKF, the case where Q and R are varied by the same multiplier (such that the Q/R ratio remains the same), the UKF is affected, as seen in below in Figure 5-24. This provides evidence in support of the discussion regarding the higher independence of Q and R for an UKF compared with an EKF solution. Like the EKF solution, Figure 5-25 and Figure 5-26 show that this formulation is more sensitive to manipulating the lower portion of Q than it is to the manipulation of the Q/R ratio. Although Figure 5-24 shows one instance of extreme divergence (multiplier of 0.001), the other 5 multipliers show little sensitivity, Figure 5-26: GPS Aided Inertial Navigation UKF - Tuning Parameter Multiplier (Lower Portion of Q Only) shows significant sensitivity with each multiplier. Note that in both the roll and pitch axes of Figure 5-26, the solution diverges completely at ~70sec; therefore, the magnitude of the error reported in the boxplots for the multiplier of 1000 appears much less than it actually is.

```
rkc1=0.0003048;
rkc2=0.0006096;
qkc1=0.0001;
qkc2=1e-11;
noise_on=1;
gyro_bias=0;
gyro_cov=5;
accel_cov=0.003;
Qonly=0;
qkc2only=0;
```

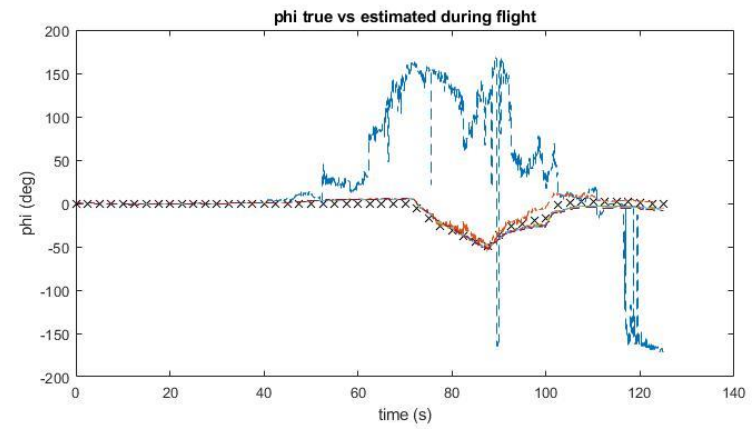
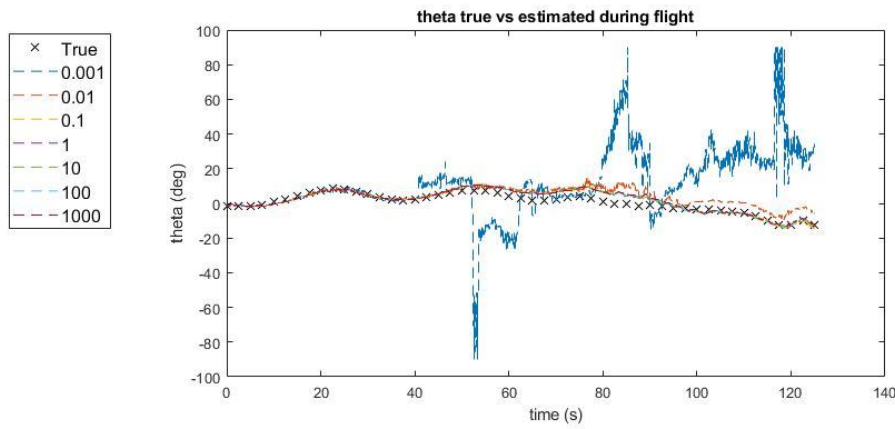
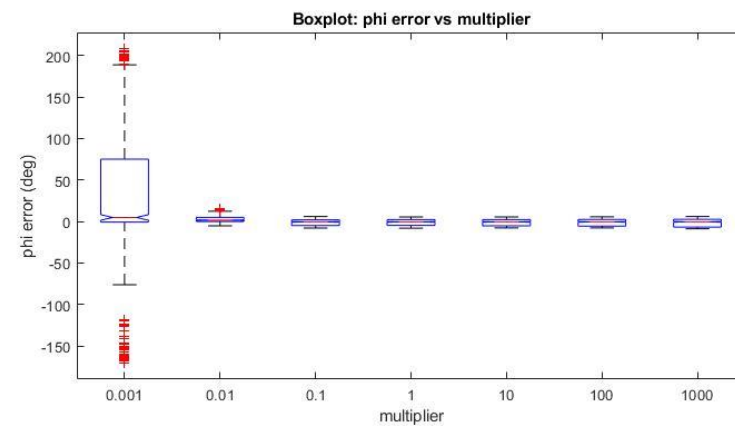
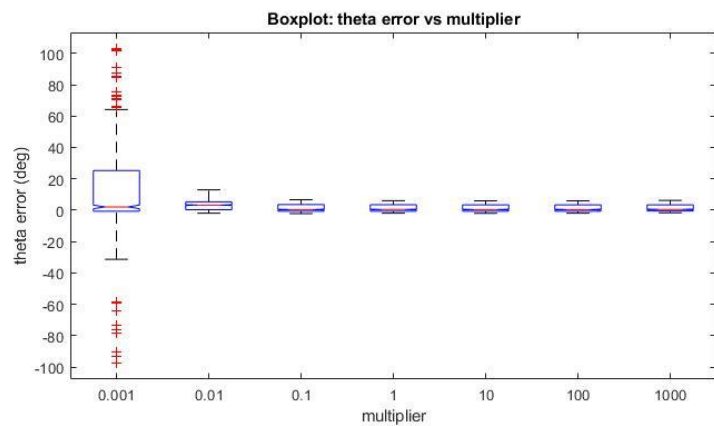


Figure 5-24: GPS Aided Inertial Navigation UKF - Tuning Parameter Multiplier (Q and R)

```
rkc1=0.0003048;
rkc2=0.0006096;
qkc1=0.0001;
qkc2=1e-11;
noise_on=1;
gyro_bias=0;
gyro_cov=5;
accel_cov=0.003;
Qonly=1;
qkc2only=0;
```

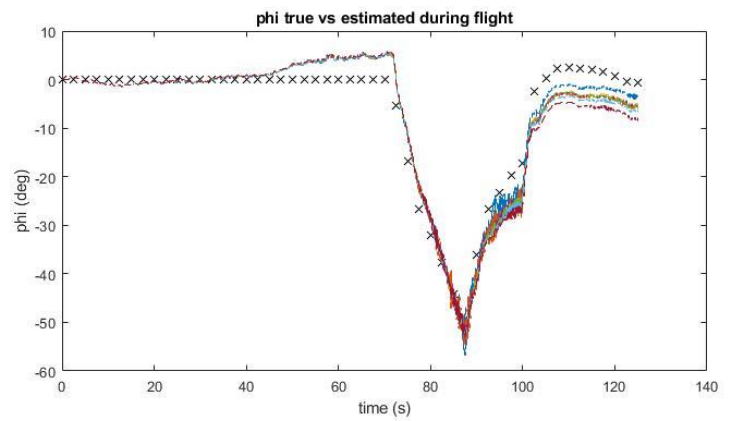
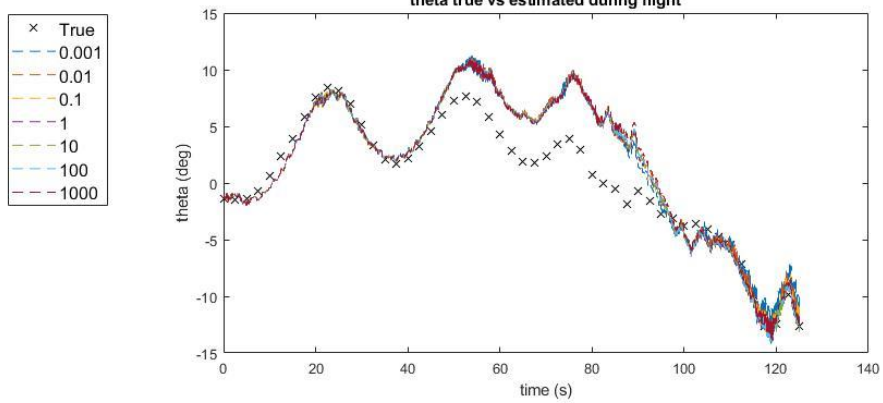
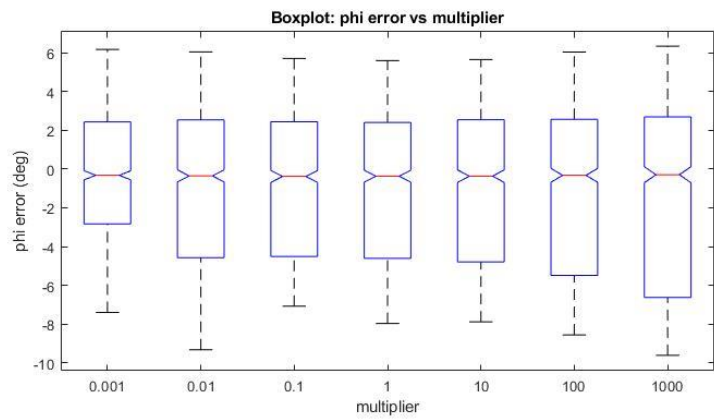
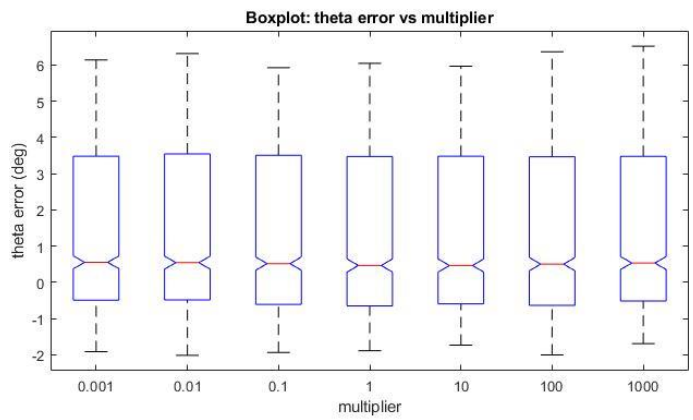


Figure 5-25: GPS Aided Inertial Navigation UKF - Tuning Parameter Multiplier (Q Only)

```

rkc1=0.0003048;
rkc2=0.0006096;
qkc1=0.0001;
qkc2=1e-11;
noise_on=1;
gyro_bias=0;
gyro_cov=5;
accel_cov=0.003;
Qonly=1;
qkc2only=1;

```

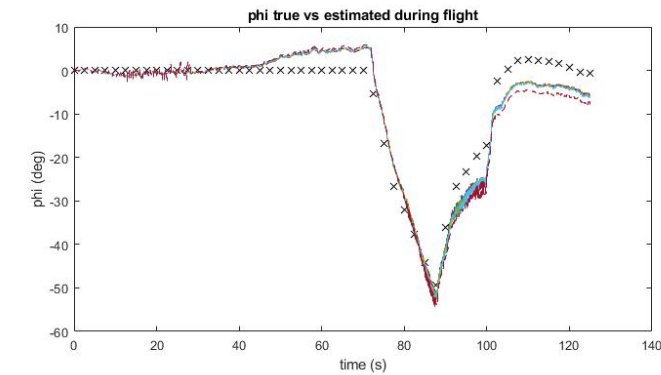
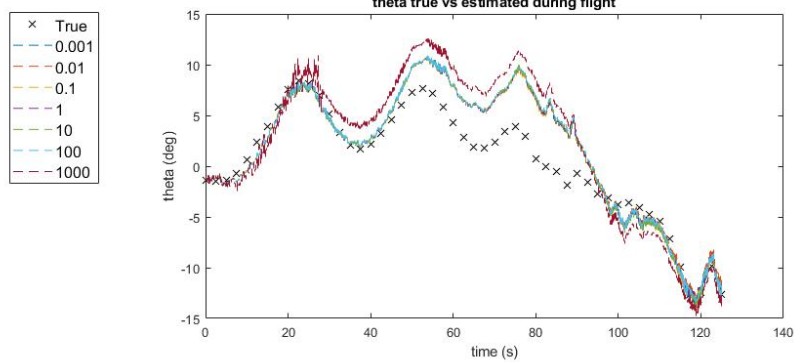
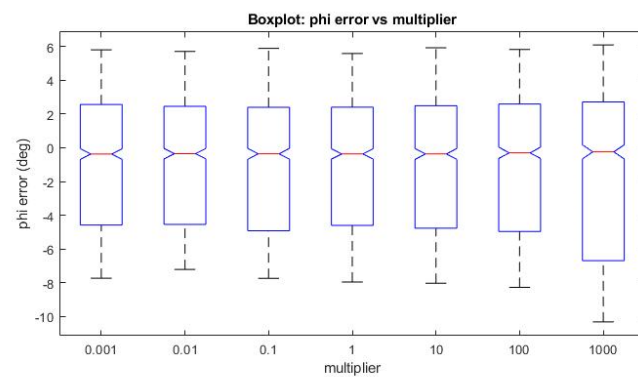
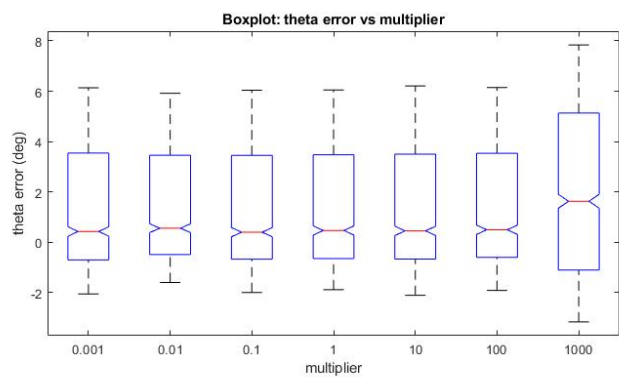


Figure 5-26: GPS Aided Inertial Navigation UKF - Tuning Parameter Multiplier (Lower Portion of Q Only)

5.2.5. Discussion

Given the significant difference of the Q/R and qkc1/qkc2 between the Method 3 EKF and Method 4 UKF, these results cannot be directly compared. It might be worth, for future study, choosing Q and R values that provide an adequate estimate for both the EKF and UKF and comparing those sensitivities. This is suggested over choosing the experimentally optimal Q and R for each, the EKF and UKF, then comparing sensitivities.

From the "Sensitivity to Tuning Parameters" Analyses, a few conclusions can be drawn about the sensitivity of the Kalman Filter estimators. It was shown that an experimentally optimal EKF is dependent upon the Q/R ratio, rather than the individual Q and R values. This was demonstrated for both formulations that used the EKF. It was also shown that, unlike the EKF, the UKF solution relies on independently optimally chosen Q and R values. The final conclusion from this section is that the Method 3 and Method 4 formulations are most sensitive to the ratio of the upper half w.r.t. lower half of Q. This was not shown for the Method 2 EKF, therefore cannot be concluded to be a property of Kalman Filters, or Kalman Filters for attitude estimation. Though, it is an interesting observation.

5.3. Bias Sensitivity

Each of the filter/formulations was run with different gyro biases ranging from 0 to 6 deg/s. An equal bias was inserted on each gyro axis. The results of each are plotted below in Figure 5-27 through Figure 5-30. The tuning parameters used for the bias runs are the chosen optimal parameters from Section 5.1 "Optimal Tuning Parameters". These parameters are printed in the upper left of each figure.

None of the estimators handled gyro bias adequately. Given that the estimator's optimal tuning parameters were chosen without gyro bias included in the noise, the parameters favored the integration of the gyro rates; therefore, they are susceptible to gyro bias. Additional simulations were done, adjusting tuning parameters as to create a more optimal result for the conditions with gyro bias. As the Method 1 CF and Method 2 EKF decreased tau or the Q/R ratio, respectively, the estimators would track the higher frequency dynamics in each axis better; however, would show no resemblance to the actual attitude angles with any amount of bias. The Method 3 and Method 4 solutions showed no improvement in bias tolerance as their qkc1/qkc2 ratio was increased as to drive the solution away from the integration of the gyros.

Though the Method 3 EKF and Method 4 UKF, that use quaternion renormalization, they were still greatly affected by the gyro bias. This is due to the fact that this formulation does not have direct estimation of the Euler angles; i.e. the Euler corrections are a byproduct of the DCM.

Though none of the estimators were able to produce an adequate estimate with gyro bias, the Method 1CF and Method 2 EKF appear to handle the bias better than the Method 3 EKF and Method 4 UKF solutions. This is a somewhat qualitative conclusion based on the fact that the Method 1 and Method 2 solutions do not diverge with the smallest amount of bias and tend to track the actual attitude, though with a biased estimate.

5.3.1. Complementary Filter ("Method 1")

Figure 5-27, below, shows that this estimator tracks the actual attitudes, but contains a bias for biases up to 2 deg/s/s. Larger biases cause the estimator to diverge. Interestingly though, for the 1 and 2 deg/s/s bias cases, the roll estimate converges on actual roll at higher roll attitudes, while driving the pitch estimate erroneous.

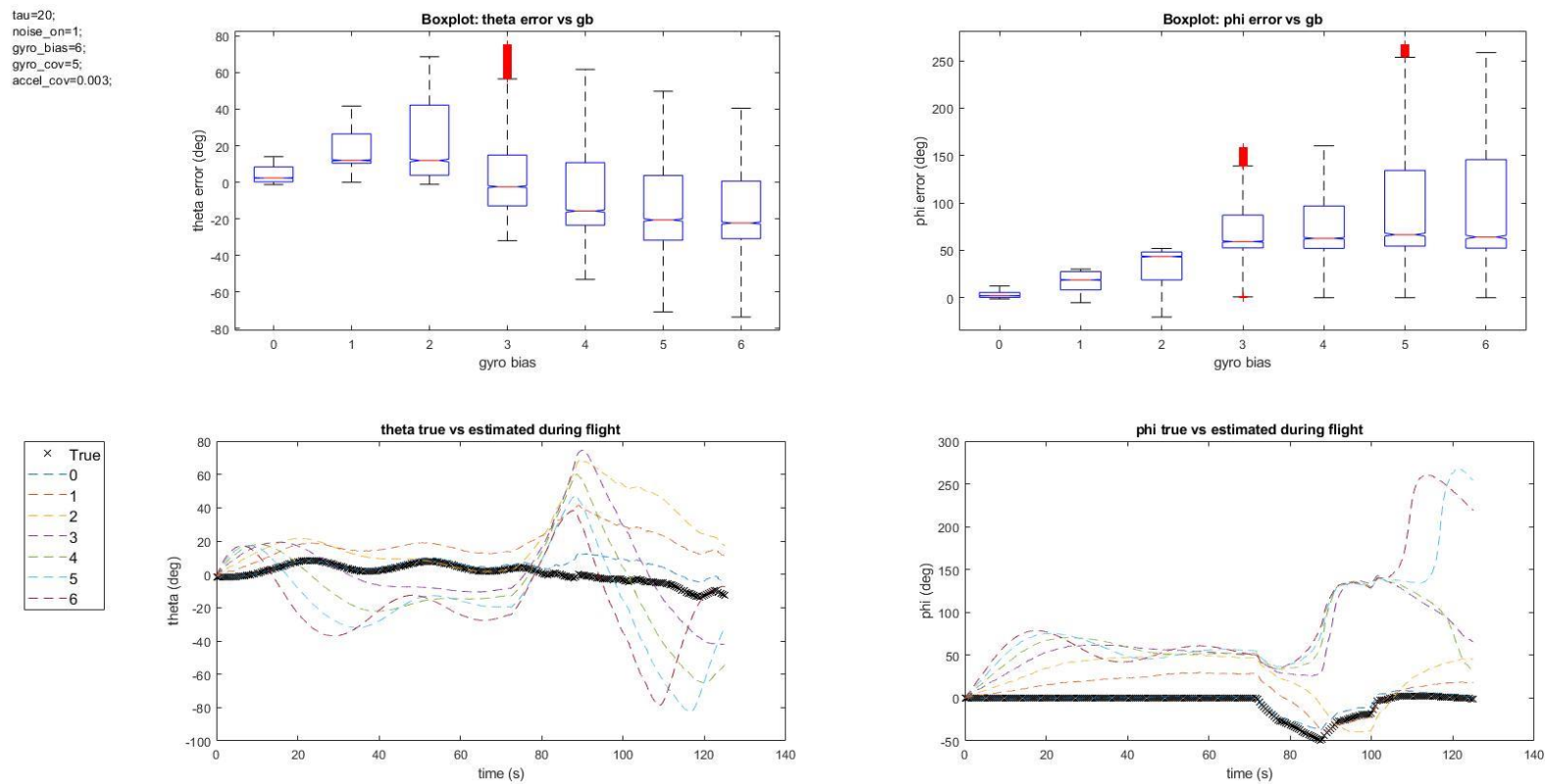


Figure 5-27: CF - Gyro Bias Sweep (0-6deg/s)

5.3.2. Airspeed Aided Inertial Attitude Extended Kalman Filter ("Method 2")

The Q and R that were chosen were within the experimentally optimal bounds discussed in Section 5.1.

They were chosen as to draw the solution away from only the integration of the gyros, while remaining within the aforementioned experimentally optimal bounds. That is Q was chosen to be the largest and R was chosen to be the smallest within those bounds.

Figure 5-28 shows that this estimator's error follows a trend as the bias increases. Interestingly, unlike the other estimators, even with a bias of 4deg/s, the roll estimate converges to the actual roll when the roll angle is large. This is likely due to the fact that the C and h matrices in this estimator are a function of Euler angles such that the Kalman gain, and error by which the Kalman gain is multiplied, become larger as Euler angle magnitude increases. With how close this estimator can come to actual, coming from a diverged solution, it is apparent that some component of this estimator has an accurate estimate of the attitude during higher angles. It's also possible that this component has an accurate estimate of the attitude during lower angles, but given that the feedback loop of this estimator is highly dependent on the magnitude of the Euler angles (C and h matrices), the estimator cannot converge to this component's solution. This adds additional rationale for having sliding tuning parameters.

```

rk_c=1000;
qk_c=0.0001;
noise_on=1;
gyro_bias=6;
gyro_cov=5;
accel_cov=0.003;

```

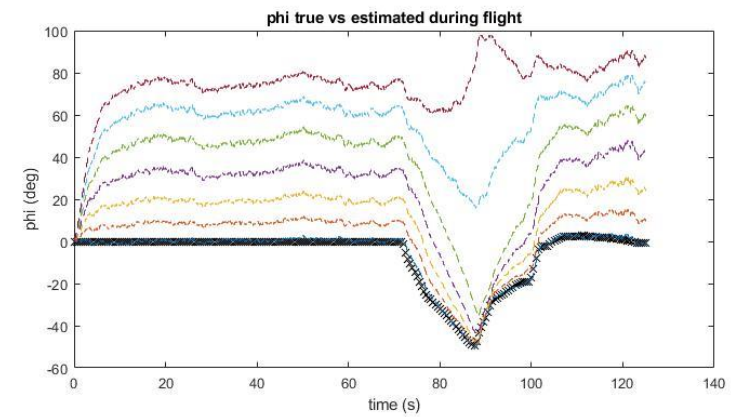
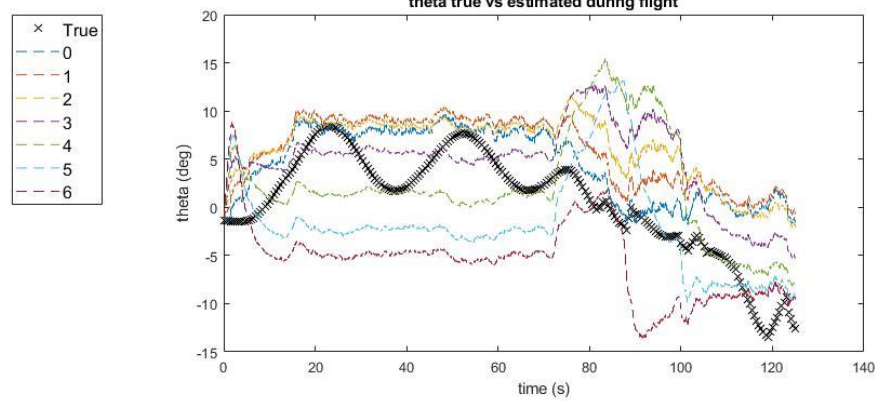
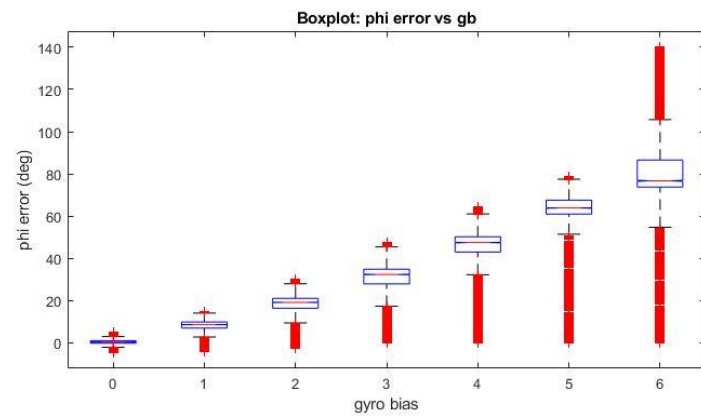
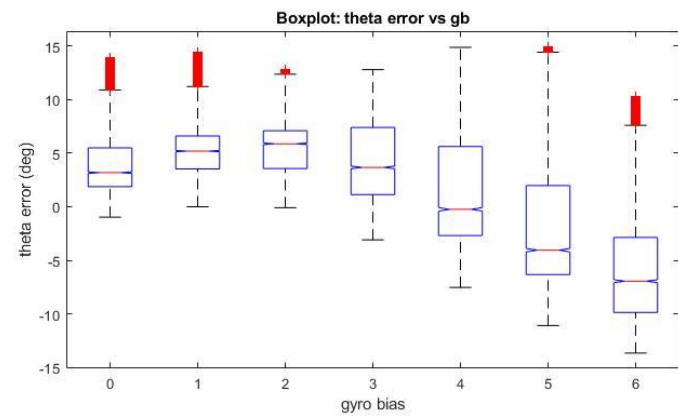


Figure 5-28: Airspeed Aided Inertial Attitude EKF - Gyro Bias Sweep (0-6deg/s)

5.3.3. GPS Aided Inertial Navigation Extended Kalman Filter ("Method 3")

The Method 3 EKF is not at all tolerant to gyro bias, even with the quaternion re-normalization. This can be seen in Figure 5-29, below. This is likely due to the fact that this formulation does not have a direct estimate of attitude. The attitude estimate is a byproduct of the position and velocity corrections through the Kalman gain.

```
rkc1=99999999;
rkc2=99999999;
qkc1=1000;
qkc2=1;
noise_on=1;
gyro_bias=6;
gyro_cov=5;
accel_cov=0.003;
```

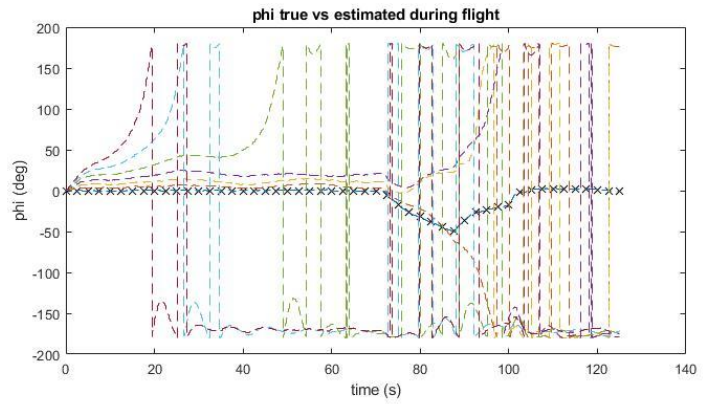
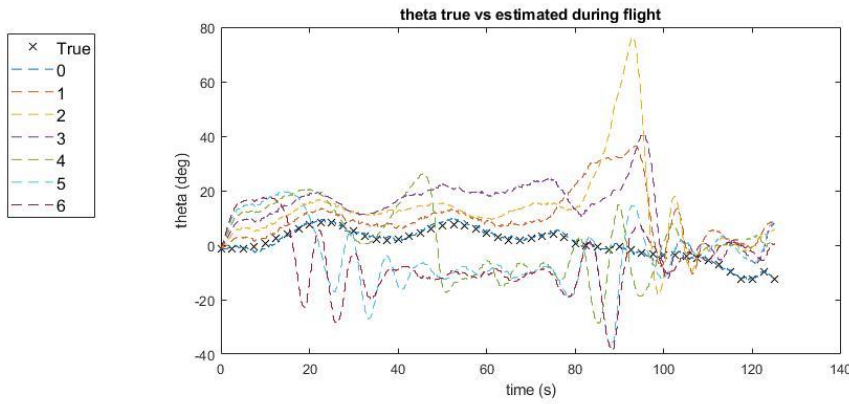
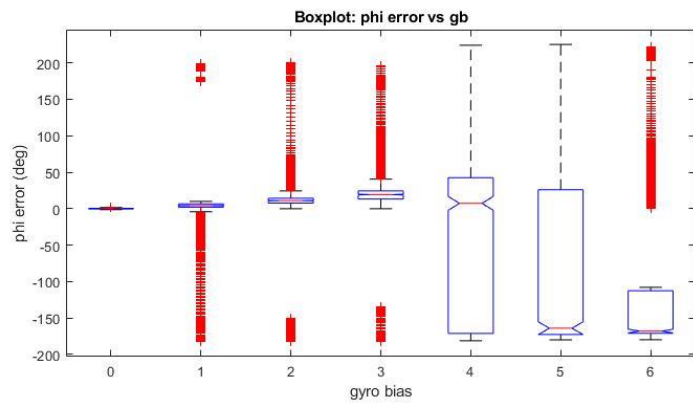
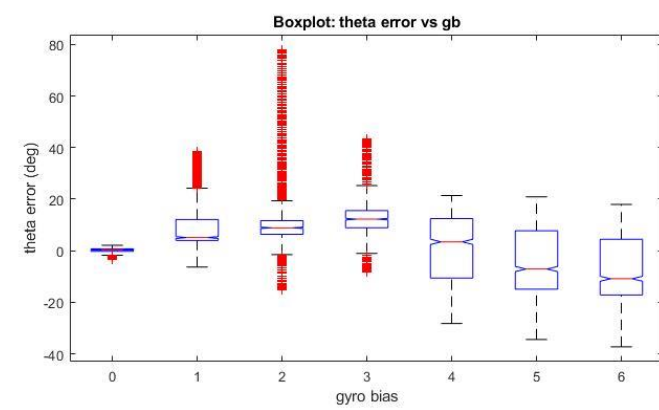


Figure 5-29: GPS Aided Inertial Navigation EKF -Gyro Bias Sweep (0-6deg/s)

5.3.4. GPS Aided Inertial Navigation Unscented Kalman Filter ("Method 4")

Like the EKF, the Method 4 UKF is not at all tolerant to gyro bias. This can be seen in Figure 5-30, below. This is likely due to the same reason as for the EKF—the particularities of the formulation of this estimator.

```
rkc1=0.0003048;
rkc2=0.0006096;
qkc1=0.0001;
qkc2=1e-11;
noise_on=1;
gyro_bias=6;
gyro_cov=5;
accel_cov=0.003;
```

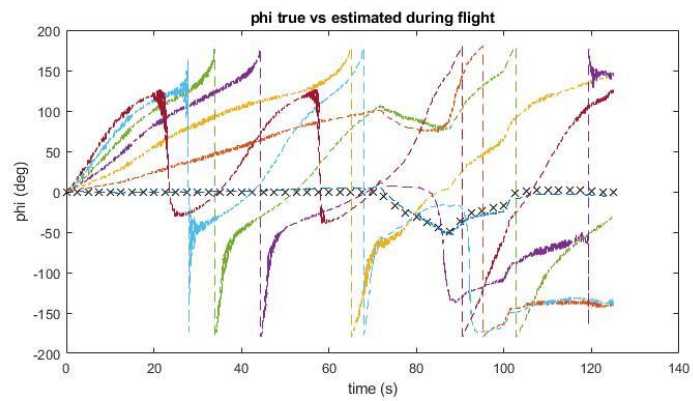
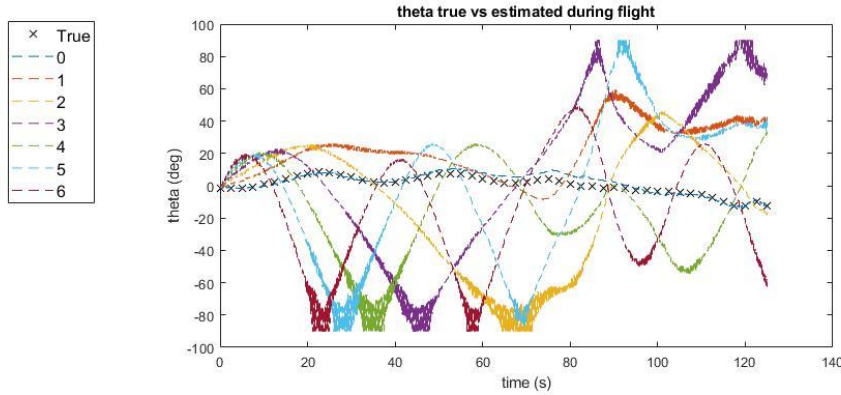
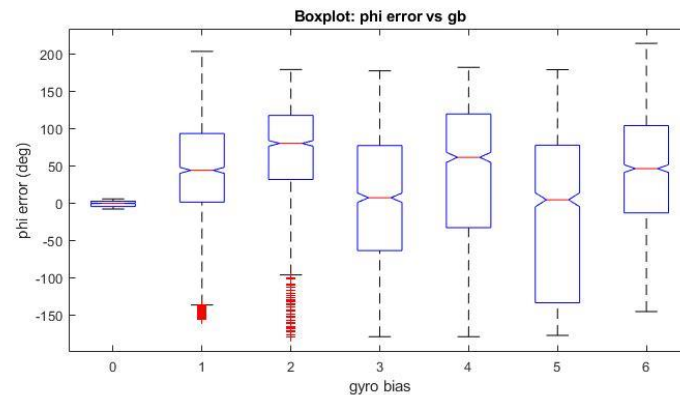
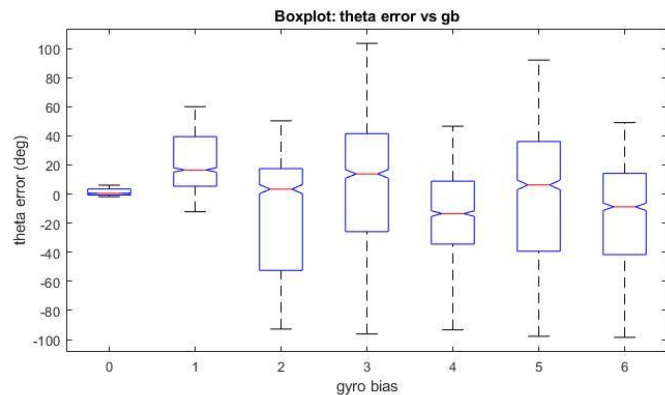


Figure 5-30: GPS Aided Inertial Navigation UKF - Gyro Bias Sweep (0-6deg/s)

5.4. Initialization Error

Each estimator's ability to converge to the correct solution after being initialized with error was evaluated. This was done by initializing one Euler axis (pitch) with 25 degrees of error for a perfect trim condition. The tuning parameters used for each estimator are those chosen in Section 5.1 "Optimal Tuning Parameters". Each estimator was subject to the same noise used throughout this analysis: gyro covariance of 5deg/s, accelerometer covariance of 0.003 g's; No gyro bias was used for the initialization error analysis.

5.4.1. Complementary Filter ("Method 1")

The complementary filter was initialized with 100 degrees of error in the pitch axis that was maintained for 2 seconds. This was done to show the immediate convergence of this estimator even with large initial and sustained error. These results can be seen in Figure 5-31, below.

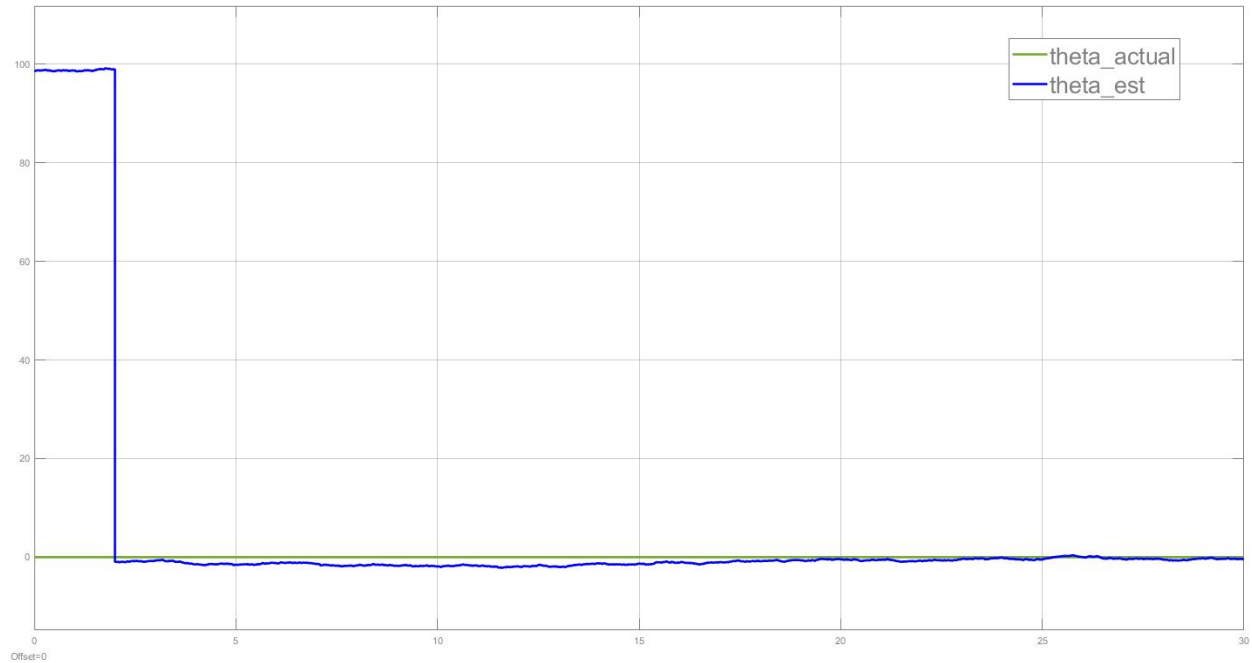


Figure 5-31: Initialization Error - Complementary Filter

5.4.2. Airspeed Aided Inertial Attitude Extended Kalman Filter ("Method 2")

The EKF was initialized to 25 degrees of error in the pitch axis. This error was created using an initial condition block in Simulink, therefore was not sustained for more than one sample. As seen in Figure 5-32 the error converges quickly (~10s), relative to the results from the 3 state solution in [3] which converged in >20 sec. This estimator's convergence is comparable to the convergence performance of the 6 and 12 state EKF and UKFs in Rhudy et. al. Additionally, the diagonal of the covariance matrix ($P(1,1)$ and $P(2,2)$) are shown, in Figure 5-33, below, to converge to a steady value at approximately the same time the error converges to zero.



Figure 5-32: Initialization Error - Airspeed Aided Inertial Attitude EKF

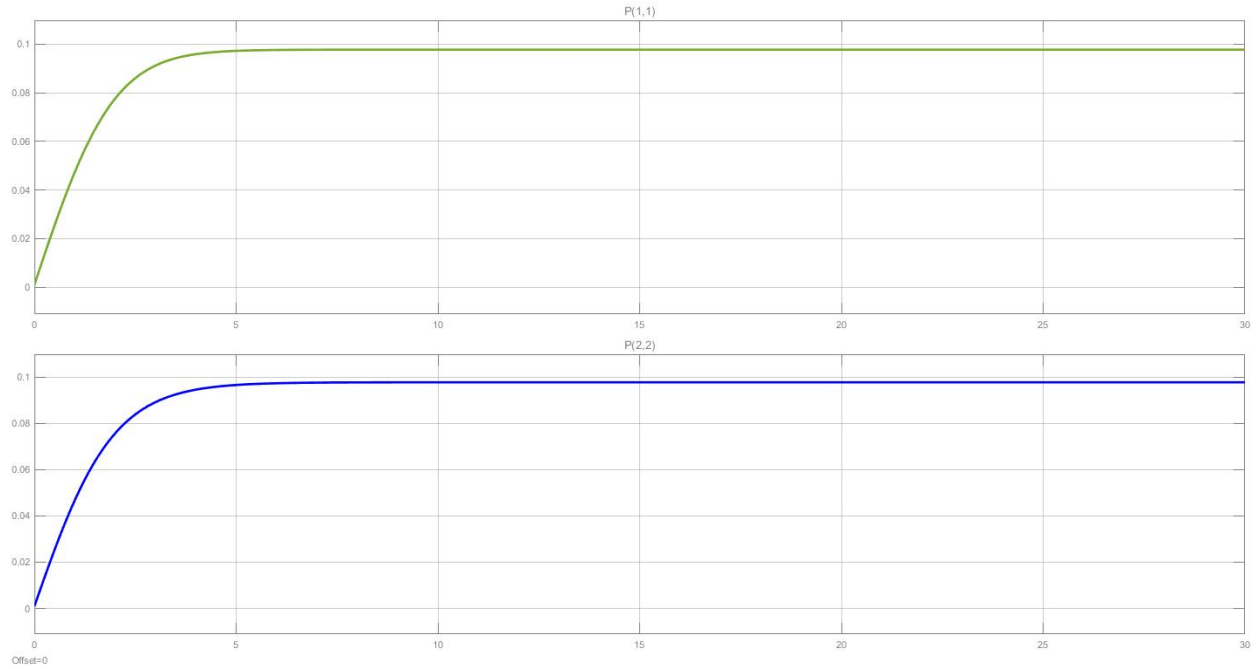


Figure 5-33: Covariance - Initialization Error - ExtendedKalman Filter (Method 2)

5.4.3. GPS Aided Inertial Navigation Extended Kalman Filter ("Method 3")

The EKF ("Method 3") was initialized to 25 degrees of error in the pitch axis. This error was created using an initial condition block in Simulink, therefore was not sustained for more than one sample. As seen in Figure 5-34, below, the error converges ($\sim 22s$). While this convergence is not fast relative to other estimators, it performs adequately. The diagonal of the covariance matrix ($P(1,1:10)$) are shown, in Figure 5-35, below, to converge to a steady value at approximately the same time the error converges to zero.

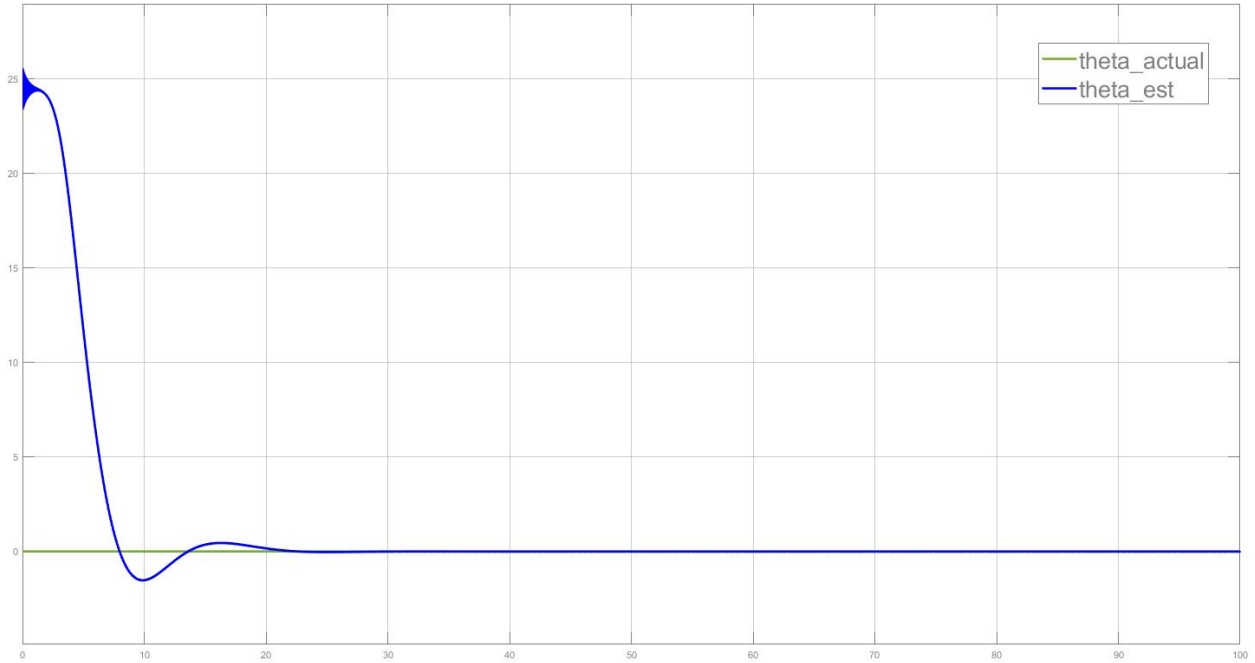


Figure 5-34: Initialization Error - GPS Aided Inertial Navigation EKF

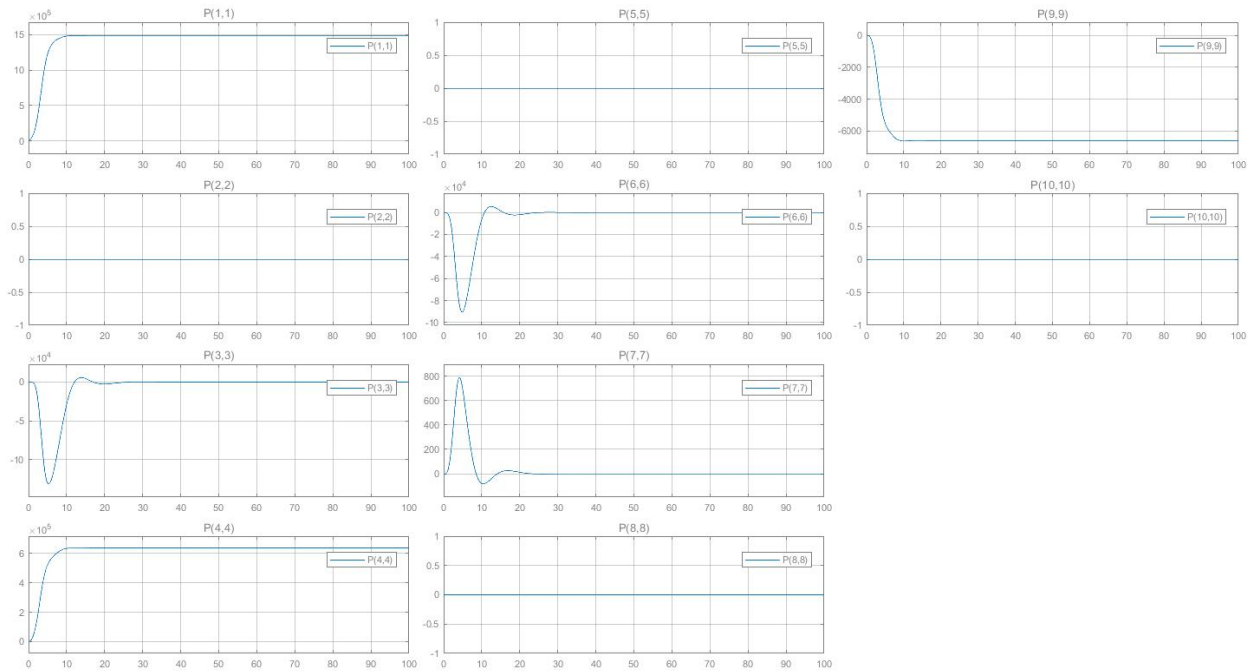


Figure 5-35: Covariance - Initialization Error - GPS Aided Inertial Navigation EKF

5.4.4. GPS Aided Inertial Navigation Unscented Kalman Filter ("Method 4")

The Method 4 UKF, using the experimentally optimal tuning parameters, was not able to converge from an initialized error, as seen in Figure 5-36, below. This is not a property of the Unscented Kalman Filter, as UKF formulations have been shown to perform similarly to their EKF equivalents in multiple other analyses. This estimator's inability to converge could be attributed to the choice to use the experimentally optimal tuning parameters from the Monte Carlo run—which were not chosen based on the covariance of the sensors. It is possible, and likely that another set of tuning parameters, that also would produce an adequate Euler estimate, would demonstrate convergence. This suggests that convergence might need to be considered when choosing the experimentally optimal tuning parameters.

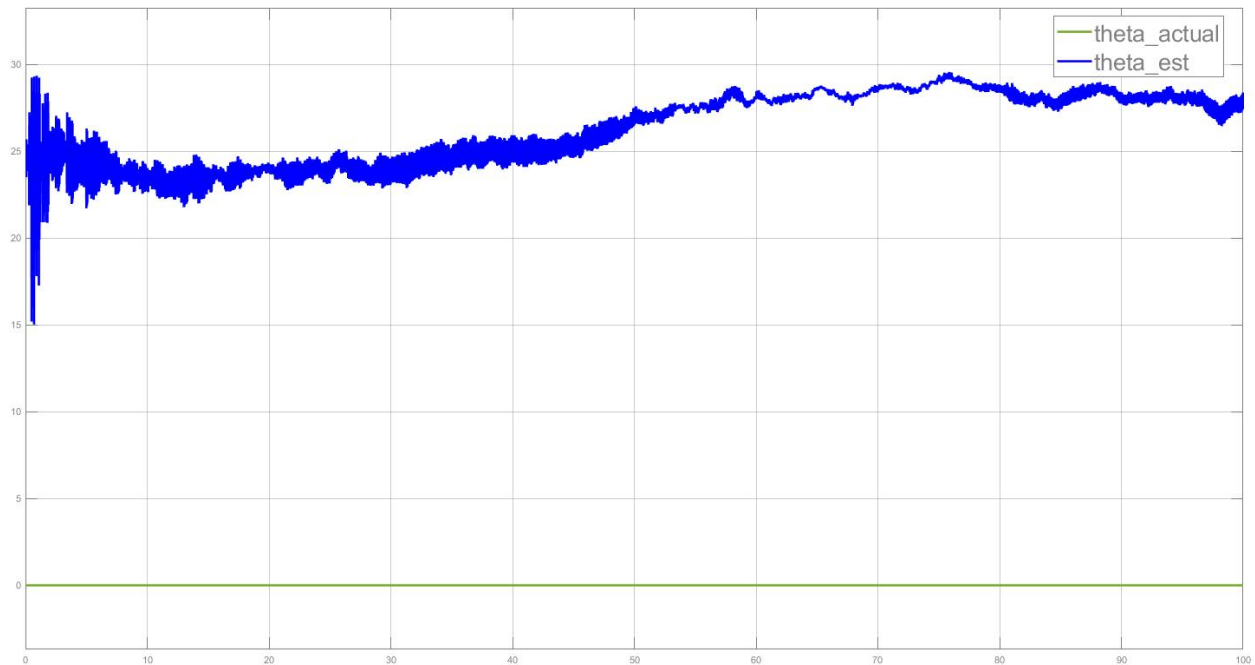


Figure 5-36: Initialization Error - GPS Aided Inertial Navigation UKF

5.4.5. Discussion

The Complementary Filter converged from the initialization error effectively instantaneously (one time step). Both EKFs converged from their errors rather quickly, with the Method 2 solution being on par with other estimators from other analyses (~10s to converge) (Rhudy et. al.), and the Method 3 EKF performing adequately, but not as well (~20s to converge). The UKF formulation, with the tuning parameters chosen, did not converge from an initial error.

The lack of convergence property for the UKF formulation (as tuned) did not affect its performance in the other analyses; however, this property might provide enough rationale for this estimator (as tuned) to not be chosen over other options. This unexpected result motivated a suggestion for future research to include convergence time as part of the Monte Carlo results for choosing the experimentally optimal tuning parameters. This suggestion is further detailed in Section 6 "Conclusions & Recommendations".

5.5. Baseline Comparison

Figure 5-37 is a plot of each estimator's solution for roll (top) and pitch (bottom) vs truth. It is visually apparent that, overall for these conditions, the Airspeed Aided Inertial Attitude EKF performed the best. Though, as time increases through the run, the estimator that performs the best and worst changes multiple times. For example, in the pitch axis, the Airspeed Aided Inertial Attitude EKF begins performing better than the CF, then begins to perform worse than the CF (~80s-100s), then finishes the flight performing better than the CF. Each estimator's performance being a function of the particular conditions has been seen throughout this analysis.

The Method 3 EKF, again, shows the interesting property that it, once diverged, begins to converge quickly at higher phi. This convergence also occurs in the pitch axis, though the higher attitude angle is in the roll axis. The original divergence, in both axes, becomes worse than that of the UKF; however, is able to converge as to be a better estimate.

The UKF performed the worst for these conditions. Intuitively, the UKF and EKF should perform similarly. The UKF's poor performance compared to the EKF (with the same formulation) could be attributed to the lack of UKF specific parameter (α , β , w_c) inclusion in the Monte Carlo runs. Additionally, the non-intuitive tuning parameters (Q and R) of the Method 3 EKF and Method 4 UKF solutions, implies that the "standard" choices for α , β , and w_c may not be "standard" as well—while, for this analysis, α , β , and w_c were held constant at the "standard" choices.

It is also possible that choosing the UKF's experimentally optimal tuning parameters based on a single metric led to poor performance. Given that the Total Euler Errors were similar ($\pm \sim 1\text{deg}$) for multiple tuning parameter combinations (Table 5-7: Monte Carlo Results from UKF ("Method 4") - With Noise), it is quite possible that a more optimal choice exists with respect to other performance metrics. The CF and Method 2 EKF experimentally optimal tuning parameters were chosen based on maximum *and*

mean error with respect to each individual axis, while the Method 3 EKF and Method 4 UKF parameters were chosen based on a single metric for both axes. Additionally, the visual nature of the box-and-whiskers and boxplots used for the Method 1 CF and Method 2 EKF in Section 5.1 "Optimal Tuning Parameters", gave a sense trends w.r.t. the tuning parameters. Trends were much less obvious from tables used for the Method 3 EKF and Method 4 UKF estimators' tuning. Box-and-whiskers was not used for the Method 3 EKF and Method 4 UKF estimators' tuning as it would've been impractical for evaluating the 1000s of combinations. Additionally, the Method 3 EKF and Method 4 UKF "Total Euler Error" included the heading error. This was done as not to pick parameters that produced good pitch and roll, but inaccurate heading—similar to how parameters would not be chosen if they produced inadequate velocity and position estimates even though the only states of interest were pitch and roll.

Most analyses utilize only one or few metrics in order to tune their estimators. This could be contributing to the existence of conflicting results in the literature, as seen by Rhudy et. al. It is likely that utilizing more metrics, when choosing experimentally optimal parameters, will result in an estimator that is more optimal. This is discussed further in Section 6 "Conclusions & Recommendations".

It should be noted that these results are the results of the combination of the filter and the formulation. That is, the prior conclusions do not intend to state that a complementary filter or EKF are better than a UKF. It is the combination of the filter and formulation that is being evaluated. Additionally, the UKF tracks the high frequency dynamics of the attitude well, even after the estimate accrues bias. The UKF's inability to converge from the accrued bias was alluded to by its inability to converge from an initial error in the previous section.

```
noise_on=1;  
gyro_bias=0;  
gyro_cov=5;  
accel_cov=0.003;
```

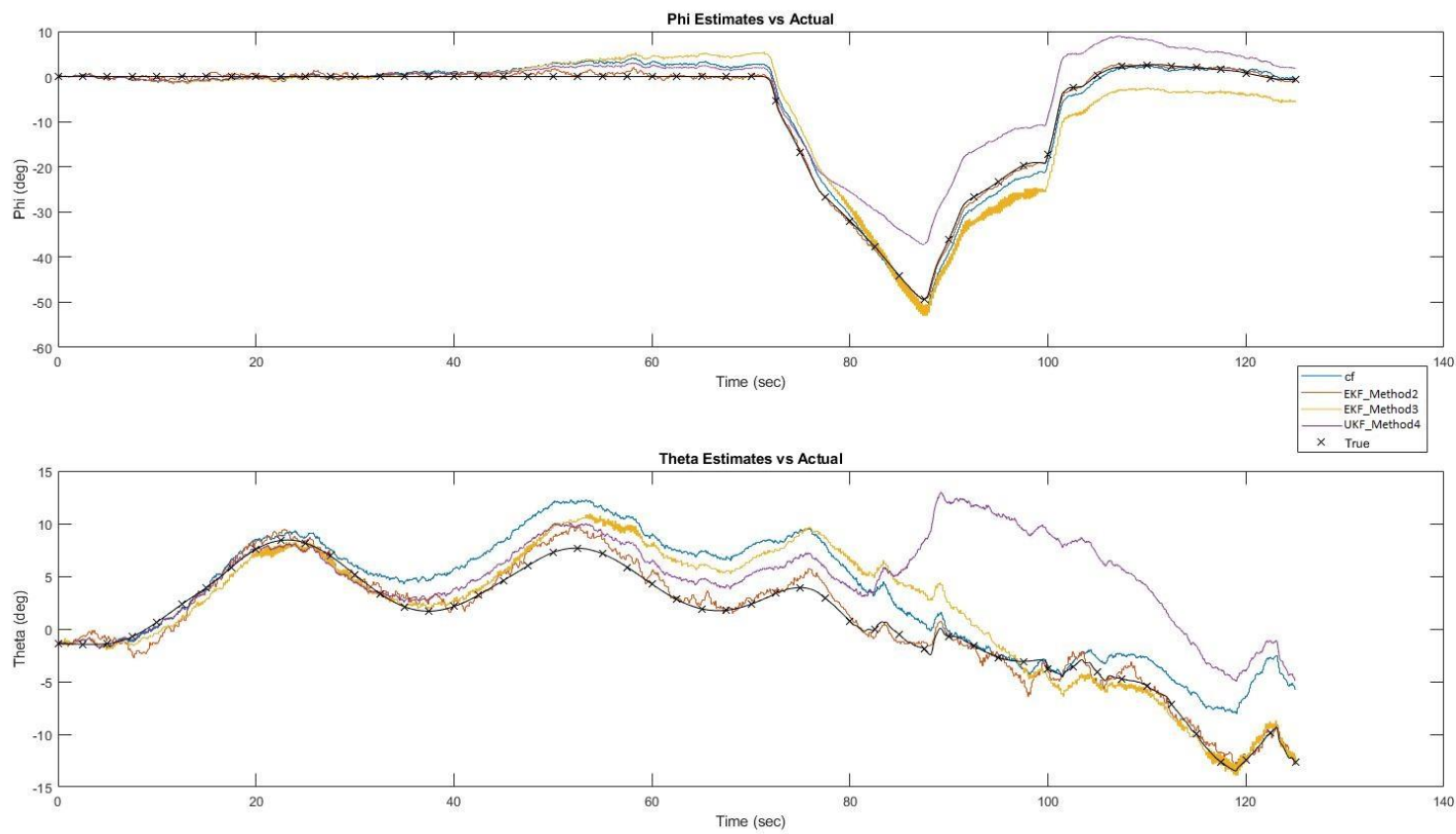


Figure 5-37: Baseline Plot - Comparing All Estimators with Respect to Phi and Theta

The inadequate performance of the UKF is much more evident in Table 5-9, below, particularly when comparing Mean Square Error. Had MSE been considered in choosing the best tuning parameters for this estimator, other parameters may have been chosen. Also note in Table 5-9 that the 3 sigma error for the UKF is better than that of the Method 3 EKF. This provides further evidence that multiple metrics should be considered when comparing estimators or choosing experimentally optimal tuning parameters.

Table 5-9: Baseline Table - Comparing All Estimators with Respect to Phi and Theta

Estimators	Phi (deg)			Theta (deg)			Total_Euler_Error (deg)
	MSE	RMSE	3sigma	MSE	RMSE	3sigma	
CF (Method 1)	3.13	1.77	6.05	11.64	3.41	6.5	4.13
EKF (Method 2)	0.29	0.54	1.97	0.76	0.87	2.9	1.13
EKF (Method3)	13.78	3.71	15.34	6.76	2.6	7.06	4.92
UKF (Method 4)	23.1	4.81	10.78	39.24	6.26	13.84	7.8

6. Conclusions & Recommendations

The conclusions, supporting evidence, and recommendations will be summarized in Table 6-1, below. This summary will be expanded upon in the following subsections.

Table 6-1: Conclusions & Recommendations Summary

Subject	Conclusion	Evidence	Recommendation
Optimal Tuning	Traditional choices (sensor covariance) for tuning parameters (Q/R) of KFs may not be experimentally optimal.	Optimal Tuning Parameters Sections	When using formulations whose inputs to the KF are not direct measurements, a Monte Carlo analysis should be used to determine best possible tuning parameters.
	Additional metrics should be considered when choosing optimal parameters.	Poor UKF performance seen in Baseline Comparison Section 5	Gyro bias and convergence (from initial error), at minimum, should be considered in choosing best tuning parameters.
Metrics	Different single metrics identify different experimentally optimal tuning parameters and top performers	Baseline Comparison Section 5	2σ , 3σ , 4σ , max, mean, and mode errors, at minimum, should be considered.
	Commonality and consistency between estimator comparison studies impedes discernment.	Conflicting research results [3]	A simple, easy to implement, estimator (the IMU-only CF) is recommended to be used as a common baseline across studies. Also, historical INS comparison standards should be re-evaluated for applicability.
Future Configurations	Bias elimination is unlikely a by-product of a configuration, unless specifically designed for.	Bias Sensitivity Section 5.3	Designed bias elimination is essential.
	Each individual state did not have the same optimal tuning parameters.	Optimal Tuning Parameters Sections	Future configurations might consider independent estimates of states.
	Magnitude of states drove improved accuracy of estimate.	Figure 5-28	Sliding tuning parameters should be investigated for their ability to produce similar results.

6.1. Optimal Tuning

Conclusions:

Previous research demonstrated the need to fairly compare estimators [3]. That research, though, only compared one configuration using two different filters with the same tuning parameters. This analysis compared estimators with multiple different configurations and formulations. Different configurations and formulations were hypothesized to perform at their individual bests with different tuning parameters. This was shown in the comparison of two EKF estimators with different formulations/configurations as well as in the comparison of an EKF and UKF using the same formulation/configuration.

Additionally, this analysis showed that the experimentally optimal tuning parameters for each estimator were not based on the covariances of the sensor inputs. This is demonstrated by the chosen experimentally optimal estimators in the "Optimal Tuning Parameters" Sections: 5.1.2, 5.1.3, and 5.1.4. Such a finding could be explained by the differences between the configuration/formulation for the infamous first practical implementation for the Apollo mission and the estimators typical of SUAS (See Section 1.3.2.2.2.2 in the Introduction).

Though experimentally optimal, based on the chosen metric, the UKF performance showed that a single performance metric is not adequate for choosing a "best" set of tuning parameters. This is evident in the UKF "Initialization Error" and "Baseline Comparison".

Recommendations:

In order to compare different configurations and/or formulations, some analysis must be conducted to ensure they're both tuned to an equivalent level of their individual bests. Given the recursive nature of state estimators, a Monte Carlo analysis is highly recommended. The metrics suggested for comparing

the Monte Carlo output are: error statistics, error convergence rate, and performance under gyro biases. "Error statistics" are being recommended as results have shown that 2σ , 3σ , 4σ , max, mean, and mode, and other single metrics, if used alone, would identify different experimentally optimal tuning parameters (See Metrics" in Section 6.2, below).

Somewhat of a sensitivity analysis is recommended in order to choose the experimentally optimal tuning parameters. While it may not seem practical to incorporate bias and initialization error in a Monte Carlo analysis, it is more practical than hand checking the top percent performers (20 or 50 of many thousands). For example, none of the top UKF tuning parameters performed adequately for initial error convergence. The only feasible way to have identified an adequate performer with error convergence properties would have been to include this in the Monte Carlo criteria.

6.2. Metrics

Conclusions:

A single metric is not adequate for comparing estimators. Results show that 2σ , 3σ , 4σ , max, mean, mode, and other single metrics, if used alone would identify different experimentally optimal tuning parameters. This is apparent in previous research [3], box-and-whisker plots (Optimal Tuning Parameters - Complementary Filter Section 5.1.1) , and Table 5-9 in Section 5.5 "Baseline Comparison".

It is not intuitive, by comparing previous research from multiple sources, which estimators perform the best. There are hundreds, if not thousands, of papers claiming some kind of improved performance of their novel estimator. Without some kind of a common baseline, though, results are difficult to discern. Including a comparison to an extremely simple estimator, in Section 5.5 "Baseline Comparison" was qualitatively insightful.

Recommendations:

It is being recommended that multiple common and intuitive metrics be used when comparing estimators. Error statistics such as 2σ , 3σ , 4σ , max, mean, and mode are a good first step. It's possible, and likely that other metrics be useful in determining performance of an estimator, and possibly help determine sources of error. Late in this research a few promising metrics were discovered, but not evaluated. The first is the Allan Deviation; it is intended to detect drift [30]. The others include using moving averages or integrals of error and/or the statistics of these; These may be indicative of bias or random walk. The former of these late findings had formal documentation; the latter did not.

A simple, easy to implement, estimator is being suggested for use as a common baseline by which to compare across different research. The simple IMU-Only CF is being suggested as it would not require much effort. Though a simple estimator may not provide massive amounts of insight, it would be an easy to take step in the right direction w.r.t commonality of estimator comparisons. It is also being recommended that historical INS comparison standards be re-evaluated for applicability for the new navigation systems [4]. It appears that this has not been done, based on lack of inclusion or reference in recent comparison studies.

6.3. Future Configurations

Conclusions:

Of all of the estimators analyzed in this thesis, Method 2 performed the best. Method 3 performed the second best. The basic CF (Method 1) performed rather well for how simple it is. Method 4 did not perform well.

It was hypothesized that some estimator configuration/formulations would handle gyro bias better than others. This, though, was not obviously the case. All estimators in this study did not perform adequately

after adding in gyro bias. Though the estimators were not tuned using any gyro bias, it is apparent that estimators may not have any inherent ability to reject the significant gyro bias typical of MEMS.

Each individual state did not have the same optimal tuning parameters. This was most apparent in the EKF and UKF "Optimal Tuning Parameters" Sections 5.1.3 and 5.1.4 in that the optimal attitude solutions did not always produce adequate position and velocity estimates. This is likely due to the indirect method by which the attitude solutions received their corrections from the KFs. Though this indirectness is a known feature of the Method 3 and Method 4 formulation, other formulations have coupling between the state estimates, through the Kalman gain, that are more of a byproduct than an intention. Such a finding could be evidence against a single estimator, unlike the 6, 9, 12, and 15 state estimators common to research today.

It was also observed that estimators' performance changed with respect to the dynamics of the system. Dynamics, in this case, are not referring to quantification of non-linearity, but w.r.t. magnitude of inputs and/or states. Particularly, it was seen that estimators would converge or diverge at particular attitudes (i.e. Figure 5-28).

Recommendations

Though Method 2 performed the best, it is not immediately recommendable. This method still requires the addition of bias removal. If an adequate bias removal component for Method 2 was created, though, that same bias removal algorithm may also close the gap between the simple Method 1 CF and the more accurate Method 2 EKF. That is, based on the performance vs complexity, the author's next steps will be to analyze Method 1 and Method 2 with a bias removal component. The rationale is that these are the most simple attitude estimators, of those analyzed, and they both show potential for simple adequate solutions.

It is strongly recommended that a fundamental/initial design consideration for any attitude estimator be the handling of gyro bias. Most research found regarding this utilized some estimate of gyro bias. Though, it may be possible to handle bias without estimating it. Regardless, this should be an initial consideration—not an afterthought.

Removing the coupling of corrections, via the Kalman gain, between state estimates may produce better estimates. This could be done by creating multiple estimators that only estimate states together that have relevant coupling in their dynamics. Additionally, sliding parameters within the estimator could permit coupling only when the dynamics are also coupled.

Sliding tuning parameters could produce improved performance by weighting one input over another in conditions in which it is known one estimate would be better. Figure 5-28 shows converge of an estimate from a significant bias during particular states. Such an affect could be created under desired conditions by design by making the accurate component of the estimate more influential at higher attitudes. That is, the tuning parameters could be variable such that they are a function of attitude magnitude. It is also possible that these tuning parameters be varied based on magnitude of the sensor inputs for the following reasons. The first reason is that it is known that drift is less of a contribution to the overall measured rotation rate at high rates. Therefore, at high rotation rates, one might want to weight the gyro inputs more. The second reason is that it is known that the measured accelerations are not measuring only gravity (less accurate of an attitude measurement) when total acceleration is not equal to 1g. For this reason, one might want to vary the tuning parameters as to increase weight of the accelerometer when total acceleration is close to 1g, and de-weight as a function of $(1g - |total\ acceleration|)$.

Bibliography

- [1] Daniel J. Biezad, *Integrated Navigation and Guidance Systems*. Reston, VA: American Institute of Aeronautics and Astronautics, 1999.
- [2] Jason N Gross, "Sensor Fusion Based Fault-Tolerant Attitude Estimation Solutions for small Unmanned Aerial Vehicles," 2011.
- [3] Matthew Rhudy, Yu Gu, Jason Gross, Srikanth Gururajan, and Marcello R Napolitano, "Sensitivity Analysis of Extended and Unscented Kalman Filters for Attitude Estimation," *Journal of Aerospace Information Systems*, vol. 10, no. 3, pp. 131-143, 2013.
- [4] Kenneth R. Britting, *Inertial Navigation Systems Analysis*. Boston: Artech House, 1971/2010.
- [5] Heikki Hyyti and Arto Visala, "A DCM Based Attitude Estimation Algorithm for Low-Cost MEMS IMUs," *International Journal of Navigation and Observation*, 2015.
- [6] Sperry Marine. (2018) Sperry Marine. [Online]. <http://www.sperrymarine.com/corporate-history/sperry-marine>
- [7] Watler Wrigley, "History of Inertial Navigation," *Journal of the Institute of Navigation*, pp. 1-6, 1977.
- [8] Charles S. Draper, Walter Wrigley, and John Hovorka, *Inertial Guidance*. New York: Pergamon Press, 1960.
- [9] Paul G. Savage, *Introduction to Strapdown Inertial Navigation Systems*, 11th ed. Maple Plain, MN: Strapdown Associates Inc., 2005/1981.
- [10] David Hoag. (1963, April) Apollo Guidance and Navigation Considerations of Apollo IMU Gimbal Lock. [Online]. <https://www.hq.nasa.gov/alsj/e-1344.htm>
- [11] Steven Johnson, *Where Good Ideas Come From*. New York: Riverhead Books, 2011.
- [12] Wilfried Elmenreich, "An Introduction to Sensor Fusion," 2002.
- [13] Jason A. Jarrell, "Employ Sensor Fusion Techniques for Determining Aircraft Attitude and Position Information," Morgantown, 2008.
- [14] Randal W. Beard and Timothy W McLain, *Small Unmanned Aircraft Theory and Practice*. Princeton: Princeton University Press, 2012.
- [15] B. Talyor, C. Bil, and S. Watkins, "Horizon Sensing Attitude Stabilisation: A VMC Autopilot," in *International UAV Systems Conference*, vol. 18, Bristol, 2003.

- [16] Walter T. Higgins, "A Comparison of Complementary and Kalman Filtering," *IEE Transactions on Aerospace and Electronic Systems*, pp. 321-325, 1975.
- [17] Mark Euston, Paul Coote, Robert Mahony, Kim Jonghyuk, and Tarek Hamel, "A Complementary Filter for Attitude Estimation of a Fixed-Wing UAV," 2008.
- [18] Tae S. Yoo, Sung K. Hong, Hyok M. Yoon, and Sungsu Park, "Gain-Scheduled Complementary Filter Design for a MEMS Based Attitude and Heading Reference System," *Sensors*, pp. 3816-3830, 2011.
- [19] Zheming Wu, Zhengua Sun, Wenzeng Zhang, and Qiang Chen, "A Novel Approach for Attitude Estimation Based on MEMS Inertial Sensors Using Nonlinear Complementary Filters," *IEEE Sensors Journal*, pp. 3856-3864, 2016.
- [20] Leonard A. McGee and Stanley F. Schmidt, "Discovery of the Kalman Filter as a Practical Tool for Aerospace and Industry," 1985.
- [21] Simon J. Julier and Jeffery K. Uhlman, "A New Extension of the Kalman Filter to Nonlinear Systems," in *Signal Processing, Sensor Fusion, and Target Recognition VI*, Orlando, 1997.
- [22] jinsihou19. (2015) Acantha Project. [Online]. <https://github.com/jinsihou19/Acantha>
- [23] Mats Jirstrand and Johan Gunnarsson. (2001) Code Generation for Simulation and Control Applications. [Online]. http://www.mathematica-journal.com/issue/v8i2/features/codegeneration/contents/html/Links/index_Lnk_3.html
- [24] Richard Fitzpatrick. (2006, Feb.) University of Texas - Lectures (301). [Online]. <http://farside.ph.utexas.edu/teaching/301/lectures/node100.html>
- [25] Artist Unknown. (2015, Oct.) Robotics.StackExchange. [Online]. <https://robotics.stackexchange.com/questions/8191/rotation-matrix-to-euler-angles-with-gimbal-lock>
- [26] User: DMahalko. (2018, May) Wikipedia. [Online]. https://en.wikipedia.org/wiki/Gimbal_lock
- [27] R. G. Brown, "Integrated Navigation Systems and Kalman Filtering: A Perspective", " *Journal of the Institute of Navigation*, vol. 19, no. 4, pp. 355-362, 1972.
- [28] Rudolph van der Merwe, Eric A. Wan, and Simon I. Julier, "Sigma-Point Kalman Filters for Nonlinear Estimation and Sensor Fusion- Applications to Integrated Navigation," 2004.
- [29] Marc O. Rauw, "A SIMULINK environment for Flight Dynamics and Control analysis - application to the DHC-2 'Beaver'," 1993.

- [30] Oliver J. Woodman, "An Introduction to Inertial Navigation," 2007.
- [31] AER Shabeyek, Cedric Demonceaux, Oliver Morel, and David Fofi, "Vision Based UAV Attitude Estimation: Progress and Insights," *Journal of Intelligent Robotic Systems*, pp. 295-308, 2011.
- [32] Gregory L. Andrews, "Implementation Considerations for Vision-Aided Inertial Navigation," Boston, 2008.
- [33] Borui Li, Chundi Mu, Tao Wang, and Qian Peng, "Comparison of Feature Point Extraction Algorithms for Vision Based Autonomous Aerial Refueling," 2014.
- [34] Jacob W Langelaan, "STATE ESTIMATION FOR AUTONOMOUS FLIGHT IN CLUTTERED ENVIRONMENTS," 2006.
- [35] Eugene Morelli, "Real-Time Aerodynamic Parameter Estimation without Air Flow Angle Measurements," Hampton, 2009.
- [36] (2012) Mathworks. [Online].
https://www.mathworks.com/tagteam/74250_Paper%20Number%2012AEAS-0090-finalweb.pdf
- [37] Marc Compere. (2015, Jan.) Mathworks. [Online].
<https://www.mathworks.com/matlabcentral/answers/98195-how-can-i-have-the-to-file-block-use-the-file-name-from-a-workspace-variable-in-simulink-6-5-r2006b>
- [38] Mathieu Marmion, "Airborne attitude estimation using a Kalman filter," Longyearbyen, Norway, 2006.
- [39] William Premerlani and Paul Bizard, "Direction Cosine Matrix IMU: Theory," 2009.
- [40] F. Landis Markley, John L. Crassidis, and Yang Cheng, "Nonlinear Attitude Filtering Methods," 2005.
- [41] Nojan Madinehi, "Rigid Body Attitude Estimation: An Overview and Comparative Study," London, Ontario, Canada, 2013.
- [42] Eun-Hwan Shin, "Estimation Techniques for Low-Cost Inertial Navigation," Calgary, 2005.
- [43] Pedro Batista, Carlos Silvestre, and Paulo Oliveira, "Journal of Intelligent & Robotic Systems Attitude Estimation: Analysis, Design, and Performance Evaluation," *IEEE TRANSACTIONS ON AUTOMATIC CONTROL*, vol. 57, no. 8, pp. 2095-2100, 2012.
- [44] Alexandra Moutinho, Miguel Figueiroa, and Jose Raul Azinheira, "Attitude Estimation in SO(3): A Comparative UAV Case Study," *Journal of Intelligent & Robotic Systems*, vol. 80, pp. 375–384, 2014.

- [45] John L. Crassidis, F. Landis Markley, and Yang Cheng, "Survey of Nonlinear Attitude Estimation Methods," *Journal of Guidance, Control, and Dynamics*, vol. 30, no. 1, pp. 12-28, 2007.
- [46] Calvin Coopmans, Austin M. Jensen, and YangQuan Chen, "Fractional-Order Complementary Filters for Small Unmanned Aerial System Navigation," *Journal of Intelligent & Robotic Systems*, vol. 73, pp. :429–453, 2014.
- [47] Tarek Hamel and Robert Mahony, "Attitude estimation on SO(3) based on direct inertial measurements," in *IEEE International Conference on Robotics and Automation*, Orlando, 2006.
- [48] Jason Gross, Yu Gu, Srikanth Gururajan, Brad Seanor, and Marcello R. Napolitano, "A Comparison of Extended Kalman Filter, Sigma-Point Kalman Filter, and Particle Filter in GPS/INS Sensor Fusion," in *AIAA Guidance, Navigation, and Control Conference*, Ontario, 2010.
- [49] Shyam M. Mohan, Naren Naik, R.M.O. Gemson, and M.R. Ananthasayanam, "Introduction to the Kalman Filter and Tuning its Statistics for Near Optimal Estimates and Cramer Rao Bound," Kanpur, 2015.
- [50] Robert Mahony, Tarek Hamel, and Jean-Michel Pflimlin, "Complementary filter design on the special orthogonal group SO(3)," in *IEEE Conference on Decision and Control, and the European Control Conference*, Seville, 2005, pp. 1477-1484.
- [51] Scott M. Bezick, Alan J. Pue, and Charles M. Patzelt, "Inertial Navigation for Guided Missile Systems," *JOHNS HOPKINS APL TECHNICAL DIGEST*, vol. 28, no. 4, pp. 331-342, 2010.
- [52] Sebastian O.H. Madgwick, "An efficient orientation filter for inertial and inertial/magnetic sensor arrays," 2010.
- [53] Shane Colton, "The Balance Filter," 2007.
- [54] R. J. Noriega-Manez, "Inertial Navigation," 2007.
- [55] John L. Crassidis and F. Landis Markley, "Unscented Filtering for Spacecraft Attitude Estimation," *JOURNAL OF GUIDANCE, CONTROL, AND DYNAMICS*, vol. 26, no. 4, 2003.
- [56] Dan Simon, "Kalman Filtering," *Embedded Systems Programming*, pp. 72-79, 2001.
- [57] Dan Simon, *Optimal State Estimation*.: John Wiley & Sons, Inc, 2006.
- [58] John Junkins and John L. Crassidis, *Optimal Estimation of Dynamic Systems, Second Edition*.: CRC Press, 2011.

[59] Anton H. de Ruiter, Christopher Damaren, and James R. Forbes, *Spacecraft Dynamics and Control: An Introduction*.: Wiley, 2012.

[60] George J. Vachtsevanos and K. Valavanis, *Handbook of Unmanned Aerial Vehicles*.: Springer Netherlands, 2015.